10/12-10-96 9858 (1)

LBNL-39028
UC-2000

ERNEST ORLANDO LAWRENCE
BERKELEY NATIONAL LABORATORY

Lance Water Injection Tests Adjacent to the 281-3H Retention Basin at the Savannah River Site, Aiken, South Carolina

B. Freifeld, L. Myer, G. Moridis, P. Cook,
A. James, L. Pellerin, and K. Pruess
Earth Sciences Division

September 1996

Available to DOE and DOE Contractors
from the Office of Scientific and Technical Information
P.O. Box 62, Oak Ridge, TN 37831
Prices available from (615) 576-8401

Available to the public from the
National Technical Information Service
U.S. Department of Commerce
5285 Port Royal Road, Springfield, VA 22161

LBNL-39028
UC-2000

Lance Water Injection Tests Adjacent to the 281-3H Retention Basin at the Savannah River Site, Aiken, South Carolina

B. Freifeld, L. Myer, G. Moridis, P. Cook, A. James, L. Pellerin, K. Pruess

Earth Sciences Division
Lawrence Berkeley National Laboratory
Berkeley, CA 94720

September, 1996

This work was supported by the Subsurface Contamination Focus Area, Office of Technology Development, Office of Environmental Restoration and Waste Management, US Department of Energy, under contract DE-AC03-76SF00098.

TABLE OF CONTENTS

LIST OF FIGURES

LIST OF TABLES

1. Introduction

1.1 Background

A pilot-scale field demonstration of waste isolation using viscous-liquid containment barriers has been planned for the 281-3H retention basin at the Savannah River Site, Aiken, SC (Moridis, 1996). The 281-3H basin is a shallow retention/seepage basin contaminated mainly by radionuclides. The viscous-liquid containment barrier utilizes the permeation of liquid grout to either entomb the contaminants within a monolithic grout structure or to isolate the waste by drastically reducing the permeability of the soils around the plume. A clear understanding of the hydrogeologic setting of the retention basin is necessary for proper design of the viscous liquid barrier. To aid in the understanding of the hydrogeology of the 281-3H retention basin, and to obtain critical parameters necessary for grout injection design, a series of tests were undertaken in a region immediately adjacent to the basin.

A direct push lance injection method, used in the grouting industry as a technique for chemical grout emplacement, was selected to perform hydrologic injection tests adjacent to the 281-3H site. In the lance injection method, a narrow diameter tube with a pointed tip and injection ports is hydraulically driven into the ground. Surface pumps ensure continuous fluid movement through the lance as it is lowered into the soil. The benefits identified in lance injection as opposed to more conventional techniques such as Tube-à-Manchette or hollow stem augured holes with grout pipe emplacement include:

- Ability to rapidly make numerous closely spaced "lancings"
- Good control over location and volumes of grout injection as a function of depth
- Practical real time adjustment of barrier emplacement as a function of the formations ability to take grout.
- Ability to form continuous grout horizons within well defined horizontal layers
- Elimination of contaminated cuttings, drilling fluids, or excavated materials.

This report discusses the data collected during the Lance Water Injection Tests (LWIT), conducted June 4 to June 8, 1996, and what was learned during field operations.

1.2 Objectives

The objectives of the LWIT were:

1. To evaluate the general performance of the Lance Injection Technique for grout emplacement at the site, including the range and upper limits of injection pressures,

the flow rates applicable for site conditions, as well as the mechanical forces needed for lance penetration.

2. To obtain detailed information on the injectability of the soils immediately adjacent to the H-area retention basin.
3. To identify any high permeability zones suitable for injection and evaluate their spatial distribution.
4. To perform ground penetrating radar (GPR) to gain information on the structure of the soil column and to compare the results with LWIT data.

This report will focus on results pertinent to these objectives. Additional descriptive details of daily activities are found in the report "Technical Oversight for the Lance Water Injection Test at the H-Area Retention Basin (U)," Westinghouse Savannah River Company (WSRC), Subcontract L001015P, July 1996.

To meet the LWIT objectives, lance injections were carried out at several locations within a test plot located approximately east of the 281-3H retention basin. The test plot was a 30m by 15m (100 ft by 50 ft) rectangle, with the major axis aligned north-northeast. At a representative set of locations, the lance was pushed into the soil in 30 cm (1 ft) increments to depths of 12.2 m (40 ft). At each test interval the pressures and flow rates were recorded. In addition, strain gauges were used to monitor the loads required to push to the new depth. GPR surveys were conducted before and after lance testing was conducted.

2. LWIT Equipment & Instruments

2.1 Lance Injection Truck and Mobile Auger Rig

The central piece of equipment used for the LWIT was a truck provided by Hayward Baker (equipment number 98312), through their Fort Worth office. The Lance Injection truck is displayed in **Figures 1, 2,** and **3**. The truck which is commonly referred to as a 40 foot railroad injection unit was designed by Hayward Baker to inject lime-slurry grouts for stabilizing the bedding beneath railroad tracks. The total weight of the LWIT truck is 20,100 kg (44,220 lbs). The weight is distributed with 12,973 kg (28,540 lbs) on the rear axle and 7,082 kg (15,580 lbs) on the front. The truck mounted tank has a storage capacity of approximately 4920 liters (1300 gallons). The masthead which contains the three 12.2 m (40 foot) lances is 13.44m (44' 1") in length.

The Lance Injection truck was instrumented by Lawrence Berkeley National Laboratory (LBNL) personnel to perform the water injection tests at the H-Basin site. Modifications to the truck included:

1. the addition of a Teel multi-stage booster pump,
2. the installation of flow meters downstream of the pump,
3. the inclusion of pressure transducers within the lance tips, and
4. the placement of strain gauges to monitor the axial loading of the lance.

In addition to the Lance Injection truck, Alliance Drillers supplied a Mobile B-61 auger rig to penetrate through hard layers that the Lance Injection unit failed to penetrate. 8.89 cm (3.5") solid stem augers were used to auger to the point of lance refusal and then the holes were split spoon sampled and augured to a depth at which it was believed that lancing could resume.

2.2 The Flow Control and Monitoring Equipment

The flow control equipment is pictured in **Figure 2**, as mounted on the Lance Injection truck. Water for injection was gravity fed into the Teel booster pump from a storage tank mounted on the rear of the truck. The Teel pump used to boost the water pressure has a maximum output of over 1.38×10^3 kPa (200 psi). At this pressure, the flow rate can still exceed 20 lpm. This would enable determination of the pressures required to fracture the formation, a situation to be avoided while permeation grouting. A recirculation line was fed back into the water storage tank from the outlet of the booster pump to enable the pump to operate at a wide range of flow rates and pressures. By

throttling open the recirculation line, excessive back pressures which would limit the service life of the pump, can be avoided.

Visual Bourden tube gauges were used for rapid acquisition of the injection system pressures in the field. **Figure 2** shows the visual gauges at the outlet of the booster pump, at the down stream side of the pressure regulators, and at the outlet of the flowmeters. The pressure at the outlet of the flowmeters was logged manually in a bound notebook during field testing. Automatic pressure data were logged electronically using strain gauge pressure transducers manufactured by Druck™, Inc. and KPSI™. Druck™ transducers with an absolute full scale range of 1.38×10^3 kPa (200 psi)were mounted at the inlet and outlet of the flowmeters. At the tip of the lance, KPSI™ transducers with a full scale sealed reference range of 6.90×10^2 kPa (100 psi) provided in-situ pressure measurements. The KPSI™ pressure transducers reflect the true injection pressure and are not subject to the head losses and transients of the surface mounted sensors. The KPSI™ transducers had an accuracy within 0.2% of full scale.

Figure 4 shows the lance tips partially assembled. **Figure 5** is an engineered sketch for the lance tip. The lance tip, shown connected to the pressure transducer, has both internal female threading and an external male thread. The pressure transducer is threaded into the inner female thread. The lance tip body connects the lance tip to the lance rods. Water is channeled around the outside of the pressure transducer and exits through twelve 4.8 mm (3/16") holes in the lance body. Small 1.6mm (1/16") holes connect the volume in front of the pressure transducer diaphragm to the flowing water. Testing of the assembly and of the injection pattern is shown in **Figure 6**.

Four flow meters were mounted downstream of the pressure regulating valves. The flowmeters are referred to by the nominal pipe size of the fluid lines. All flowmeters were turbine wheel type. The two flow meters with the lowest range were manufactured by McMillan Company. They had calibrated ranges of 0.06 lpm to 1.0 lpm and 0.2 lpm to 5 lpm and were referred to as 1/4" and 3/8" flowmeters respectively. The minimum detectable flow through the 1/4" flowmeter is 0.01 lpm. Accuracy within the calibrated range is 3%. The larger flowmeters, referred to as 1/2" and 3/4", were manufactured by Signet Flow. The 1/2" flowmeter had a range from 4 lpm to 50 lpm. The 3/4" flowmeter was removed from the system and was not used during field testing.

Data were collected using a Keithley Model 2001 Digital Multimeter and a Keithley Model 7001 Switch System. Control of the electronics and data acquisition were provided by Labview™ for Windows 95, a control and data acquisition program by National Instruments Inc. All sensors were scanned at 2 second intervals during testing.

Strain gauges were bonded to a 30 cm (12") section of hardened steel lance rod and mounted below the lance drive plate (at the opposite end of the lance from the tip). Each bonded strain gauge was calibrated in a load cell with up to 20,000 lbs of load prior

to field use. The strain gauge signal was monitored by the same Keithley electronics as was used for monitoring the pressure transducers and flowmeters.

All sensors and electronic instruments had current calibrations as required in the Quality Assurance Project Plan for the LWIT, WSRC May 1996, section 6.0.

3. Testing Procedures and Operations

3.1. Water Injection Test Procedure

Constant pressure injection tests were conducted adjacent to the 281-3H retention basin. The lance was lowered in 30 cm (1 ft) increments while water pressure in the lance tip was maintained above lithostatic pressure. The constant water pressure prevents clogging of the lance tip ports while raising or lowering the lance. At the targeted depth the lance tip was kept stationary, while both pressures and flows were logged at two second intervals. The pressure was maintained constant using spring actuated pressure regulators while the flow rate was allowed to vary. If the measured flow rate was below the detection limit of the smallest flowmeter (0.01 lpm), the lance tip was lowered to the next interval. If flows were measurable, then the appropriate flowmeter was selected to record the flow at the current depth. After a quasi-steady state flow had been established for several minutes (usually 5 minutes), the test at that depth was concluded and the lance tip was pushed down by 30 cm (1 ft) to the next testing location. Lance injection tests were conducted down to a maximum depth of 12.2 m (40 ft).

The point at which the formation would fracture was investigated during lance testing. To test for the point at which significant soil yielding begins, the injection pressure was adjusted upward until a significant increase in flow rate occurred with a corresponding decrease in pressure. A representative fracturing test can be seen in Appendix A, at the 38' test in lancing LPT-2S.

3.2. Summary of Field Testing Operations and Data Collection

Prior to injection testing, the site was cleared of trees, the stumps were removed and a gravel pad was laid in place. The pad sloped about 4% toward the south. Details on the site preparation are found in WSRC, July 1996.

A rectangular grid, 30m x 15m (100ft x 50ft) was laid out to the east of the 281-3H basin perimeter fence. **Table 1** shows the name and location of each lancing that was conducted, as referenced to the southwest corner of the grid. Each lancing location within the test grid has been plotted in **Figure 7**.

Table 1. Location of lancings on a Cartesian coordinate system

	Grid Location	
Lancing Location Name (data file name)	Easting (ft.)	Northing (ft.)
LPT-2	35	86
LPT-5	35	54
LPT-9	35	15
LPT-11	15	5
LPT-16	15	55
LPT-19.5	15	90
LPT-20	15	95

Prior to performing the injection tests, flowmeters were volumetrically calibrated. This simple procedure required a calibrated bucket be placed below the injection lance while the time required to deliver a known volume is measured. Checks on the calibrations of the flowmeters were performed in the field on June 4, June 6, and June 7.

The Lance Injection truck was initially set up over LPT-20 on June 5. The lance was lowered in 30 cm (1 ft) increments to 1.8m (6 ft) in depth. At this point an extremely tough layer was encountered. The rig was moved back two feet and another attempt was made to penetrate to a deeper depth. With a lot of hard pushing and cycling the lance up and down the lance was able to penetrate to 2.8m (9' 4") in depth. The next lancing location attempted was midway between LPT-19 and LPT-20, at LPT-19.5. The lance was able to penetrate to a depth of 3.1m (10' 1").

Due to the inability to push the lance below the very hard layer it was decided to have the lancings augured by Alliance Drilling using a Mobile Drill B-61 Auger rig, and split spoon sampled to a depth at which it was felt the lance system could resume operation. The depth that lancing restarted was routinely 4.3 m to 4.9 m (14' to 16') below land surface. This depth corresponded to the point at which blow counts for advancing the split spoon sampler 15 cm (6") were in the range of 25 to 30. This criteria was established based on a comparison of previously obtained cone penetrometer results, lance refusal depths and blow count data. The correlation between blow count and lance penetrability was not carefully tested. The upper limit of 25 to 30 is considered to be approximate since blow count testing (Standard Penetration Testing) was not conducted as per ASTM D1586 and was only used for guidance in the field.

Lance testing continued above the hard layer at locations LPT-9, LPT-5, and LPT-2. After holes were augered and split spooned by Alliance Drilling, lance testing was performed in LPT-9S, LPT-19.5S, LPT-2S, LPT-16S, LPT-11S, and LPT-5S. The suffix S appended after the location denotes post-augered/split-spooned lancings.

The complete record for daily field activities is found in WSRC, July 1996. A synopsis of the events in the field is included here. Recorded downhole pressure and flow rate appear in Appendix A. Data collected after augering are indicated by the suffix S added to the location name (i.e. LPT-9S). In Appendix A the flows from the 1/2" flowmeter and the corresponding injection pressure are plotted on the left axis, while the lower flows monitored using the 1/4" and 3/8" flowmeters appear on the right axis. The high flow rates often appear erratic due to ground loop and 60Hz. noise. This is further discussed in section 4.2.2. Flowrates above 10 lpm and accompanied by decreasing injection pressure are indicative of the soil fracturing or yielding, and will be discussed in section 4.4.3.

3.3 Ground Penetrating Radar Survey

3.3.1 Purpose

Ground Penetrating Radar (GPR) data were acquired on June 5 and June 11, 1996 within the LWIT test site by the company Microseeps using a GSSI Sir 10 system equipped with both 100 and 300 MHz antennas. The purpose of the GPR survey was to provide an understanding of the subsurface structure and lithology within the vicinity of the LWIT site and determine GPR's potential for future characterization activities within the 281-3H basin. The specific goal of the survey was to estimate the depth and continuity of lithologic features as delineated by the auger drilling and lance testing.

3.3.2 Survey Specifications

The lines of GPR coverage, labeled GPR1-GPR12, are illustrated in **Figure 7**. Data were acquired using the GSSI Sir 10 system before and after the lance water injection. The 300 MHz data were acquired in the mono-static mode (single antenna unit with zero offset), while the 100 MHz data were acquired in the bi-static (separate transmitter/receiver antenna) mode with a six foot offset utilizing a very high powered transmitter. The 300 MHz data were sampled at 250 picosec/sample rate and the 100 MHz data were sampled at 500 picosec/sample rate. All data sets were collected using a 256 ns record length.

During the pre-injection phase of coverage (6/5/96), the presence of a drill rig prevented data collection in the northwestern corner of the site. The post-phase of coverage included the entire 30m x 15m (50ft x 100ft) area due to the absence of obstructing equipment. Plots of several lines from the 300 MHz data set are shown in **Figures 19** to **24**. Analysis of the GPR survey is presented in section 4.6.

4. Field Observations and Results of the LWIT

4.1. Synopsis

- Permeability measurements were taken at 171 discrete points in seven different locations.
- High injection pressures were needed to inject water into the formation (much higher than lithostatic pressures) and injection flow rates varied from below the detectable limit (0.01 lpm) to 35 liters per minute.
- A hard layer was encountered at a depth below land surface of between 1.5m and 3.1m (5 and 10 ft), which could not be lanced through.
- The bottom of the hard layer was routinely 4.3 m to 4.9 m (14 to 16 ft) below land surface, although this was not rigorously tested.
- Almost all injection tests conducted above this layer resulted in flows below the detection limit.
- Below the hard layer, injection flow rates varied from below the detection limit, up to 35 liters per minute.
- Within the hard layer no injection tests were conducted, although injection tests conducted at the top interface of the hard layer resulted in no measurable flow, even at very high injection pressures. The top of the hard layer also proved extremely resistant to hydraulic fracturing.
- There was very little vertical correlation in injectability. Intervals 30 cm apart could exhibit drastically different behavior.
- High flow rates were indicative of fracturing of the soil column. This occurred at injection pressures that varied from 3.79×10^2 kPa to 1.03×10^3 kPa (55 to 150 psi).
- No continuous high permeability horizons were identified.
- Even at reasonable injection rates, the pressure and flow rate data indicate a relationship which cannot confirm permeation of the formation. Although numerical simulations (see section 4.5.3 and **Figure 18**) managed to predict similar behavior to the measured flow rates, there is strong indication that the water uptake is not due to permeation, but to incipient yielding or soil fracturing. If this is the case, numerical simulation could not easily predict such behavior because none of the available models of flow and transport account for effects in soil with significant yield.

4.2. Equipment Performance

4.2.1 Lance Truck Performance

Several limitations were identified in using the 40' lance railroad unit for injection. As configured, the 40' lance injection rig was unable to penetrate an areal persistent hard layer which was encountered between 1.5 m and 3.1 m (5 and 10 ft) below ground surface. Although the rig is very heavy (at 20,100 kg) it has been designed for use on nearly level railroad tracks and its lack of hydraulic outriggers prevented it from fully using its hydraulic capability to maximize the downward force with the lances. As a result, operation is limited to relatively smooth, level (less than about 4% slope) surfaces. Moreover, it could not make an angled push because of its inability to lock the masthead into any position but full vertical.

Future lance testing and grout injections can resolve many of the aforementioned limitations by using alternative equipment. Hayward Baker has in the past installed the injection mast on track-mounted vehicles which has increased rig stability. A hydraulic hammer or high-frequency industrial vibrator installed at the head of the lance would also increase the lances ability to penetrate hard layers. These techniques are often referred to as sonic or vibratory methods in groundwater literature. Alternative hammer drill rigs such as the Ingersoll Rand ECM-370 or equivalent may be used because of the combined ability to push and act as a rotary drill when necessary. However, a major constraint in working with conventional rotary hammer rigs at a contaminated site is the extra health and safety precautions necessary to minimize the risk of exposure to cuttings or fluids brought to the surface.

4.2.2 Flow Control System and Pressure Sensors

The flow control system and pressure sensors were able to span the range of flows and pressures required to operate over widely varying conditions. Although many tests yielded "no flow" results, the detection limit of 0.01 lpm was considered the lowest practical flow rate due to compliances in the injection system. These compliances are primarily in the hydraulic hoses and the lance tip position. The upper injection limit was a function of pump output pressure. Maximum pump output pressure could be regulated by changing the setting on the pump recirculation valve. At injection pressures of 5.1×10^2 kPa (74 psi) a flow rate of 35 lpm could be maintained.

Accurate pre-setting of injection pressures was difficult for several reasons. First, the lance injection truck tower was approximately 45 ft. high. Thus, with the lance tip at the ground surface about 1.38×10^2 kPa (20 psi) was required to pump the water to the top

of the tower. Additional pressure was required to keep the lance full. As the lance was pushed into the ground, the relation between pressure at the pump and water pressure at the tip changed continuously. Another reason for difficulties in pre-setting pressures was that the permeability of the soils changed almost instantaneously by orders of magnitude when moving from one horizon to another. The pressure regulators were not able to control pressures during such rapid changes in flow. Thirdly, the process of advancing the lance often resulted in large pressure spikes of as much as 1.38×10^3 kPa (200 psi). It was often necessary to toggle the lance up and down in order to penetrate the formation. As soon as the lance was lifted up, water would enter the hole. As it was pushed back down, this water had to be displaced, either into the formation or back into the lance. The lower the permeability of the formation, the larger would be the pressure spike in the lance.

Due to ground loop and 60 Hz noise at the site, data obtained by the 1/2" flowmeter had a degraded accuracy. Based upon analysis of the data a conservative estimate of the 1/2" sensors accuracy is ±20% of measurement above 10 lpm and ±40% below this point. The data from the 1/2" flowmeter appears noisy but results from the calibration tests show it is repeatable.

4.2.3 Axial Load Measurements

Strain gauge measurements are included in Appendix C. A table of the peak downforce measured during each test increment appears at the beginning of the appendix. The typical response of the strain gauge to advancing it downward is a step increase when penetration was initiated. Relaxation of the down force occurs gradually and may take from several seconds to a minute or more. The height of the pressure spike correlates with the hardness of the layer and the friction between the lance and the soil column. Negative spikes occurred when the lance was being withdrawn also due to the friction between the lance and the soil. No correlation between resistance to penetration and fracturing pressure has been noticed in the data.

The average force needed to advance the lance in 30 cm (1 ft) increments was 2.14×10^4 N (4800 lbf) Maximum downward force measured was 4.01×10^4 N. The maximum downward force of 4.01×10^4 N (9000 lbf) was surprisingly less than expected, considering the weight of the truck, 20.1 metric tons, and the ability of the lance drive chain and hydraulically driven motor to produce and deliver very large forces. The problems stemmed from the truck not having outriggers or stabilizers and its operation while on a sprung suspension rather than on rigid supports. The free suspension and lack of outriggers coupled with the 4% slope of the surface led to limitations on what the lance injection truck operators felt was a safe downward force.

4.3 Review of a representative lancing (LPT 11S)

This section will provide a detailed description of the actions performed and observations made during a single lancing. The interpretative statements made here are applicable towards similar observations made for the other lancings. This section makes use of the sets of data included in Appendix A, Pressure and Flow Rate Data for Lance Injections, Appendix C, Axial Lance Load Data, Daily Activity Reports, and the sets of field notes located in WSRC, July 1996. The location for lancing LPT-11S is shown in **Figure 7**.

Lancing LPT-11S was first started by augering down to 8', with the Mobile B-61 rig. At this point the first split spoon sample was taken. Augering was then performed alternating with split spoon sampling until a depth of 14' was reached. The lance injection rig was located over the augered hole, LPT-11S, and the lance lowered to just above the bottom of the hole. The pump was turned on and the 1/2" flow meter was opened as the lance was lowered into the soil. Initially a flow rate of 35 lpm was recorded until the lance actually penetrated the formation and the flow rate dropped to 0 lpm.

Pushing the lance down to 15' required a force of 2200 lbs. No flow was recorded at this depth with an applied hydraulic head of 52 m H_20 applied. The lance was lowered to 16' with a push of 3400 lbs force. Hydraulic head was increased to 60 m H_20 without any measurable flow. The lance was lowered to 17' with a push of 3800 lbs force. At 61 m H_20 no flow was recorded.

During the push at 18', a "sticky" response was noted. It required the lance to be cycled up and down using the truck hydraulics. The axial load on the lance is seen to swing from negative force to positive, as the lance is pulled up and pushed down again. The hydraulic head in the lance shot up to 70 m H_20 and slowly decays back toward the set point of the pressure regulator. No flow is noted. The reason for this transient is that during the upward pull on the lance, fluid fills the volume below the lance tip. When the lance tip is hydraulically forced down again the pressure is increased. Since the water in the lance tip is at a higher pressure than has been set at the pressure regulator the regulator acts as a backflow preventer. The systems only outlet is through the formation. The slow decay in pressure is a function of the formation permeability.

The lance was lowered to 19' with a push of 4800 lbs. Again, no flow was recorded. The pushes to 20' and 21' were considered "sticky" and "hard" and resulted in no flow responses. It was necessary to cycle the lance up and down to get to the targeted depths. It took approximately three minutes of cycling the lance up and down to get to a depth of 22'. The axial forces measured varied from +6400 lbs to -5500 lbs. With the pressure regulator set at 63 m H_20, a flow rate of .29 to .31 lpm was recorded for a five

minute injection period. Both flow rate and pressures were very steady during this interval.

At depths of 23' and 24' no flow was measurable. At a depth of 25' with a hydraulic head of 68 m H_20 a flow rate of .1 lpm was measured. Both pressures and flow were constant during the 5 minute injection. The push down to 26' was characterized as "very hard layer, extreme" and "not sticky". The flow rate on the 3/8" flowmeter was out of range. When the 1/2" flowmeter was used a flow rate of ~9 lpm was recorded. Injection pressures stabilized at 58 m H_20.

Between 27' and 30', injections resulting in flows of 7, 5.5, 5.4, and 6 lpm were recorded with injection pressures respectively at 56, 54, 54, and 52 m H_20, with increasing depth. All penetrations took some cycling of the lance up and down to get to the targeted depth. At 31' depth with and injection pressure of 64 m H_20 the flow rate was below the detection limit. The 32' depth had a flow rate of .35 lpm at 64 m H_20.

The 33' depth injection was started with an injection pressure near 65 m H_20. After a minute of slowly falling injection pressures and an increasing flow rate, the injection rate suddenly jumped from 0.5 lpm to 2.6 lpm. This drastic change in flow rate is an indication of soil fracturing or some other sudden mechanical deformation of the injection zone. Although this particular injection test stabilized with an injection rate of 2.6 lpm, with an injection pressure of 62 m H_20, often it was seen that the flow rate would jump all the way up to 30 lpm or more with an extreme drop in injection pressure. An example of this behavior is clearly demonstrated by a test at LPT-19.5S, 26' depth.

Injections at the depth of 34', 35' and 36' were conducted at a pressure of 65 m H_20. Steady flow rates of .70 lpm 0.08 lpm and 0.30 lpm were measured. The injections at 37' and 38' conducted at 67 m. H_20 resulted in no measurable flow rate. The injection test at 39' conducted at 67 m H_20 resulted in a flow of 0.12 lpm. The pushes to reach the 39' and 40' were characterized as "easy". The last injection at 40' depth resulted in a steadily increasing flow rate which started at 0.5 lpm and ramped up over 5 minutes to 1.7 lpm. Similar to the injection at 33' depth, this injection does not represent a response that would be suggested by permeation, rather it indicates some form of fracturing of the soil or deformation of the injection zone.

At 40' depth, the lance has been inserted to its maximum depth and is withdrawn while injecting water through the 1/2" flowmeter. The flow during lance removal serves to keep the lance ports from getting plugged.

4.4 General Field Testing Observations

4.4.1 Near Surface Phenomena

Since the planned H-basin barrier included "walls" as well as a "floor," injection began essentially at the ground surface. High flow rates at injection pressures of 1.03×10^2 kPa -1.38×10^2 kPa (15-20 psi)(the minimum pressure which could be applied with this equipment) were observed at depths of 0.6m to 0.9 meters (2' to 3'). This was attributed to site preparation activities which caused surficial disturbances. At this shallow depth, preferential flow paths can develop connecting the lance tip to the surface. A common observation at these depths is that water would appear as a localized "boil" at the ground surface. A final observation of near surface injection was that the injectivity of the soils changed from high values in the top 0.6m to 0.9m (2' to 3') to essentially zero over a distance of much less than 30 cm (1 ft). Examples of this near surface behavior can be seen in the start of the pressure/flow data for lancings LPT-5 and LPT-9 presented in Appendix A.

At depths in excess of four feet, at no time, under any injection pressure, did flow ever appear at the surface. In particular, water did not establish a pathway along the interface between the lance and the soil.

4.4.2 Typical LWIT Response

The most common hydrologic response (see data plotted in Appendix A) is constant pressure with a flat or slightly increasing flow rate. Such a response was unexpected and cannot be accounted for by conventional hydrologic analysis. In a typical well test in a porous medium, a constant pressure injection would result in a transient response of decreasing flow rate. Eventually, depending on the storativity and permeability of the media, a steady state or constant flow rate is approached.

The LWIT injection tests differed in a number of ways from a typical well test. Most importantly, the elevated injection pressure was maintained continually as the lance was advanced from one injection point to the next. Since the injection points were only 30 cm (1 ft) apart, pore pressures at subsequent points may have been affected by the previous measurement as well as the process of advancing the lance. Another factor was that the low flow meters were normally not turned on until after the targeted injection depth was attained. This was done to protect the low flow meters from surges. The delay in turning on the meters was not monitored but probably varied from 5 to 30 seconds. One interval in which the meters were left on is LPT 16S from 19 to 21 feet. The process of advancing the lance resulted in a complicated pressure and flow rate response.

4.4.3 Fracture Response

Results showed that the upper limits on injection pressures and volumes for this site were set by the soil strengths. If injection pressure was too high, the soil would fracture. It should be noted that a fracture in a competent medium is evidenced by a sudden drop in injection pressure accompanied by a rapid increase in flow rate. The fracture behavior observed during the LWIT was sometimes very sudden, but more commonly "fracturing" was observed over the span of several minutes. This slower change is possibly due to a slow mechanical deformation or yielding of the soil, as opposed to the sudden formation of a discrete fracture.

The injection pressure at which a fracture would form was very variable over the site. At a depth of 9' in lancing LPT 19.5, fracturing did not occur at a fluid pressure of 1.03×10^3 kPa (150 psi) (no flow occurred either). In lancing LPT 9, a fluid pressure of 6.90×10^2 kPa to 7.58×10^2 kPa (100 psi to 110 psi) was maintained from a depth of 16' to 33' without the formation of an obvious fracture, whereas in LPT 19.5 fracture occurred at the same depths, at pressures of 3.79×10^2 kPa to 4.14×10^2 kPa (55 psi to 60 psi). In other holes, injection pressures in the range of 4.48×10^2 kPa to 5.52×10^2 kPa (65 to 80 psi) caused fractures in some intervals and not in others..

Analysis of the individual flow vs. time response curves shows that some of the locations that are not considered fractured, represent conditions of incipient soil fracturing. This response is characterized by an irreversible, increasing flow rate during a constant pressure injection. Examples of this response are in LPT 19.5S at depths of 28 and 30 feet. (At 32 feet obvious fracturing occurred in the formation.)

4.4.4 The Areal Pervasive Hard Layer

For each lancing, beginning from the lang surface, the maximum depth the lance could penetrate was between 1.5m to 3.1m (5' to 10') before an impenetrable barrier was reached. This coincided with similar depths of very high resistance (5500- 8300 psi), noted in cone penetrometer logs taken just outside the fence on the east side of the 281-3H basin (Phifer, 1996). **Table 2** shows the depth at which each lancing was aborted and augering and split spoon sampling commenced. Since the topography is dipping towards the south, the hard layer appears near horizontal.

Pedological analysis of previously obtained split spoon samples (Moridis, 1996) and visual observation in the field reveal a composition of the hard layer which is similar to the overlying medium. The one noted difference between the soil within the hard layer and the overlying soil is a greater content of quartz pebbles in the hematitic clay matrix.

During injections conducted with the lance tip at the upper boundary of the hard layer, pressures as high as 1.4×10^3 kPa (200 psi) failed to produce any measurable flow. The failure to be able to inject into the upper boundary of the hard layer reveals both the high strength and low permeability associated with this feature. Unlike a coarse gravel layer, which would have a high resistance to lance penetration along with high permeability, the hard layer contains a matrix of coarser material filled and cemented with sufficient clays to render it near impervious to flow.

Table 2. Depth to Hard Layer

Lancing	*Depth*
LPT-20	9' 4"
LPT-19.5	10' 1"
LPT-9	7' 6"
LPT-5	5'
LPT-2	9' 6"

4.5 Analysis of LWIT Results

4.5.1 Discussion of results

The need to use very high injection pressures to introduce water into the formation with surprisingly low flow rates is the single most significant observation that was made during injection testing. Without performing any hydrologic analysis on the data, this observation has serious implications for emplacement of a liquid viscous barrier. In particular, the flow rates generated are, on average, too low for practical barrier emplacement as outlined in "A Design Study for the Isolation of the 281-3H Retention Basin..." (Moridis, 1996). Some of the facts that make this observation clear include:

- Sixty-six of the 171 injections resulted in flows too low to measure.
- The 10 highest flow rate injections are all clearly indicative of formation fracturing.
- Of the 100 injections that fall between these two extremes, the hydrologic response does not follow an expected response for formation permeation and may indicate a combination of permeation and deformation of the soil.
- The average injection pressure used was 6.10×10^2 kPa (88.5 psi) resulting in an average flow rate of 0.7 lpm for the 161 tests not considered clearly fractured.
- No spatially continuous high permeability zones were located.

In order to relate these observations into quantitative parameters necessary for grout emplacement design, it is necessary to reduce the data collected into hydrologic parameters, such as permeability or hydraulic conductivity. However, there are many complexities that must be understood before applying conventional hydrologic models to analyze the data. Conventional hydrologic models fail to be able to accurately simulate much of the phenomena that controls fluid transport in systems that do not fit simple geometries and boundary condition. This is not to say that the results of modeling the data are not useful. Rather, the limitations should be understood so that the results can be interpreted objectively.

The formation underlying the 281-3H basin, like most real systems, falls into the category of a non-ideal system. Complications in analyzing the lance injection tests include (1) the possible formation of a disturbed zone around the lance that may alter formation permeability, (2) the lack of understanding of the variably saturated conditions accompanied by the difficulties in measuring actual pore pressures in very fine grained materials, and (3) the use of injection pressures far beyond confining pressures that could lead to deformation of the soil.

The soil deformation around the lance is often referred to as a "skin" in groundwater literature. A skin effect is identified as an offset in pressure at a wellbore face, which will be proportional to the flow rate across the well face. In order to quantify the presence of a skin requires the ability to differentiate between an expected ideal pressure transient response to injection, and the observed response. Since there is no characteristic pressure buildup during lance injection testing, the quantification of a skin response becomes impossible. As a result of the uncertainty of the presence of a skin effect, calculated hydraulic conductivities are acknowledged to possibly reflect a positive "skin". One possible implication is that hydraulic conductivities may be higher than estimated.

Accurate determinations of pore pressures and the water table location was not an object of the LWIT during active testing. Four piezometer tubes were installed within the LWIT grid as shown in **Figure 7**, for future monitoring. Detailed installation information can be found in WSRC, July, 1996. At the conclusion of the LWIT program, the piezometers were not yet at equilibrium and no evaluation of water table location could be made by direct measurements. Observations made while augering show the strong presence of water at about 19'. Even though lance injections were performed above and below this depth, no difference in the behavior was identified as a function of relative position to the presumed water table. It can be concluded that lance injections, as carried out during the LWIT program, are insensitive to the variations in liquid saturation that were encountered.

This insensitivity can, in part, be explained by the numerical simulations presented in (Moridis, 1996). The numerical simulations show that there is little difference in the time averaged injection rate as a function of lance tip pressure for saturated and unsaturated systems for injection tests conducted in low permeability systems. As permeability increases, differences become more noticeable. The similarity in tip pressure versus average flow rate can be attributed to different phenomena within saturated and unsaturated formations which serve to decrease the hydraulic conductivity. In the case of an unsaturated porous media, the hydraulic conductivity decreases due to decreasing formation saturation (a function of the relative permeability function). In a medium with high water saturation, the incompressibility of water and the low formation compressibility increase the injection pressures required to introduce water into the system. A full parametric study of the models used in (Moridis, 1996) would be needed to further clarify the behavior of the variably saturated system, along with supporting laboratory and field measurements.

The injection tests were conducted with pressures much higher than the overburden confining pressure. It is impossible to estimate the compressibility or other possible mechanical responses that the soil may undergo by examining the LWIT data sets. The indicators that lead one to believe the formation is undergoing a mechanical response are the uncharacteristic increase in flow rate over time and the fracturing of the formation which leads to a drop in injection pressure. When lance testing started the first series of injection tests were conducted at location LPT-20. After no flow responses were noted with an injection pressure of 2.76×10^2 kPa (40 psi), pressures were increased to 3.79×10^2 kPa to 9.65×10^2 kPa (55 psi to 140 psi) for subsequent injections. These high injection pressures were necessary to introduce measurable quantities of fluid in the ground.

Currently there are no hydrologic modeling tools that can account for yielding and fracturing of the formation during hydrologic testing. In a laboratory setting, or in high permeability media, a pressure differential can be easily created that is much smaller than confining pressures and measurements made in a reasonable amount of time on a small sample. However, in soils with permeabilities as low as we see near H-Basin, very long duration in-situ tests would be necessary to obtain data that was free from mechanical soil effects. The objectives of finding continuous high permeability zones and testing potential grout injection rates precluded the type of painstaking effort that would be needed to obtain precise measurements of very low permeabilities in the field.

The majority of tests were conducted at flow rates below what is considered practical grouting rates. That is, the low value of injectivity would mean that an impractical amount of time would be needed to inject a meaningful volume of grout. For permeation grouting, injectivity derived from flow after the soil has fractured is not meaningful, and so injection test data compiled in Appendix B has the comment "Post Fracture" appended. Depths at which groutable injection rates were noted were heterogeneously distributed both in depth and spatially over the LWIT test area. This is shown in plots of calculated hydraulic conductivity as described in section 4.5.2. The results are plotted in **Figures 8** to **15**.

4.5.2. Data Analysis: Steady State Solutions

Constant rate injection or withdrawal tests conducted in a saturated, homogeneous, isotropic porous media, are often modeled through the analytic solution of the diffusion equation, with simple geometric boundary conditions applied. The steady state solution of the diffusion equation leads to simple expressions for hydraulic conductivity as a function of flow rate and change in pressure. The steady state solution for radial flow is the familiar Thiem equation for hydraulic conductivity K,

$$K=Q/(2\pi\,\Delta H\, b)\,\ln(r/r_o)$$

while for spherical flow we have

$$K=Q/(4\pi \Delta H) (1/r - 1/r_0),$$

where r_0 is the distance to an assumed constant pressure boundary, r is the lance radius, and b is the thickness of the layer in which cylindrical flow is assumed to take place. Q is the injection rate of water and ΔH represents the change in hydraulic head from before the start of injection to the steady state pressure. Hydraulic conductivity calculated using the above solutions applied to the LWIT data are tabulated in Appendix B. The calculations are based on assumptions which include a boundary radius of 1.0 m for the spherical and radial model and a formation thickness of 0.1 m in the radial model. The thickness of the radial model is based on the spacing of the injection ports.

Although the physics which controls flow in the real physical system is not fully incorporated into the analytical model, the hydraulic conductivities calculated can serve as a way to quantitatively assess the data and spatial distribution of formation "injectivity." The numerical results also provide a means to compare the hydraulic conductivity of the split spoon samples measured in the laboratory (Moridis, 1996), with the in-situ measurements.

Figures 8 to **15** plot hydraulic conductivity as a function of depth for the lance injections. Appendix B shows results presented in tabular form, taken for each test conducted. The pressure and flow rates that appear in Appendix B represent either the steady state values attained during testing or represent average values picked from the transient responses for non-steady state tests. **Figure 15** shows hydraulic conductivities calculated for all the injection tests. Except for the tests conducted above the hard layer, there is no strong correlation between hydraulic conductivity and depth. Above the hard layer, almost all lancings resulted in flow rates below the measurable limit.

Using the radial model, the average hydraulic conductivity for the 171 injections listed in Appendix B is 9.15×10^{-7} m/s. A comparison of the analytical model results and laboratory core results presented in Moridis, 1996, shows that the hydraulic conductivities calculated from the lance injections are not significantly different than the laboratory results. The average horizontal hydraulic conductivity calculated for the 13 Shelby tube samples presented in (Moridis, 1996) is 5×10^{-7} m/s while the 161 in-situ tests that did not result in clear fracturing of the formation had an average hydraulic conductivity of 3×10^{-7} m/s.

4.5.3. Data Analysis: Numerical Simulations

In order to provide a more realistic analysis of the data, a numerical simulation was employed that includes the physics involved in fluid injection into a partially saturated soil. The TOUGH2 and ITOUGH2 codes were used with the equation of state

module EOS11 for performing numerical simulations (Pruess 1991, Finsterle 1994, Finsterle, 1993). A cylindrical domain, 30 cm thick with a radius of 1.0 m was used to simulate the test and estimate the hydraulic conductivity. Upper and lower boundaries were assumed to be of the no-flow type. The unsaturated subsurface was assumed to have a porosity of 40%. Atmospheric pressure and a uniform initial saturation of 55% were assumed for initial conditions throughout the domain. In the simulations, water was injected at a constant pressure at a single gridblock in the center of the domain over a five minute period.

The relative permeability and capillary pressure relationships used in the simulation followed van Genuchten's model:

$$P_c = -(1/\alpha)(S_e^{-1/m}-1)^{1/n}$$

$$k_{rl}=S_e^{1/2}[1-(1-S_e^{1/m})^m]^2$$

$$k_{rg}=(1-S_e)^{1/3}[1-S_e^{1/m}]^{2m}$$

where $S_e=(S_l-S_{lr})/(1-S_{lr})$ $\qquad (S_{lr}<S_l<1)$

and $m=1-1/n$.

The van Genuchten model parameters used were n=3.3 and $1/\alpha = 5.76\times10^4$ Pa. For a complete discussion of this application of the van Genuchten model see Luckner et. al. (1989).

Based on values of injection pressure and flow rate from some of the tests performed, an estimate of hydraulic conductivity was determined. **Figures 15, 16** and **17** plot flow rate versus time, comparing the near constant flow rate measured in the field and the simulated time dependent flow rate for the three different tests. The numerical model does not produce a constant flow rate as observed in the field. There is an early time transient which is not seen in the field data, although it must be remembered that the very early time flow rate data was usually not measured. This was because the 1/2" flowmeter was used during lance movement. After the lance was stopped at the targeted depth, 5 to 30 seconds elapsed before the in line flowmeter was switched to a lower range unit, when the flow rate was below the 1/2" flowmeters detection limit.

Hydraulic conductivities were adjusted so that simulated flow rates would give a close match to the observed average flow rates. **Table 3** contains results of three such simulations.

Permeabilities for the LPT-5S, LPT-11S, and LPT-19S tests, using the steady state radial flow solution, have consistently lower permeabilities than the numerical model. The fundamental reason for this difference is that the analytical solution assumes

full saturation of the matrix while the numerical model uses an unsaturated initial condition. The intrinsic hydraulic conductivity of the soil will be greater than the apparent liquid permeability at the partially saturated state.

Table 3. Comparison of numerical model with radial flow analytical model results.

Test Location	Depth (ft.)	Pressure (m H_20)	Flow Rate (l/min)	Hydraulic conductivity (Numerical Model) (m/s)	Hydraulic conductivity (Analytical) (m/s)
LPT-5S	16	43	0.0275	1.27×10^{-7}	1.7×10^{-8}
LPT-11S	15	52	0.01	1.56×10^{-8}	4.8×10^{-9}
LPT-19S	17	78	0.078	1.67×10^{-7}	2.3×10^{-8}

While the numerical models show that a near constant flow rate can result from a constant pressure injection into an unsaturated medium (see **Figure 18**), it would be speculative to conclude that permeation is the only mechanism by which water is entering the formation and that the numerical simulation is capturing the physics controlling the injection response. Injection tests conducted at low injection pressures would help to differentiate between permeation and other mechanisms of introducing water into the formation. Very careful excavation after injection testing could also help describe the mechanism of fluid transport in the subsurface.

4.6 GPR Survey Data Analysis

The GPR data illustrate that substructure can be imaged, but instrument artifacts obscure lithological reflectors. The data presented in **Figures 19** through **24** are the 300 MHz pre-injection data run on lines 3, 6, 8, 10, 11 and 12. Location along the GPR line is plotted on the abscissa and the time in nanoseconds (ns) is plotted along the ordinate. **Figure 7** shows the GPR line locations. Data on lines 3, 6, 8 and 10 are plotted from west to east and lines 11 and 12 from north to south. Line numbers and cardinal directions are noted on the top of each plot and the 50, 100, 150, 200 and 250 ns marks are noted along the vertical axis. Features of interest are outlined below and noted on the figures. The following observations can be made:

- The first arrival, the solid line at about 20 ns, is evident in each record.
- Everything below about 100 ns is noise.
- There is a strong horizontal feature at approximately 25, 30, 60, and below 135 ns in every record. Due to the regularity and strongly horizontal nature these bands are attributed to an artifact of the GSSI system and are not due to stratigraphy. The GSSI system frequently exhibits these ringing features. There are breaks in these bands and

in some places they seem to follow structure, indicating that responses due to structural features may also be present in the record, and are superimposed on or interfere with the ringing.

- At the intersection of Lines 11 and 6, centered at approximately 30 ns, is an area of disturbance that correlates with the removal of a tree stump that was subsequently backfilled with soil and somewhat compacted. A rough depth estimate would put this feature at 3-4 feet.
- A reflector indicating a depression in the shallow lithology is apparent on line 12 south of line 6, on line 8 to the east of line 11, and on line 10 to the east of line 12 from roughly 30 to 65 ns. (approximately 1.2 to 2.4m)(4 to 8 ft).
- A steep response, dipping to the north, is apparent in lines 11 and 12 to the south of line 6, and centered at line 3, between 60 and 100 ns. This anomaly can also be seen, to a lesser extent, in line 3. The steep angle of this features indicates a 3-D scatterer as opposed to a reflective horizontal layer. This target probably has relatively large dimensions as opposed to a point scatterer, such as a pipeline, that would give a distinct hyperbolic refraction pattern.

The data are strongly contaminated by ringing that dominates the response of layered structures, such as the hard layer. No velocity measurements were made during this survey, severely limiting any reliable depth estimates and correlation with the hard layer as delineated by lance refusal and auguring. It is recommended that future surveys for characterization of the local stratigraphy be repeated using a Sensors and Software Pulse Echo system, which tends to be free of ringing problems. A velocity analysis should also be undertaken to obtain reliable depth estimates.

5. Conclusions

An areal persistent hard layer was found in the LWIT test plot which proved to be a barrier to penetration by the standard lance injection equipment. The elevation of this layer corresponds approximately to the elevation of the bottom of H basin. No field hydrologic data were acquired within this layer, which varied from about 1.5m to 4.6m (5 to 15 ft) in depth. Results showed that the upper limit on injection pressure which should be used for permeation grouting was determined by the resistance of the soil to fracturing. Severe fracturing was found to occur with injection pressures that varied between 3.8×10^{2} kPa (55 psi) to over 1.03×10^{3} kPa (150 psi), but no consistent trends or correlation to other measurements were observed. Thus, a maximum injection pressure of 3.4×10^{2} kPa (50 psi) is recommended. Results also show that injection at very shallow depths of 1m (3 ft) or less may be difficult to control, due to the lack of a seal forming around the injection lance.

There was no significant finding of a uniform homogeneous layer with high permeability. This is seen by the scatter of data in **Figure 14**. Hydraulic conductivities below 1×10^{-8} m/s are common and hydraulic conductivity measured above 2×10^{-6} m/s were often clearly indicative of fracturing of the formation. The ability of the soil to withstand injection pressures far in excess of lithostatic without fracturing is attributed to the high yield strength of the medium. Soils that underlay the area next to the 281-3H basin are heterogeneous in structure, as seen by the varying downforce required for lance penetration, and the widely varying range at which the formation will fracture. The injection flow rates measured indicate that most of the formation has too low a hydraulic conductivity for practical grout emplacement.

Acknowledgment

This work was supported by the Subsurface Contamination Focus Area, Office of Technology Development, Office of Environmental Restoration and Waste Management, US Department of Energy, under contract DE-AC03-76SF00098. The authors wish to thank Andrew Cohen and Kenzi Karasaki for their careful review of this manuscript.

References

"Development of a test work plan for the viscous liquid barrier demonstration (U)", Westinghouse Savannah River Company (WSRC), Subcontract C001015P, May 1996

"Technical Oversight for the Lance Water Injection Test at the H-Area Retention Basin (U)", Westinghouse Savannah River Company (WSRC), Subcontract L001015P, July 1996

Luckner, L., van Genuchten, M. Th., Nielsen, D. R., "A consistent set of parametric models for the two-phase flow of immiscible fluids in the subsurface", Water Resources Research, 25(10), 2187-2193, October 1989

Finsterle, S., ITOUGH2 User's Guide, Version 2.2, Lawrence Berkeley National Laboratory Report LBL-34581, August 1993

Finsterle, S., Moridis, G. J., Pruess, K., A TOUGH2 equation-of-state module for the simulation of two-phase flow of air, water, and a miscible gelling liquid, Lawrence Berkeley National Laboratory Report LBL-36086, May 1994

Moridis, G.,et. al. A design study for the isolation of the 281-3H retention basin at the Savannah River Site using the viscous barrier technology, Lawrence Berkeley National Laboratory Report (in preparation) 1996

Phifer, Mark, Technical information on H-Area Retention Basin, FAX to John Apps, 1/24/96

Pruess, K., TOUGH2 - A general purpose numerical simulator for multiphase fluid flow, Lawrence Berkeley National Laboratory Report LBL-29400, 1991

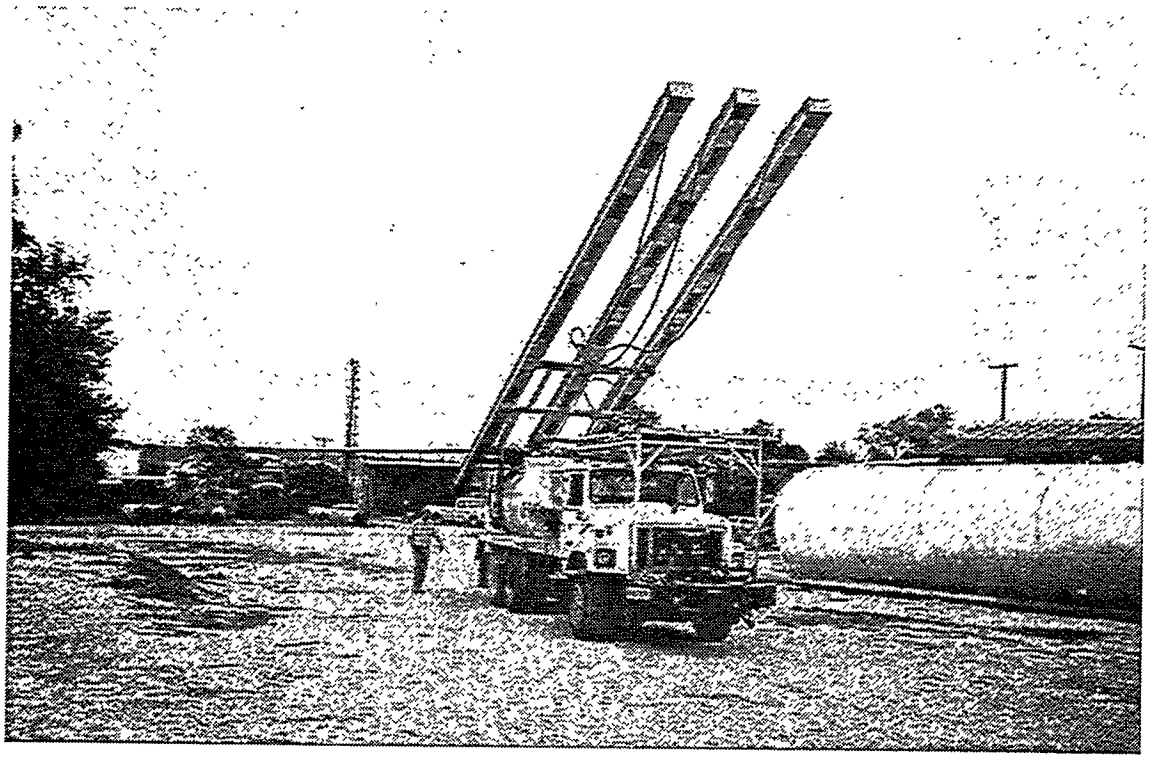

Figure 1. Lance Injection Truck with mast being raised. Total mast length is 45 feet.

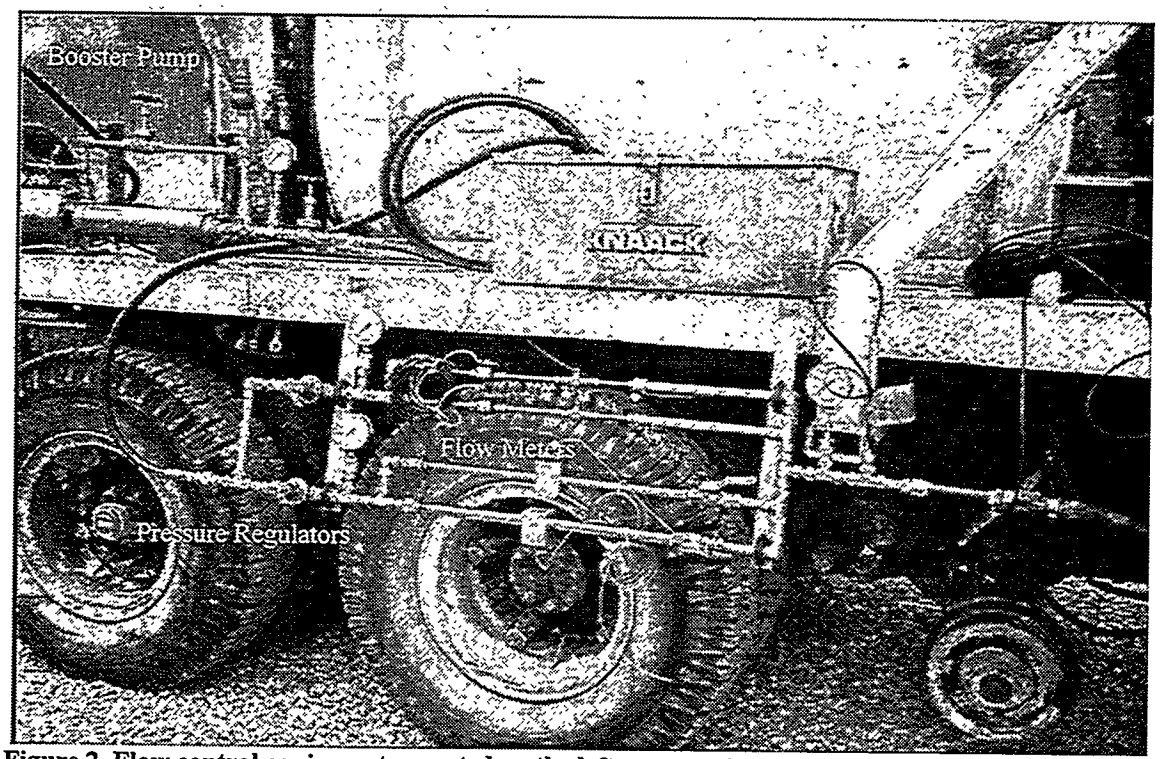

Figure 2. Flow control equipment mounted on the left rear portion of the Lance Injection truck.

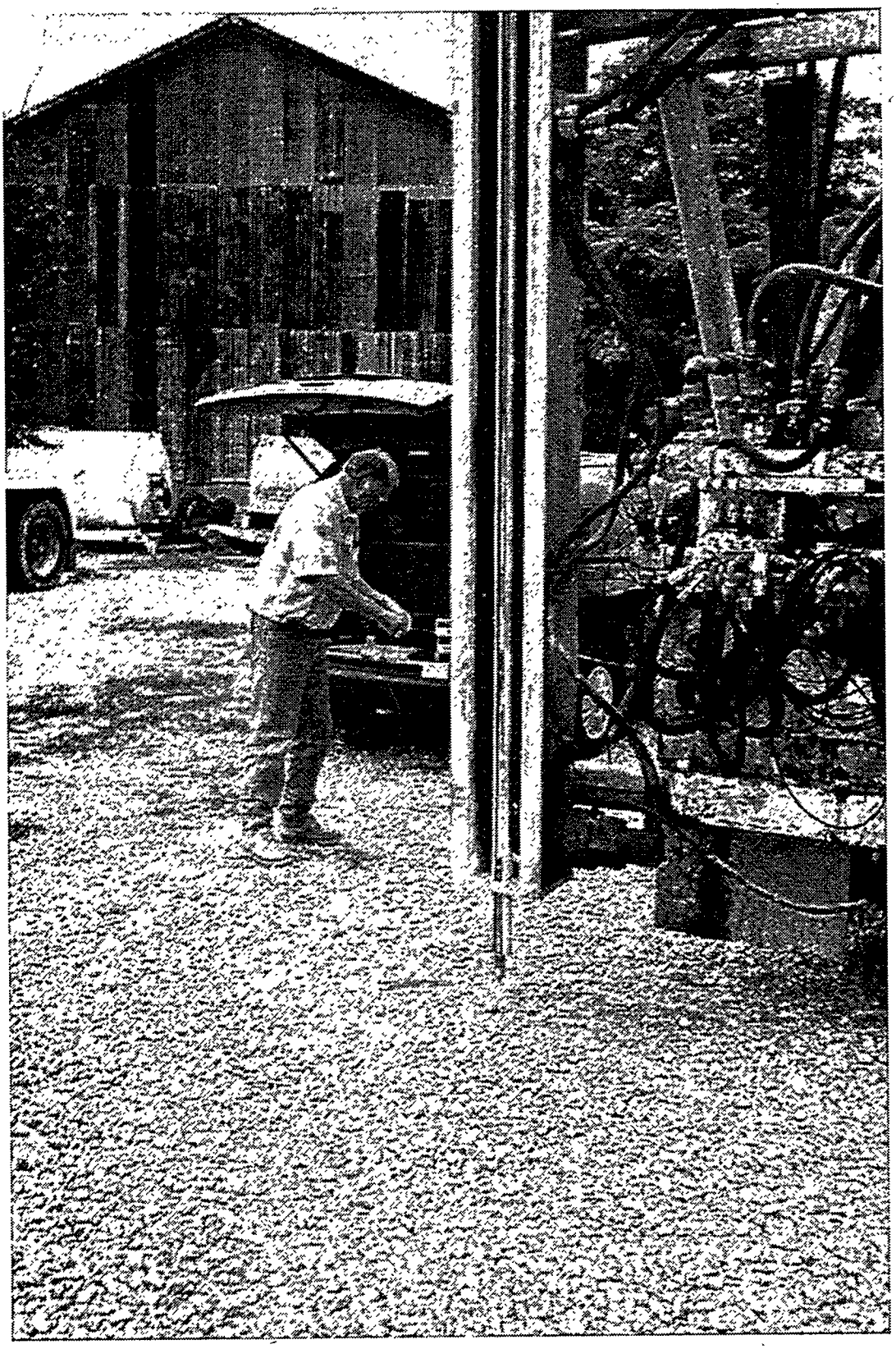

Figure 3. Lance injection truck with instrumented injection tip installed. Masthead is locked in the vertical position.

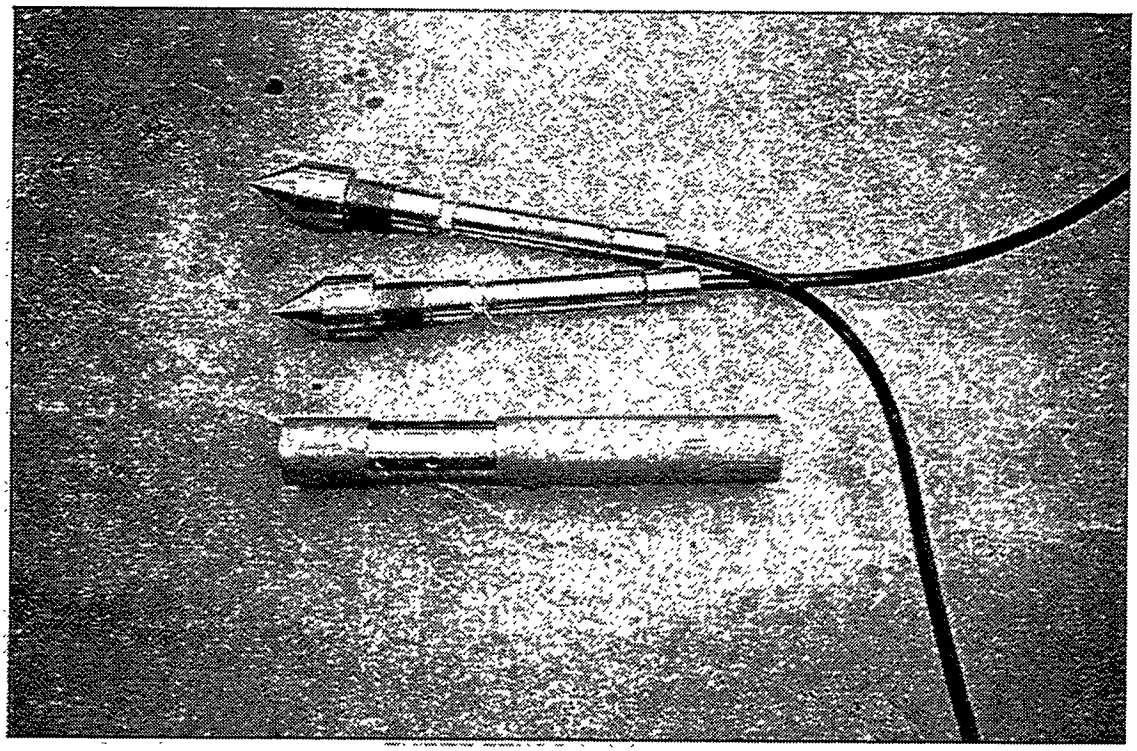

Figure 4. Lance tips with downhole pressure transducers installed.

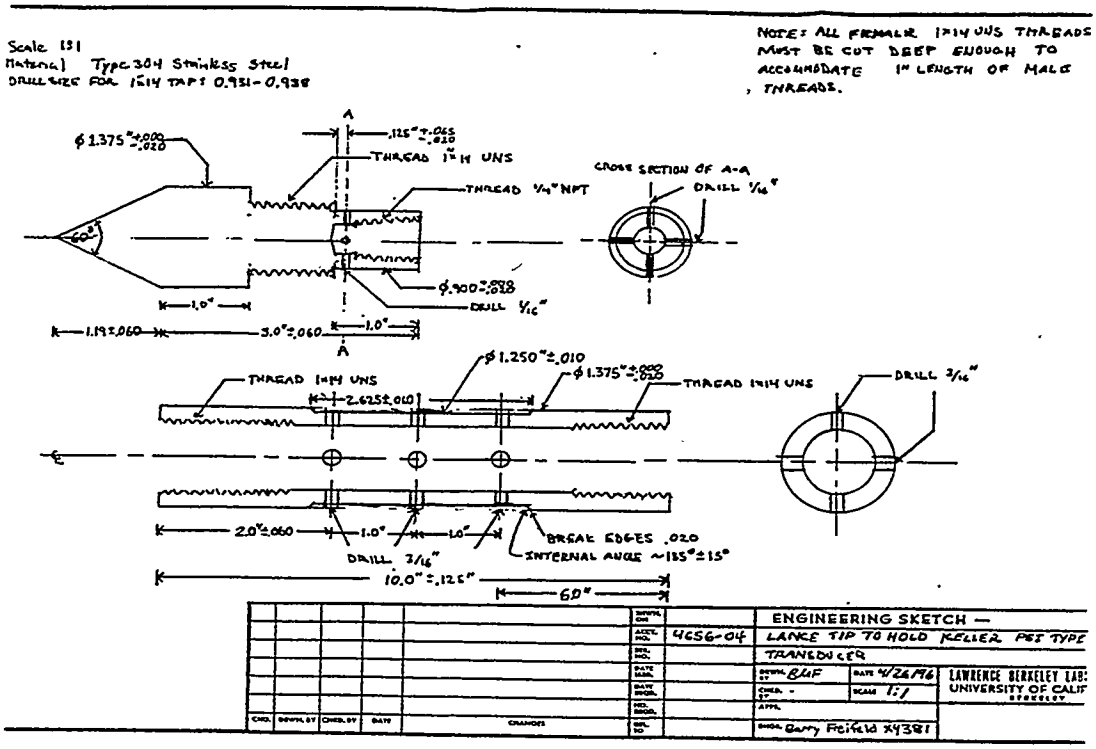

Figure 5. Engineered sketch of lance tip and lance body.

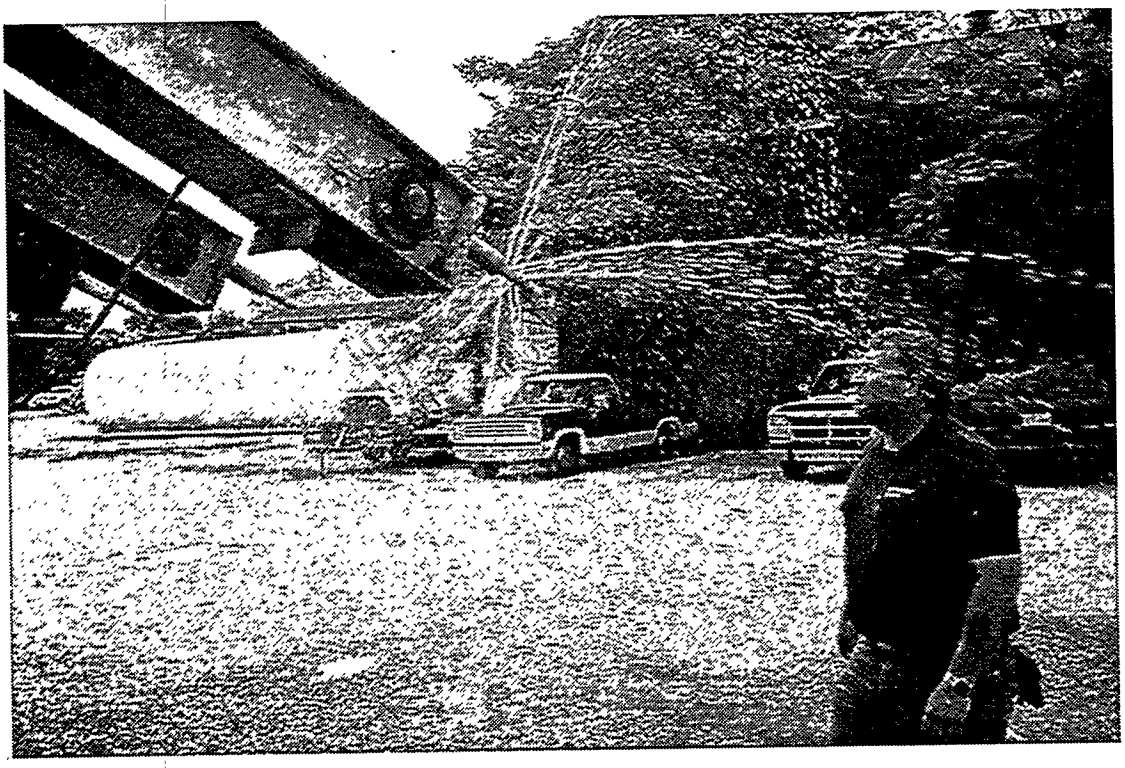

Figure 6. Testing the lance tips above the ground. Water is injected through four sets of three 3/16" holes.

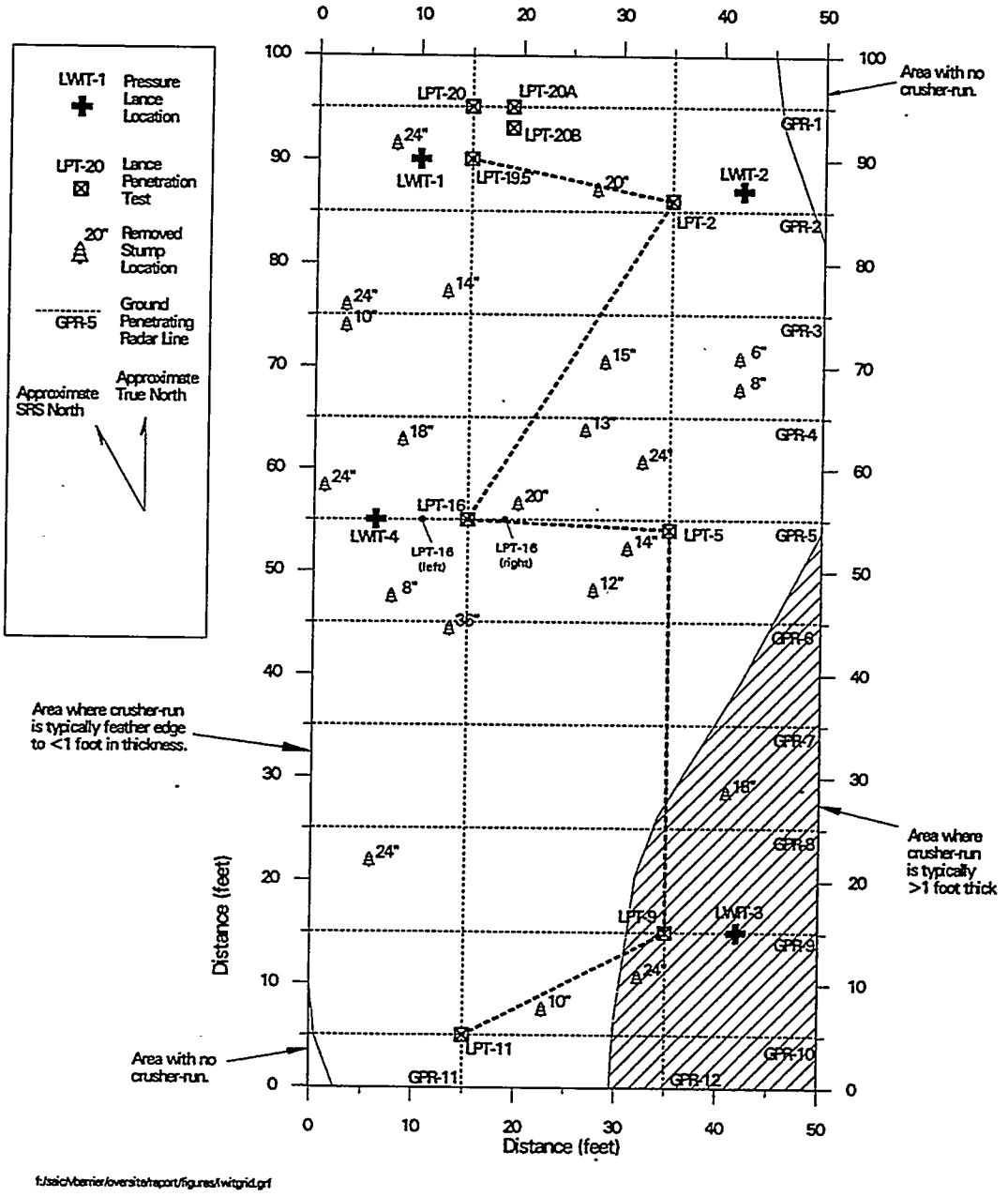

Figure 7. Location of test borings in the LWIT Footprint. Modified from WSRC 1996.

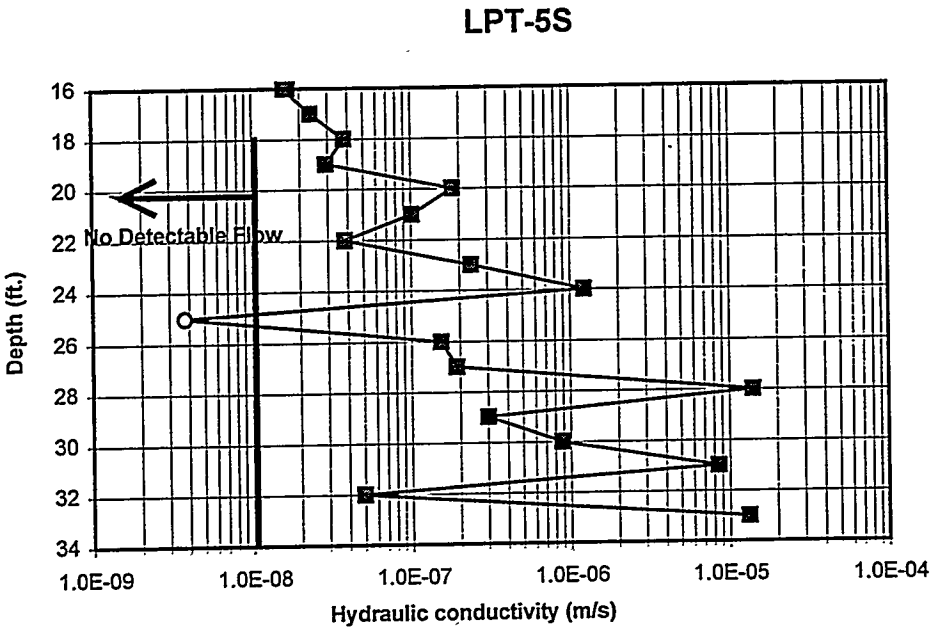

Figure 8. Injection test results at LPT-5S location. Radial flow model.

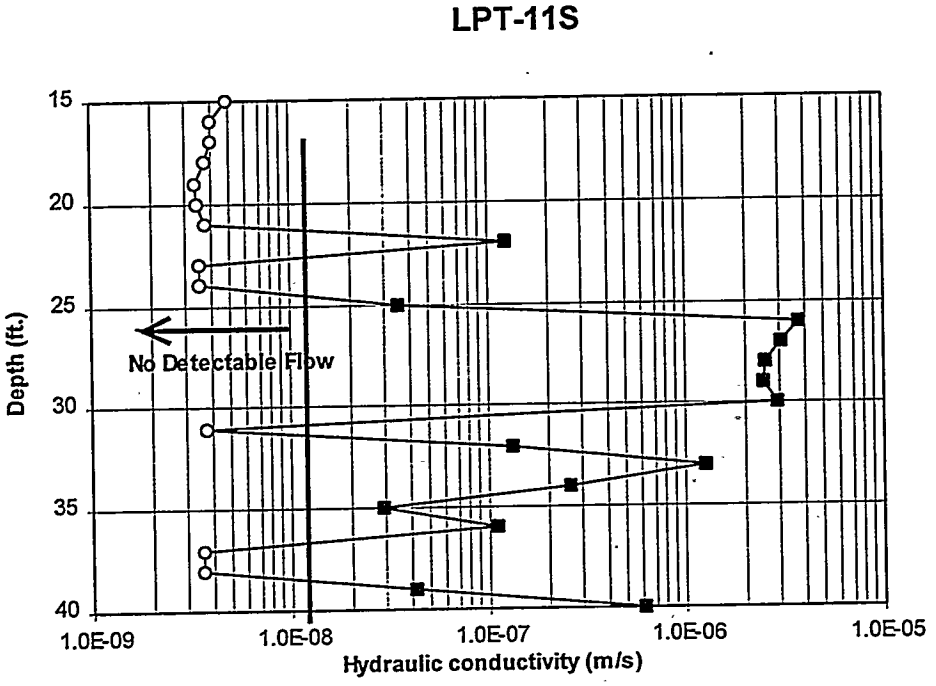

Figure 9. Injection test results at the LPT-11S location. Radial flow model.

* Note: Hydraulic conductivity for tests with no measurable flow indicates an upper bound. Actual hydraulic conductivity may be significantly less.

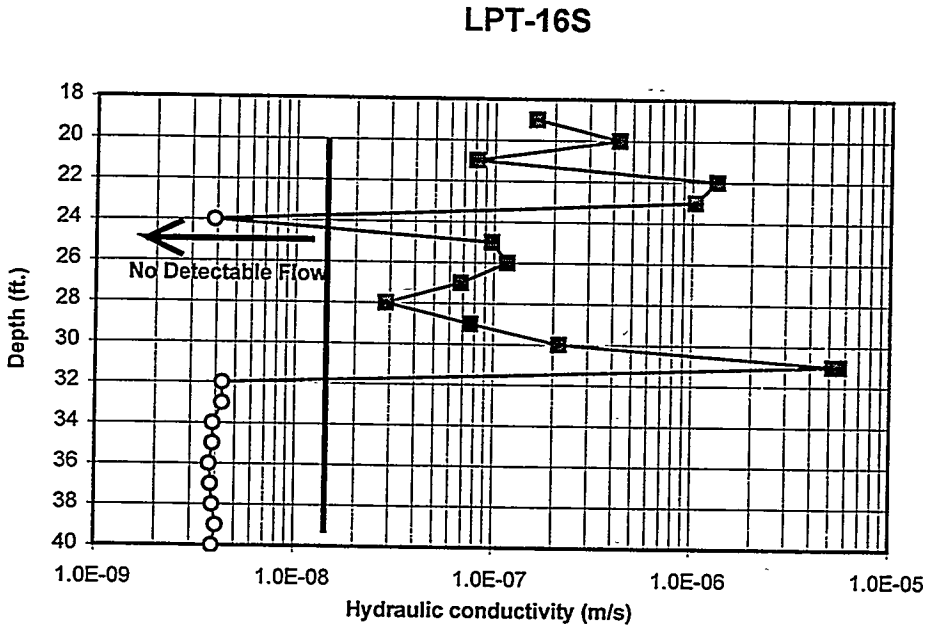

Figure 10. Injection test results at LPT-16S location. Radial flow model.

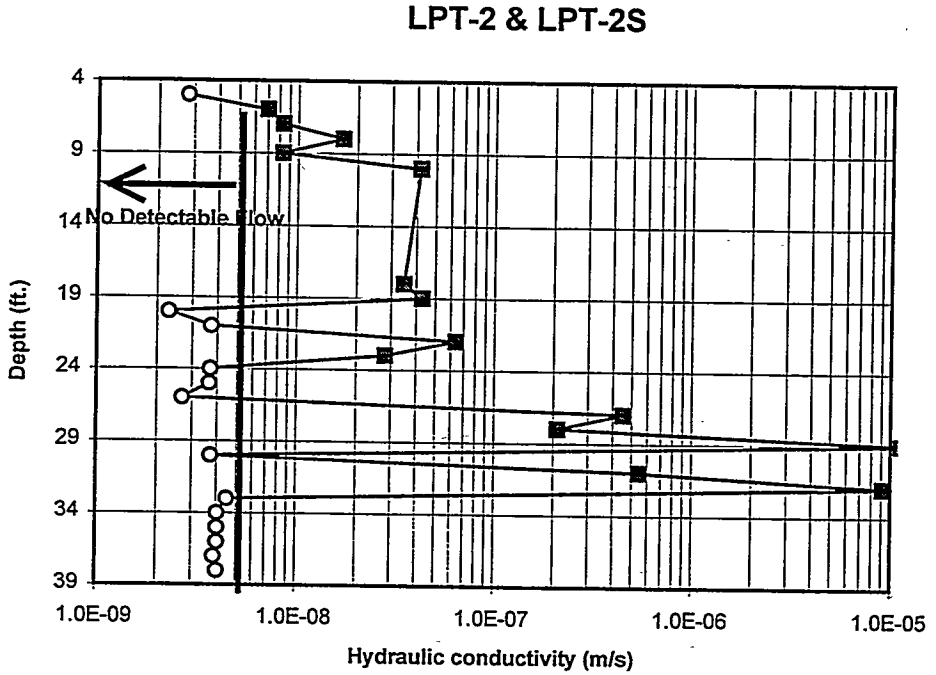

Figure 11. Injection test results at LPT-2 location. Radial flow model.

* Note: Hydraulic conductivity for tests with no measurable flow indicates an upper bound. Actual hydraulic conductivity may be significantly less.

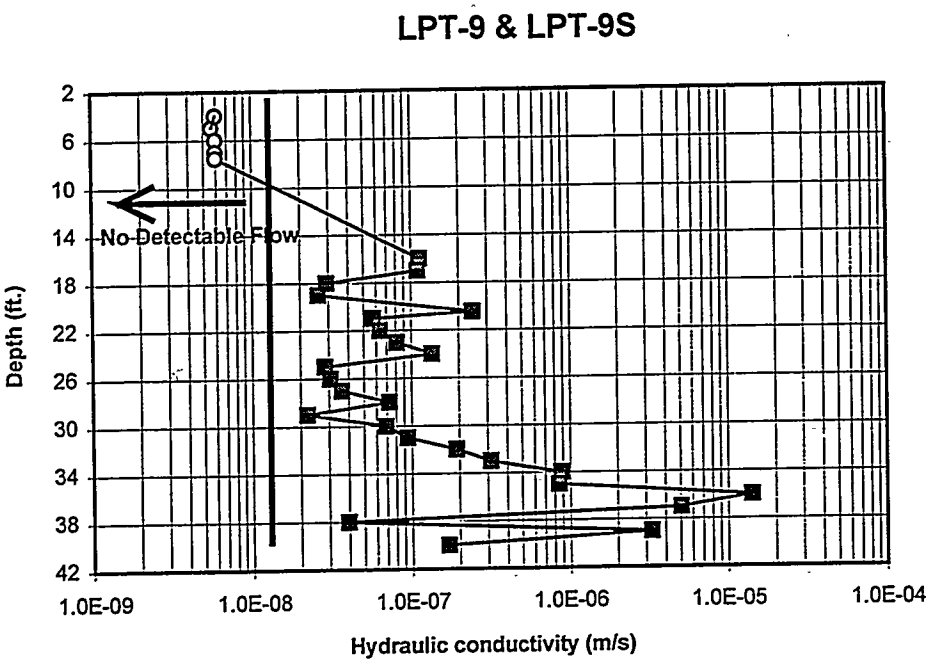

Figure 12. Injection test results at LPT-9 location. Radial flow model.

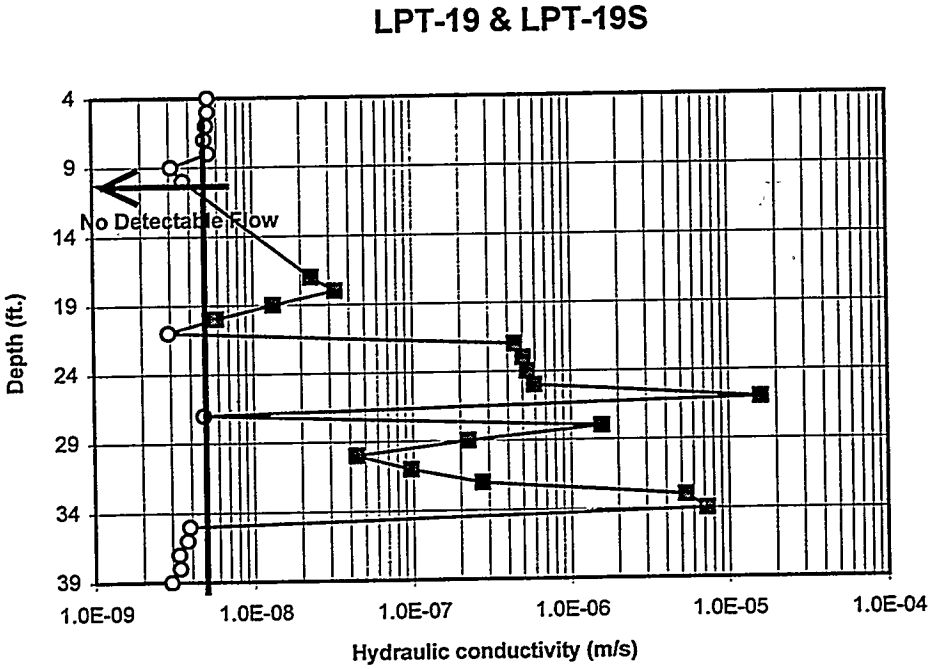

Figure 13. Injection test results at LPT-19 location. Radial flow model.

* Note: Hydraulic conductivity for tests with no measurable flow indicates an upper bound. Actual hydraulic conductivity may be significantly less.

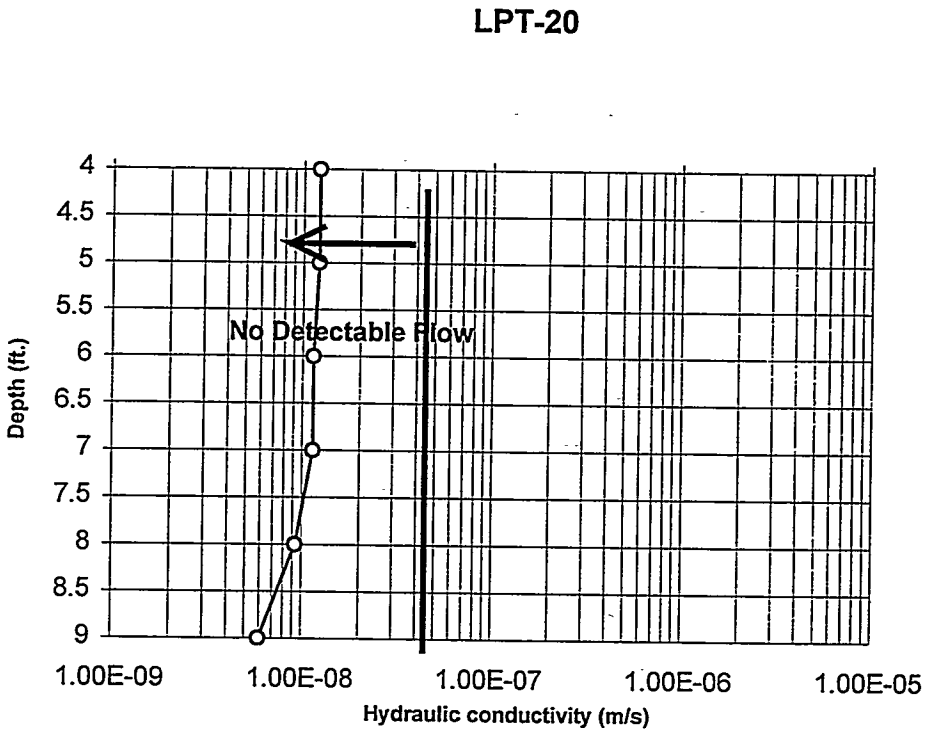

Figure 14. Injection test results at LPT-20 location. Radial flow model.

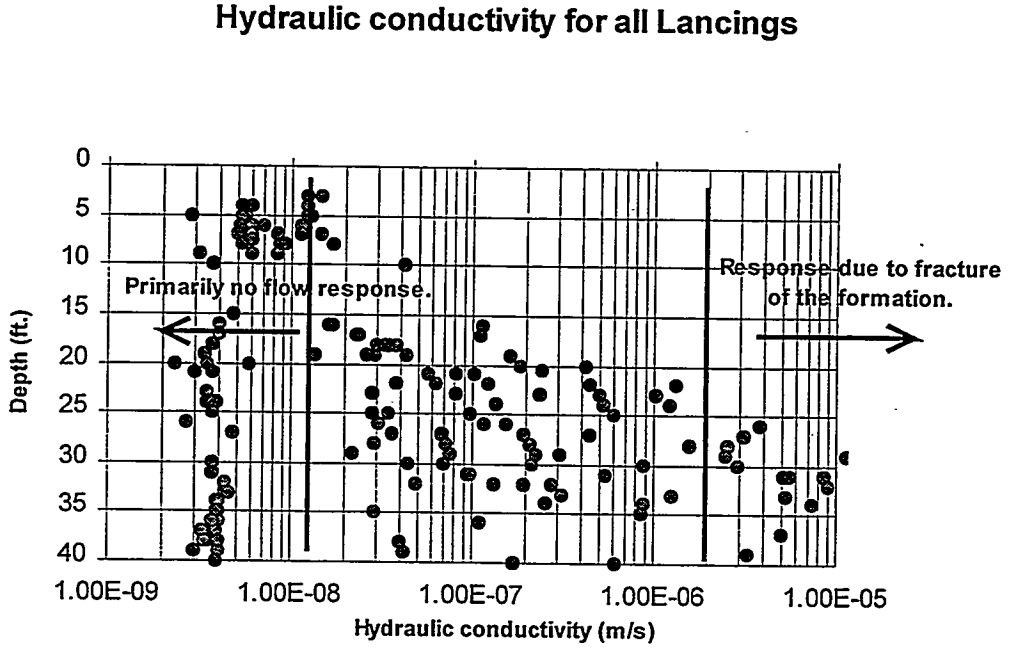

Figure 15. Estimated permeability for all injection tests using radial flow model.

* Note: Hydraulic conductivity for tests with no measurable flow indicates an upper bound. Actual hydraulic conductivity may be significantly less.

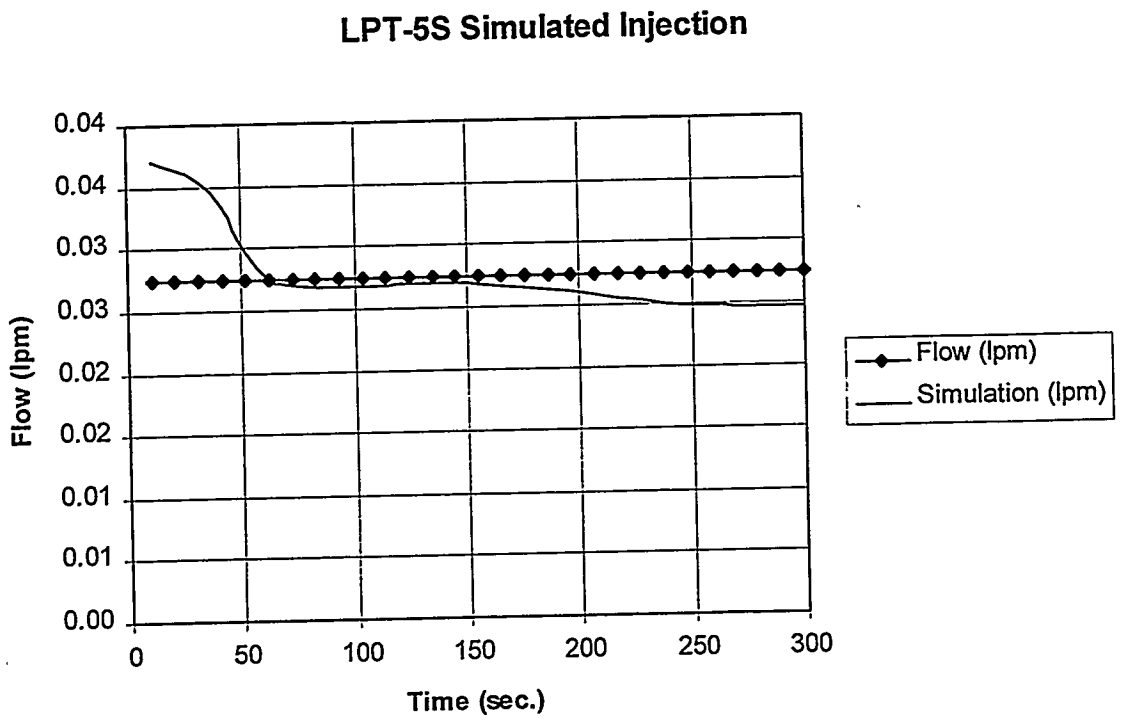

Figure 16. Comparison of LPT-5S injection at 16 ft. depth with TOUGH2 model.

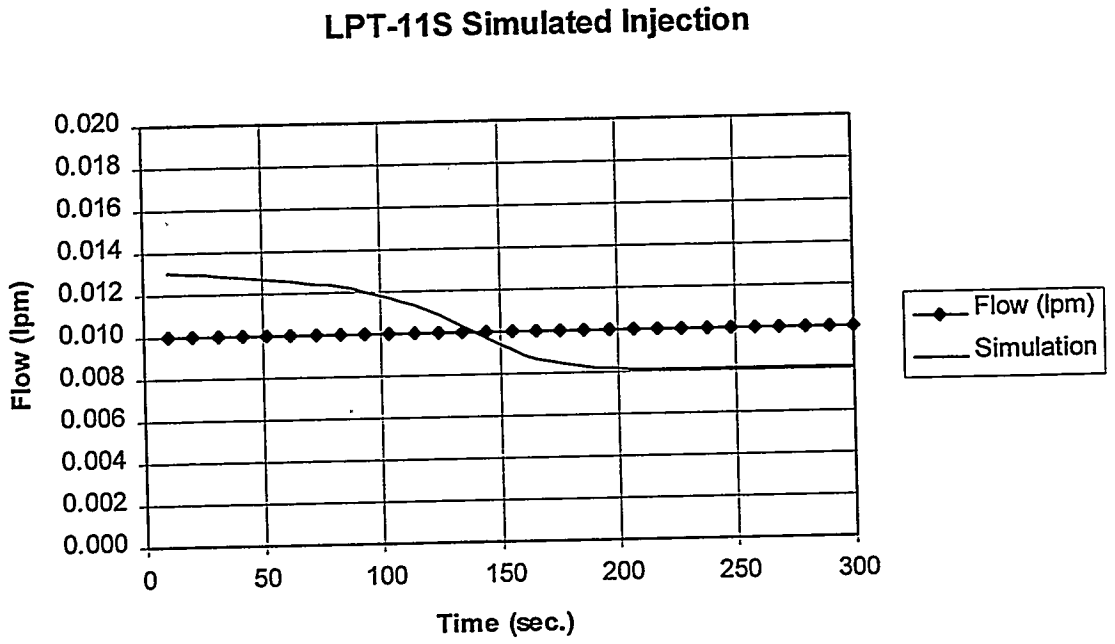

Figure 17. Comparison of LPT-11S injection at 15 ft. depth with TOUGH2 model.

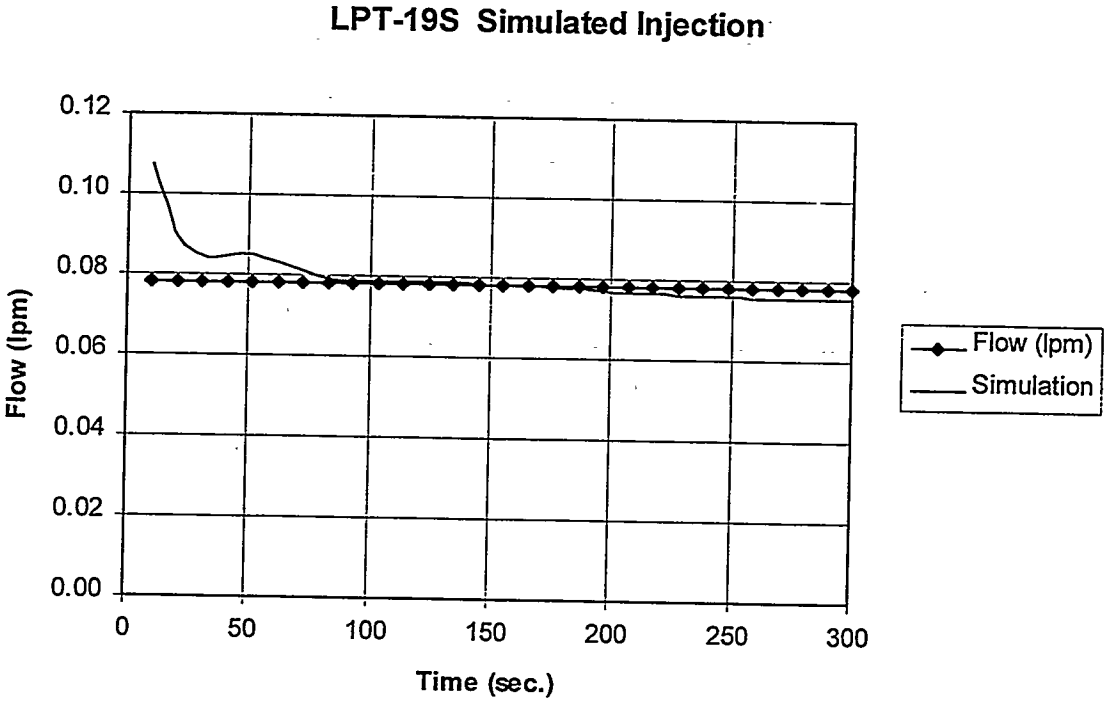

Figure 18. Comparison of LPT-19S injection at 17 ft. depth with TOUGH2 model.

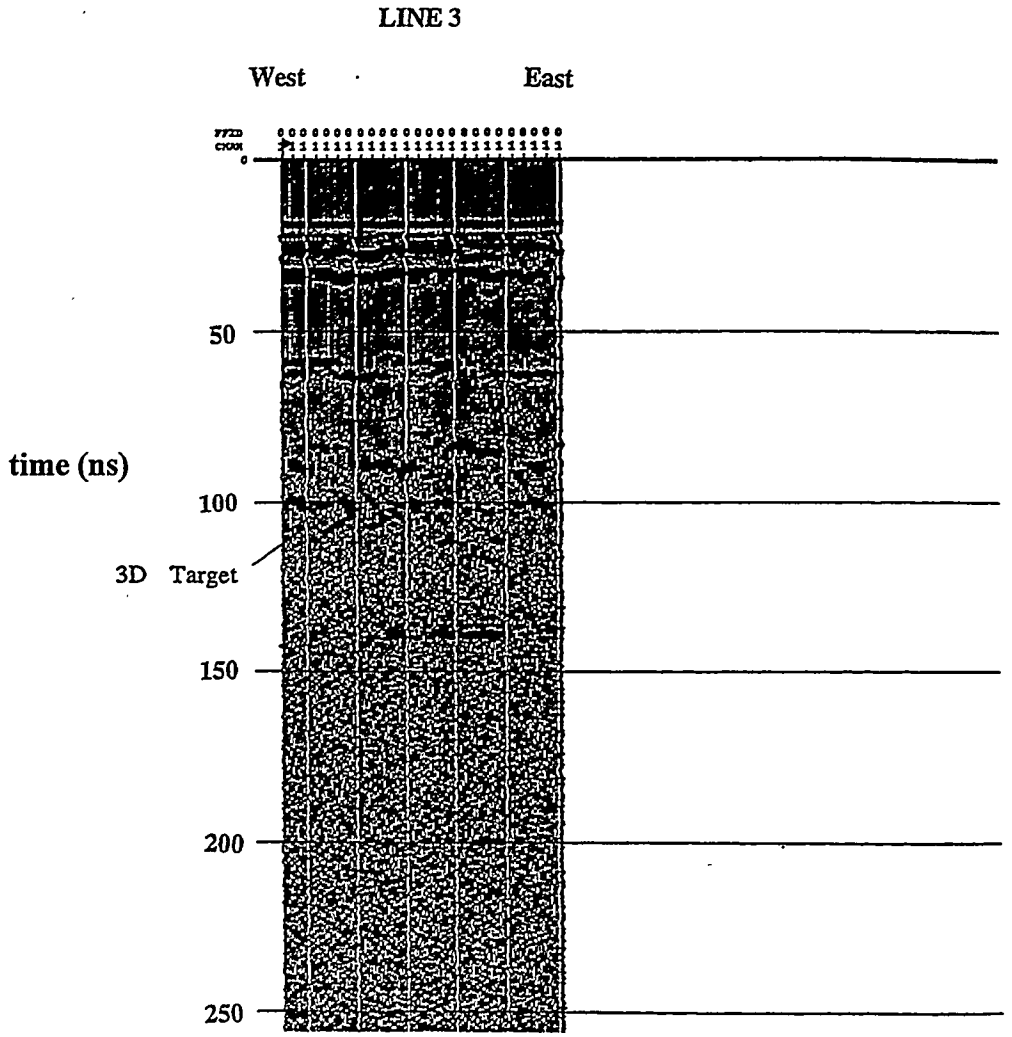

Figure 19. Ground penetrating radar taken along Line 3.

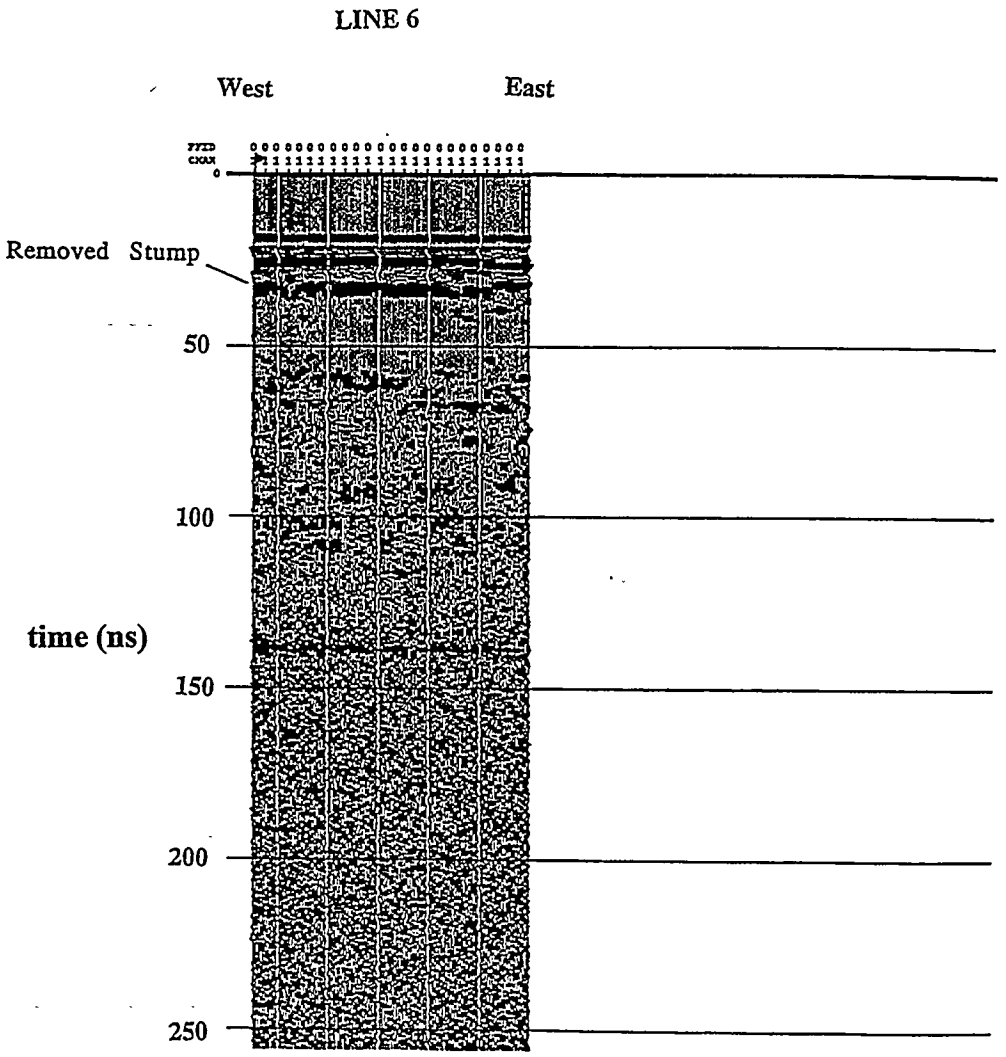

Figure 20. Ground penetrating radar taken along Line 6.

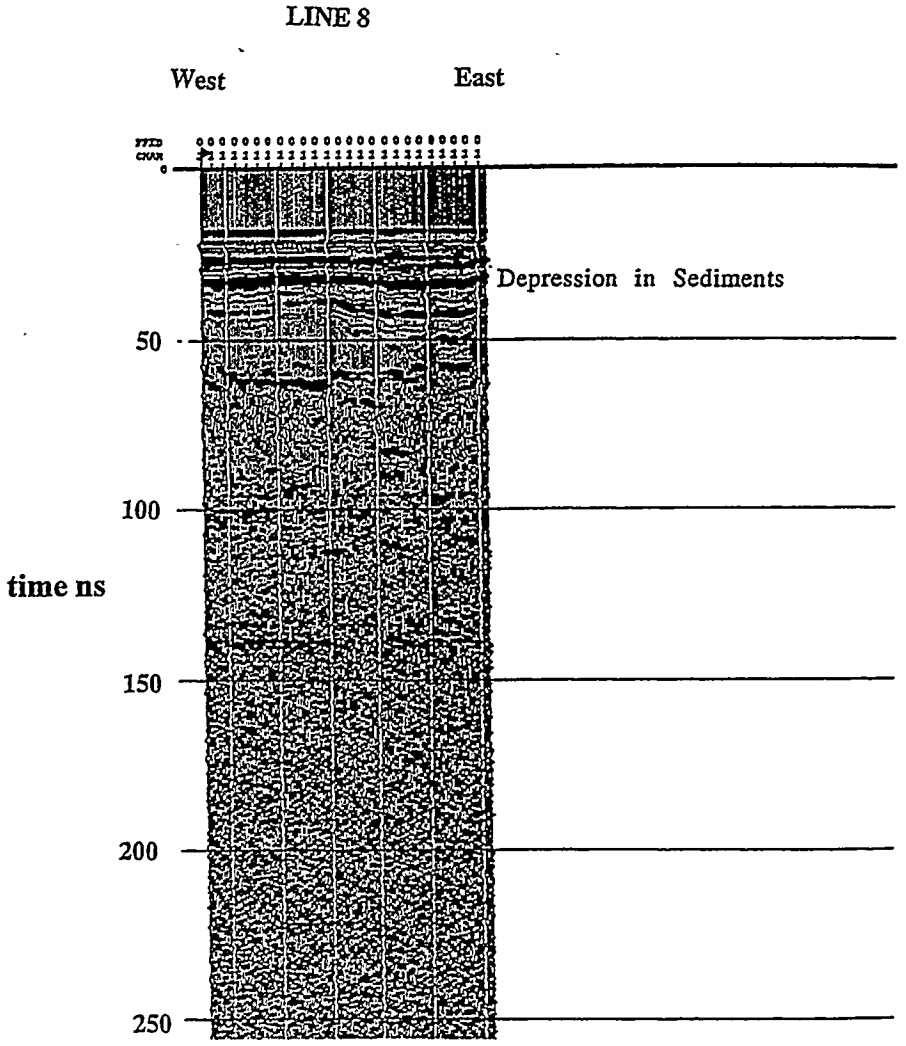

Figure 21. Ground penetrating radar taken along Line 8.

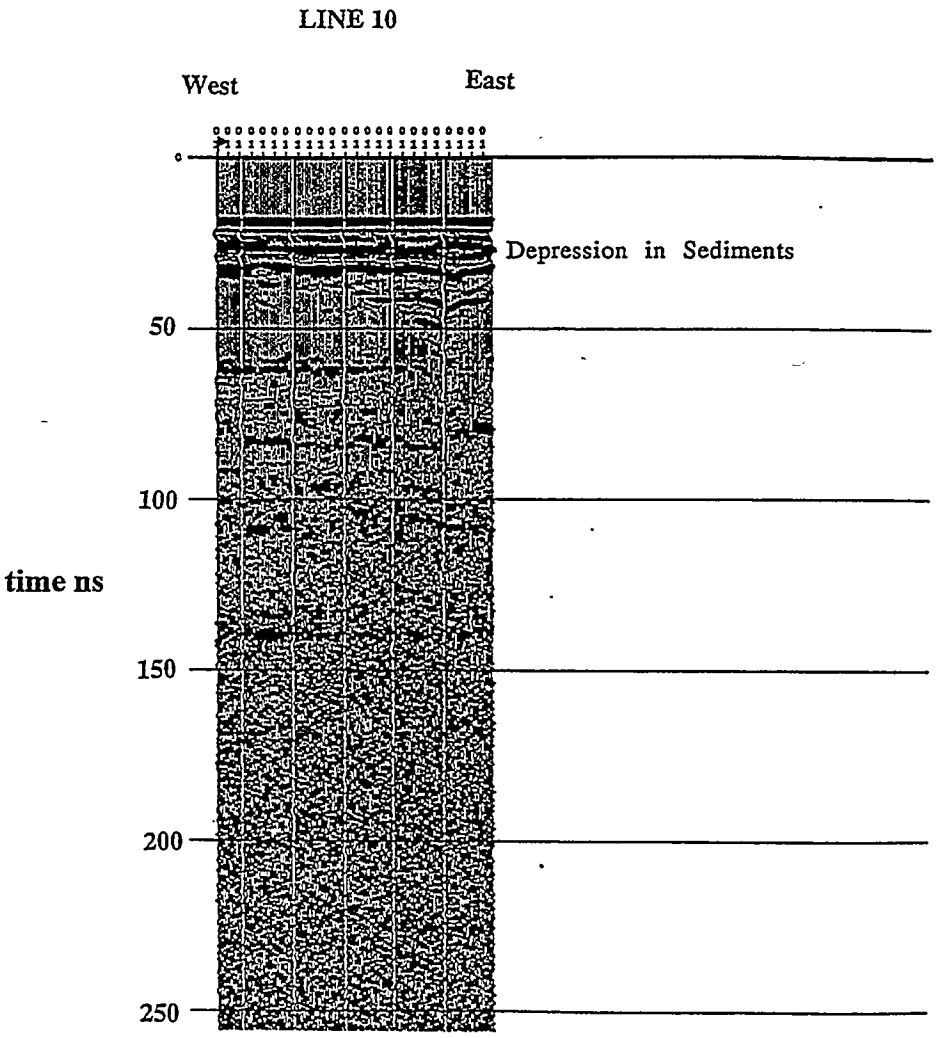

Figure 22. Ground penetrating radar taken along Line 10.

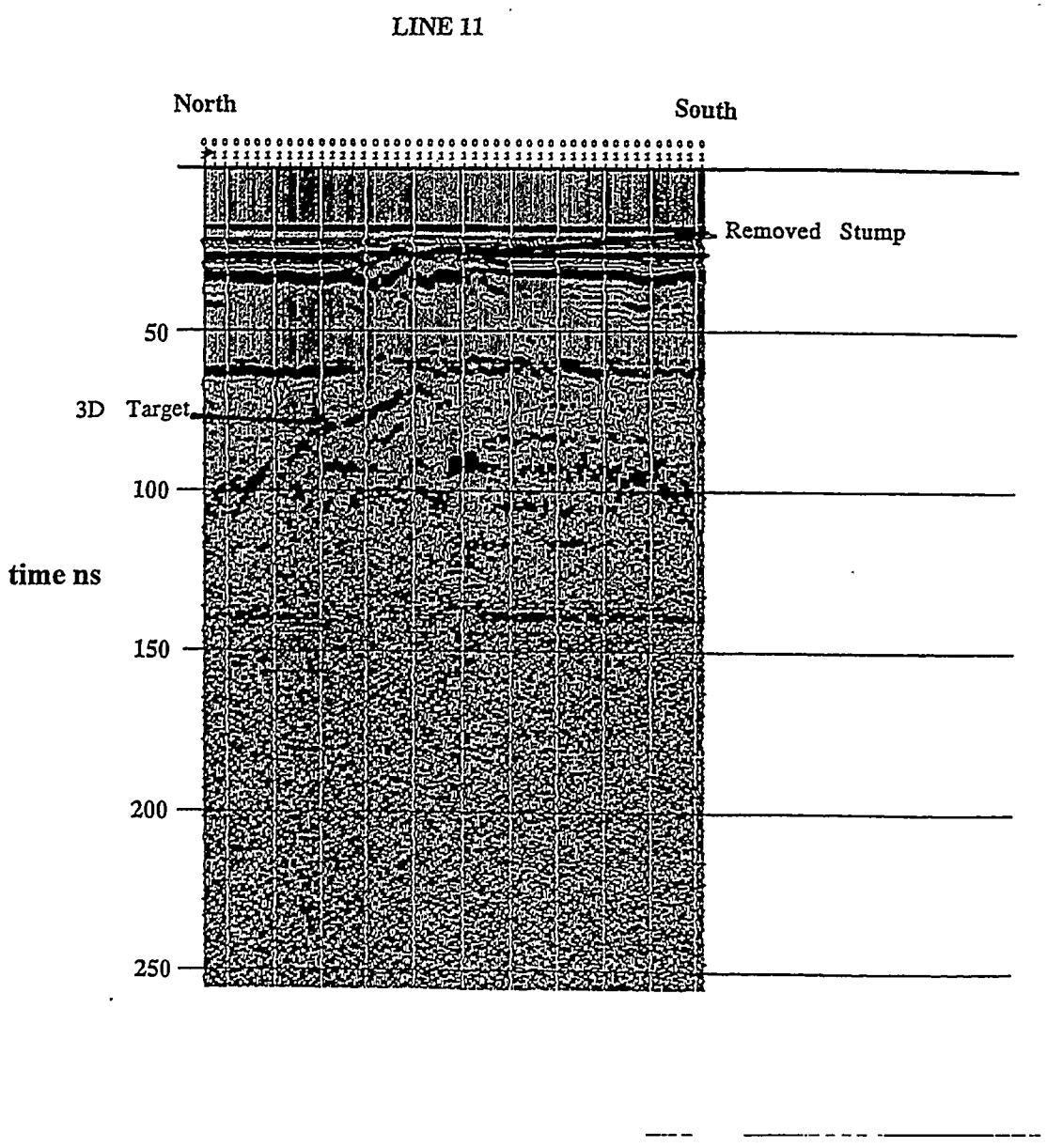

Figure 23. Ground penetrating radar taken along Line 11.

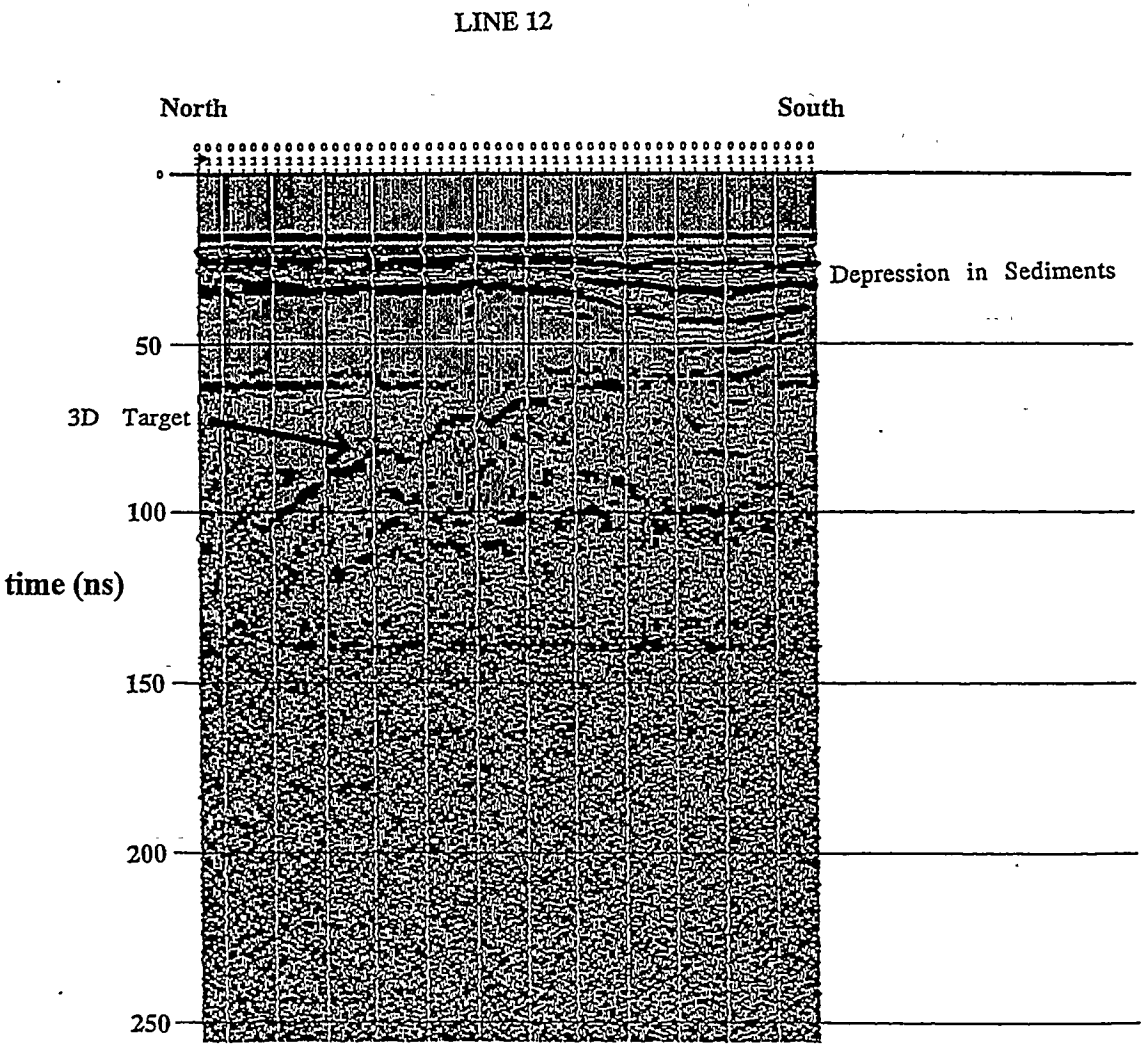

Figure 24. Ground penetrating radar taken along Line 12.

APPENDIX A

Pressure and Flowrate Data for Lance Injections

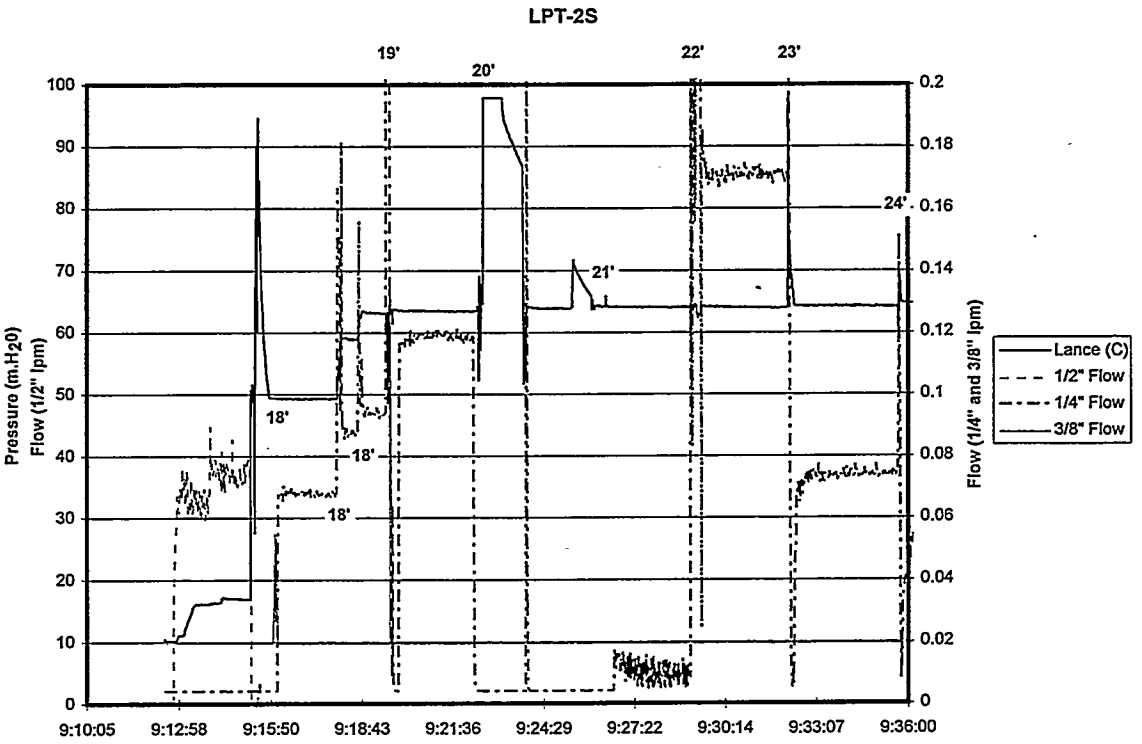
LPT-2S
19'
20'
22'
23'
24'
21'
18'
18'
18'
Pressure (m.H20)
Flow (1/2" lpm)
Flow (1/4" and 3/8" lpm)
Lance (C)
1/2" Flow
1/4" Flow
3/8" Flow
100
90
80
70
60
50
40
30
20
10
0
0.2
0.18
0.16
0.14
0.12
0.1
0.08
0.06
0.04
0.02
0
9:10:05
9:12:58
9:15:50
9:18:43
9:21:36
9:24:29
9:27:22
9:30:14
9:33:07
9:36:00

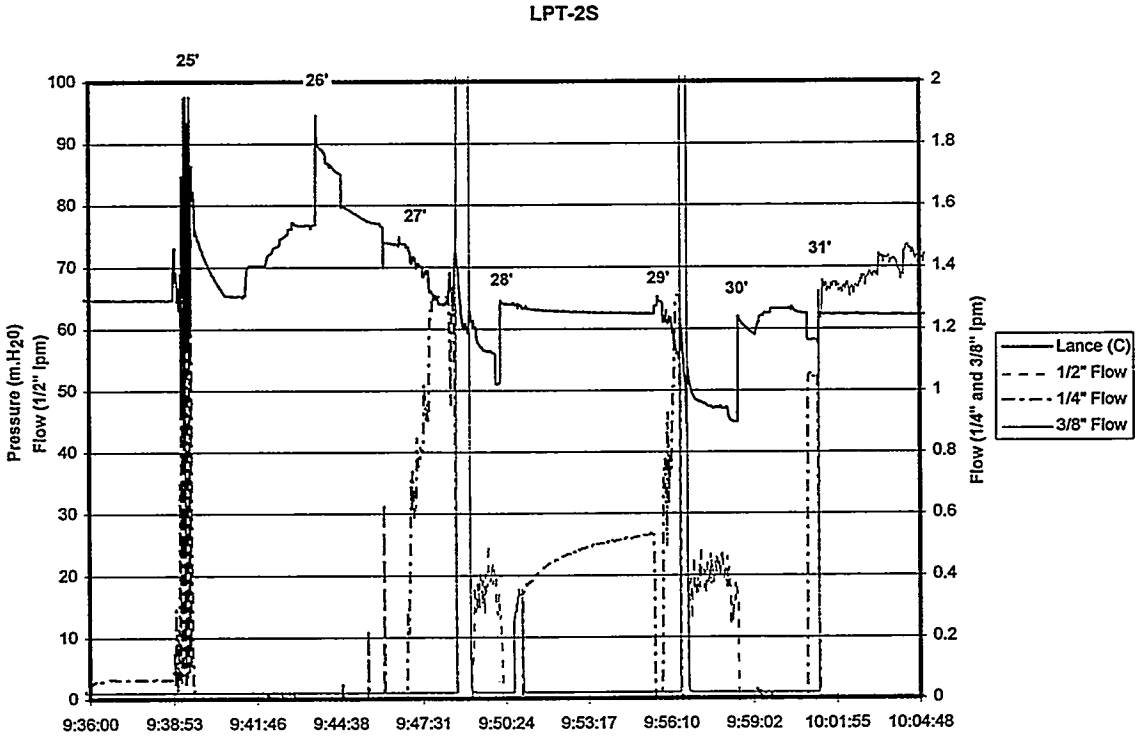
LPT-2S
25'
26'
27'
28'
29'
30'
31'
Pressure (m.H20)
Flow (1/2" lpm)
Flow (1/4" and 3/8" lpm)
Lance (C)
1/2" Flow
1/4" Flow
3/8" Flow
100
90
80
70
60
50
40
30
20
10
0
2
1.8
1.6
1.4
1.2
1
0.8
0.6
0.4
0.2
0
9:36:00
9:38:53
9:41:46
9:44:38
9:47:31
9:50:24
9:53:17
9:56:10
9:59:02
10:01:55
10:04:48

LPT-2S

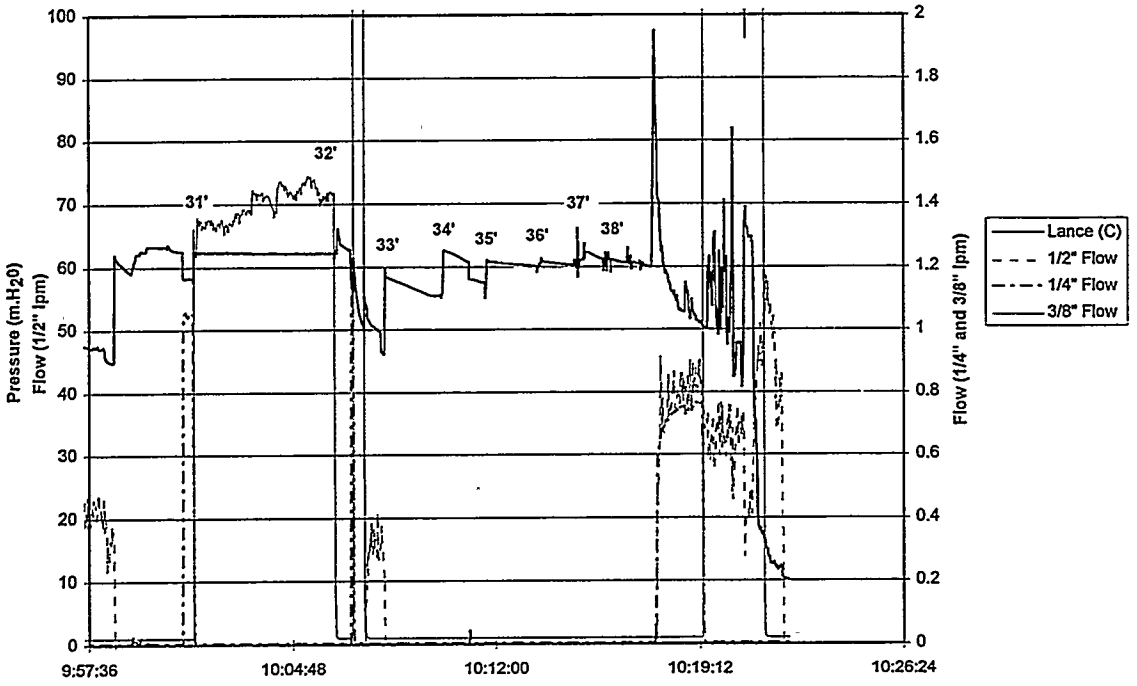
Pressure (m.H2O)
Flow (1/2" lpm)
Flow (1/4" and 3/8" lpm)
31'
32'
33'
34'
35'
36'
37'
38'
Lance (C)
1/2" Flow
1/4" Flow
3/8" Flow
9:57:36
10:04:48
10:12:00
10:19:12
10:26:24

LPT-5

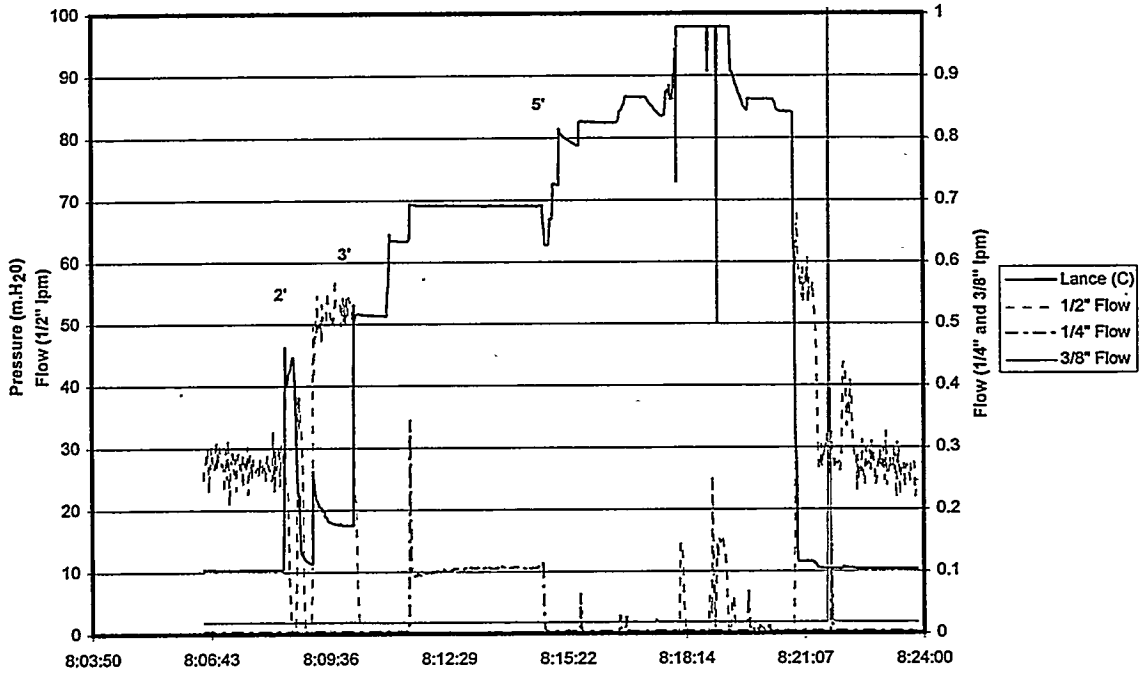
Pressure (m.H2O)
Flow (1/2" lpm)
Flow (1/4" and 3/8" lpm)
2'
3'
5'
Lance (C)
1/2" Flow
1/4" Flow
3/8" Flow
8:03:50
8:06:43
8:09:36
8:12:29
8:15:22
8:18:14
8:21:07
8:24:00

LPT-5S

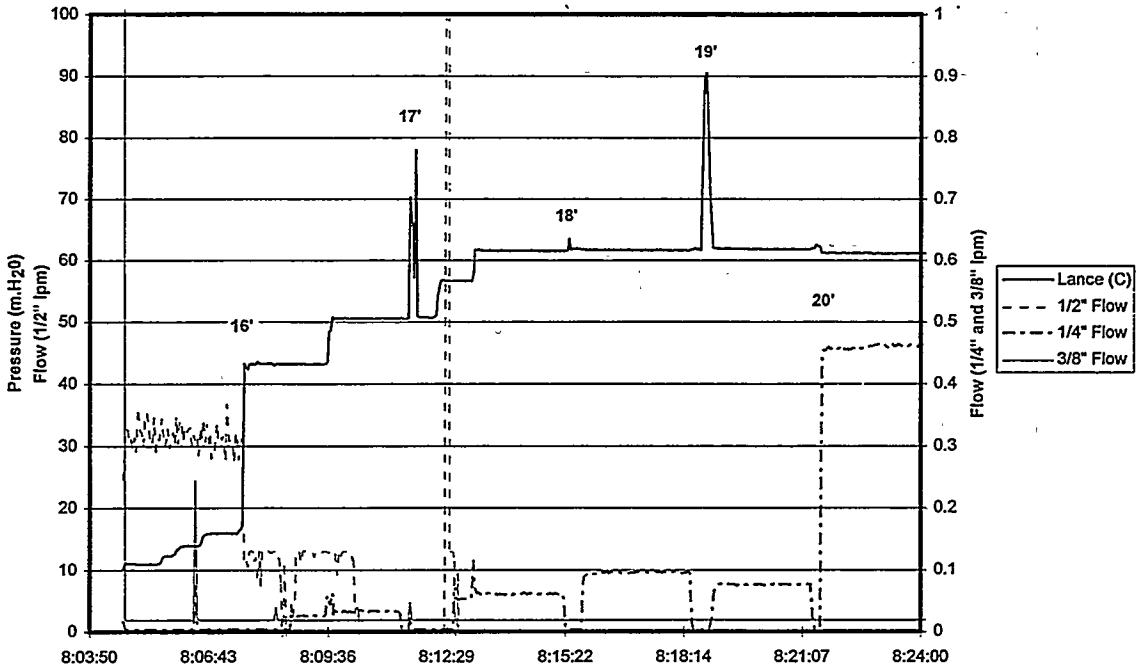
Pressure (m.H20)
Flow (1/2" lpm)
Flow (1/4" and 3/8" lpm)
16'
17'
18'
19'
20'
Lance (C)
1/2" Flow
1/4" Flow
3/8" Flow
8:03:50
8:06:43
8:09:36
8:12:29
8:15:22
8:18:14
8:21:07
8:24:00

LPT-5S

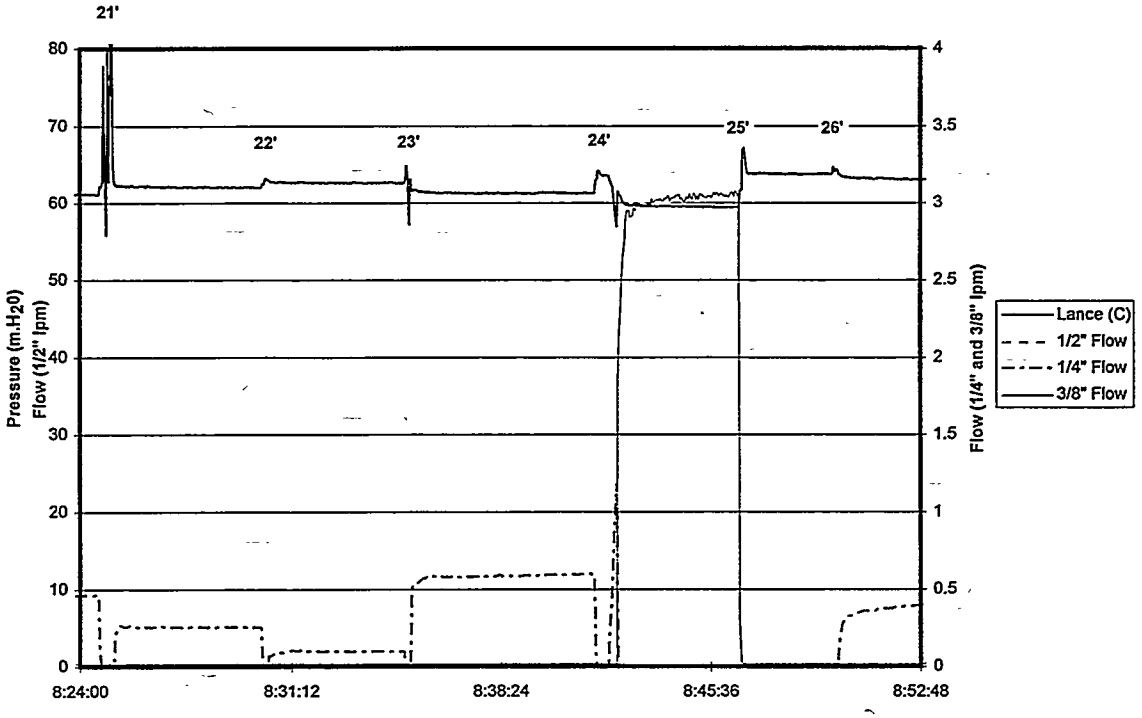
21'
22'
23'
24'
25'
26'
Pressure (m.H20)
Flow (1/2" lpm)
Flow (1/4" and 3/8" lpm)
Lance (C)
1/2" Flow
1/4" Flow
3/8" Flow
8:24:00
8:31:12
8:38:24
8:45:36
8:52:48

LPT-5S

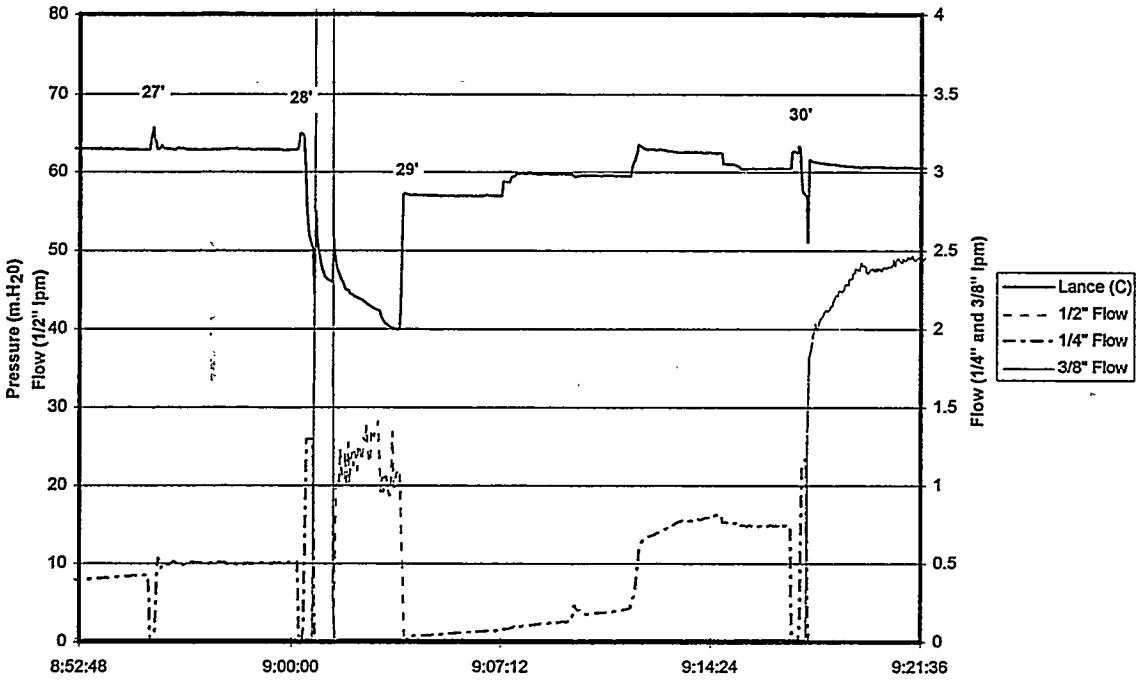
27'
28'
29'
30'
Pressure (m.H20)
Flow (1/2" lpm)
Flow (1/4" and 3/8" lpm)
Lance (C)
1/2" Flow
1/4" Flow
3/8" Flow
8:52:48
9:00:00
9:07:12
9:14:24
9:21:36

LPT-5S

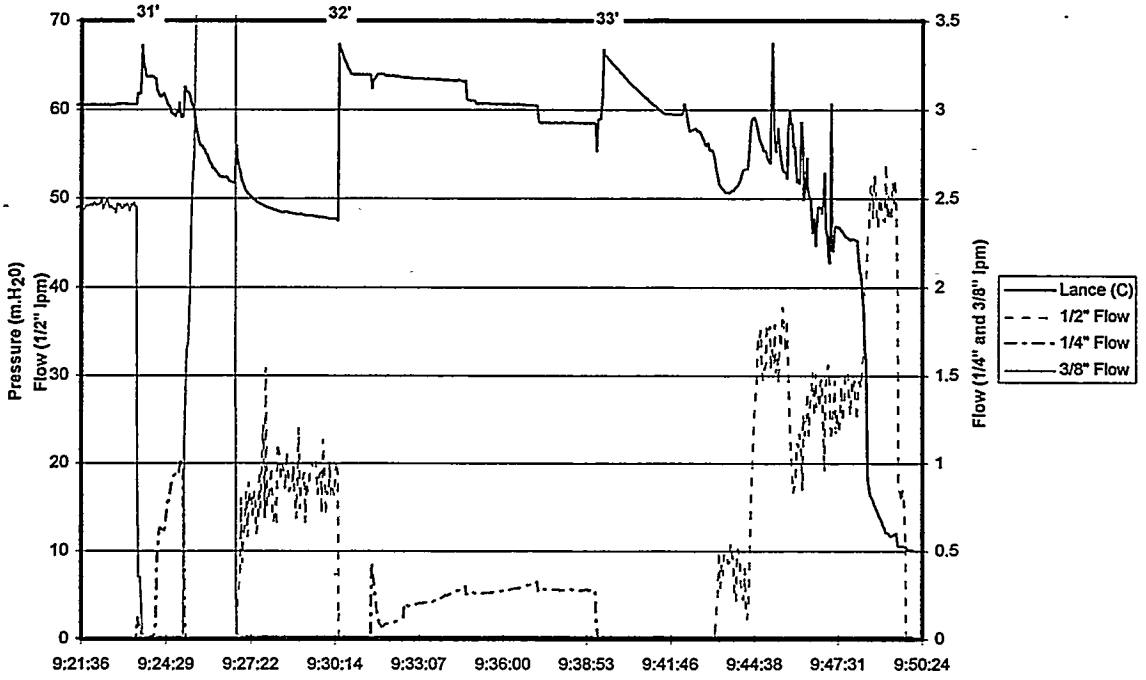
31'
32'
33'
Pressure (m.H20)
Flow (1/2" lpm)
Flow (1/4" and 3/8" lpm)
Lance (C)
1/2" Flow
1/4" Flow
3/8" Flow
9:21:36
9:24:29
9:27:22
9:30:14
9:33:07
9:36:00
9:38:53
9:41:46
9:44:38
9:47:31
9:50:24

LPT-9

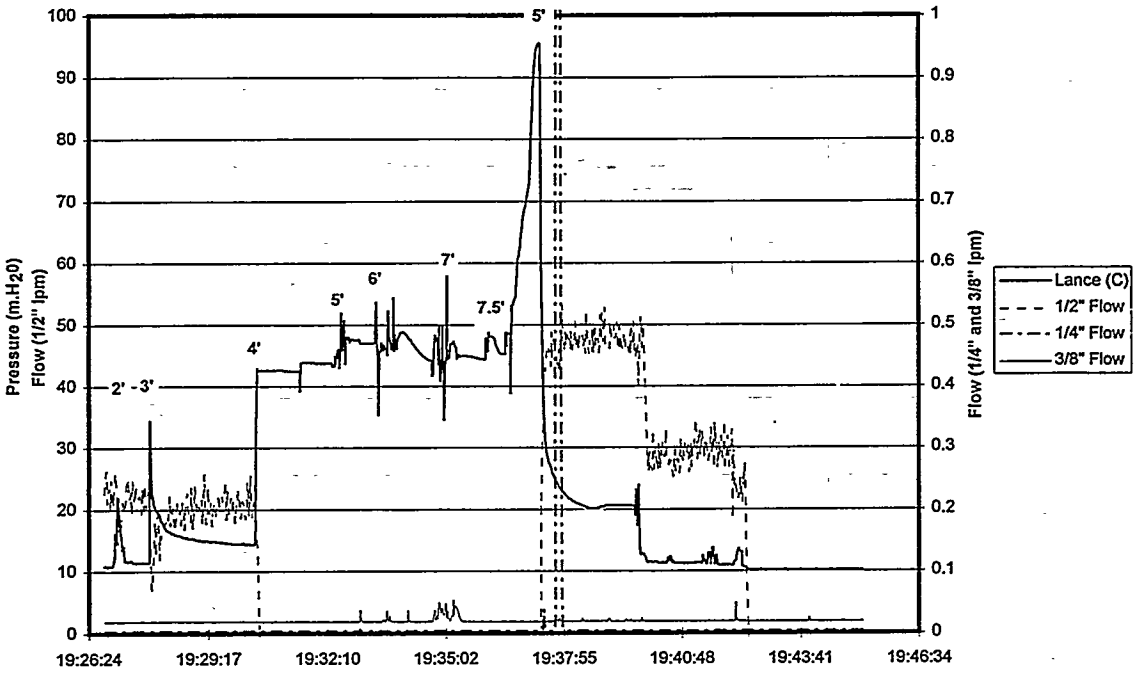
Pressure (m.H2O)
Flow (1/2" lpm)
Flow (1/4" and 3/8" lpm)
2' - 3'
4'
5'
6'
7'
7.5'
5'
Lance (C)
1/2" Flow
1/4" Flow
3/8" Flow
19:26:24
19:29:17
19:32:10
19:35:02
19:37:55
19:40:48
19:43:41
19:46:34

LPT-9S

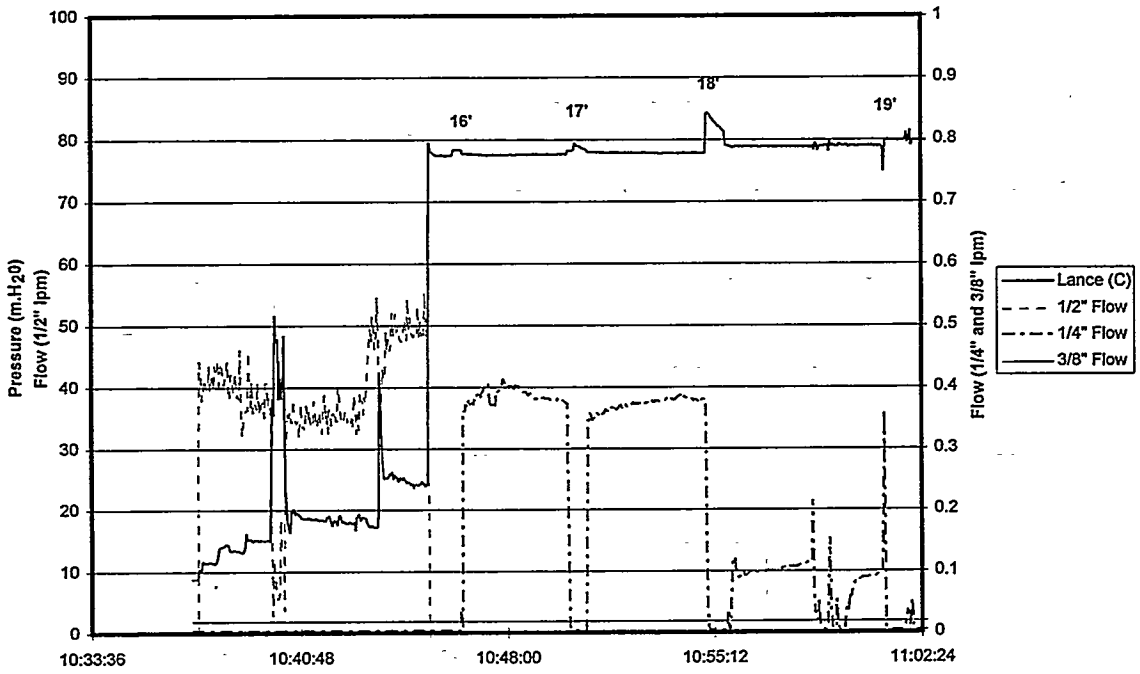
Pressure (m.H2O)
Flow (1/2" lpm)
Flow (1/4" and 3/8" lpm)
16'
17'
18'
19'
Lance (C)
1/2" Flow
1/4" Flow
3/8" Flow
10:33:36
10:40:48
10:48:00
10:55:12
11:02:24

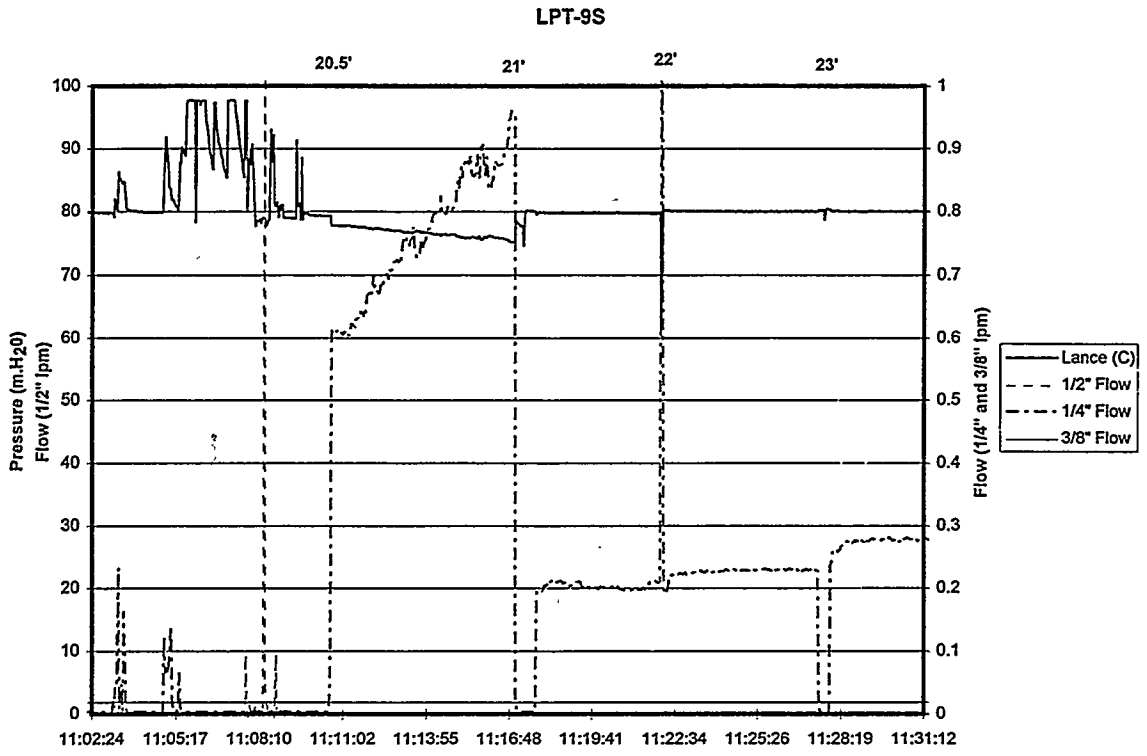
LPT-9S
20.5'
21'
22'
23'
Pressure (m.H2O)
Flow (1/2" lpm)
Flow (1/4" and 3/8" lpm)
Lance (C)
1/2" Flow
1/4" Flow
3/8" Flow
11:02:24
11:05:17
11:08:10
11:11:02
11:13:55
11:16:48
11:19:41
11:22:34
11:25:26
11:28:19
11:31:12

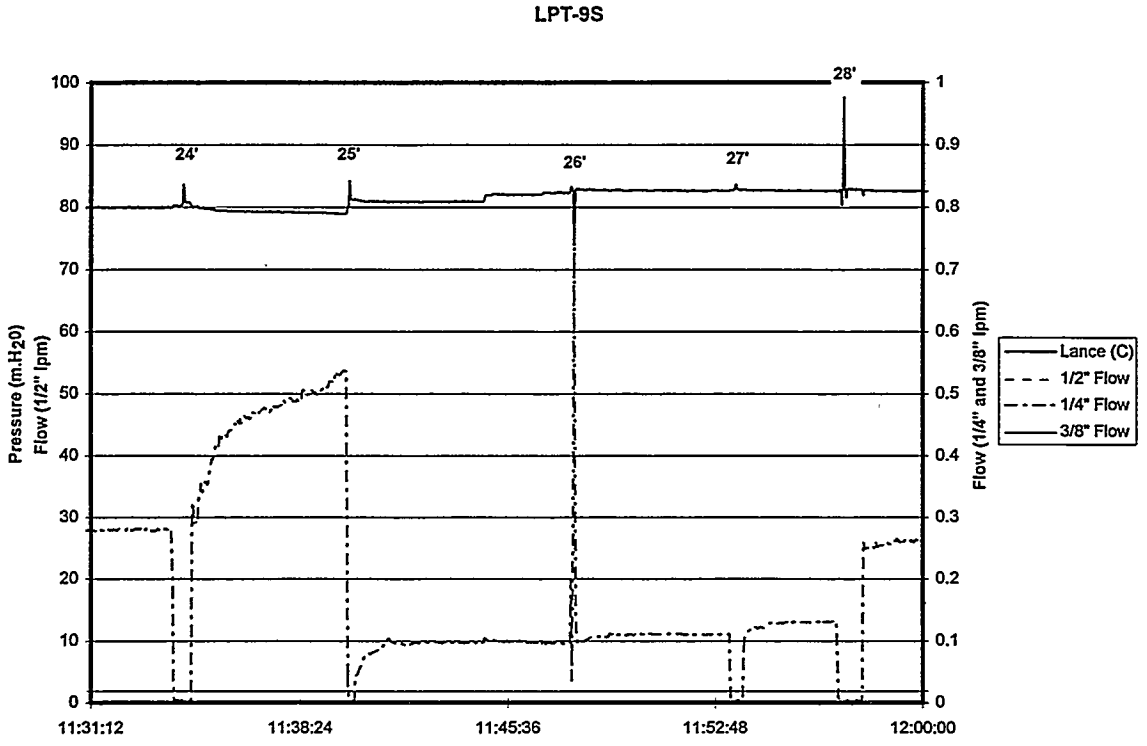
LPT-9S
24'
25'
26'
27'
28'
Pressure (m.H2O)
Flow (1/2" lpm)
Flow (1/4" and 3/8" lpm)
Lance (C)
1/2" Flow
1/4" Flow
3/8" Flow
11:31:12
11:38:24
11:45:36
11:52:48
12:00:00

LPT-9S

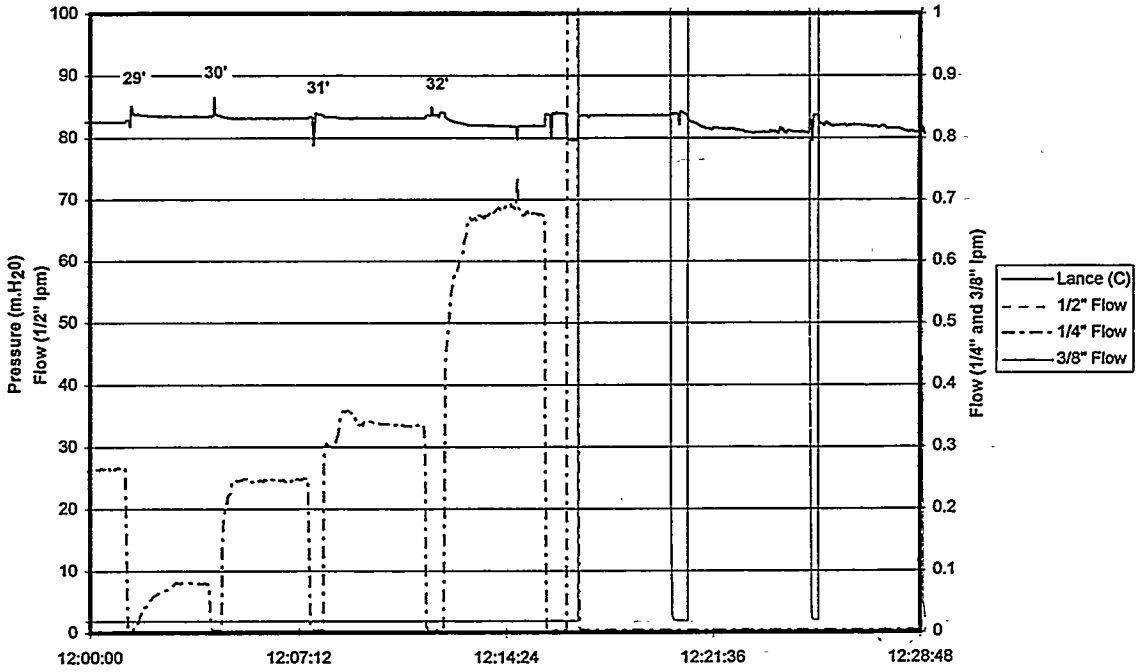
29'
30'
31'
32'
Pressure (m.H20)
Flow (1/2" lpm)
Flow (1/4" and 3/8" lpm)
Lance (C)
1/2" Flow
1/4" Flow
3/8" Flow
12:00:00
12:07:12
12:14:24
12:21:36
12:28:48

LPT-9S

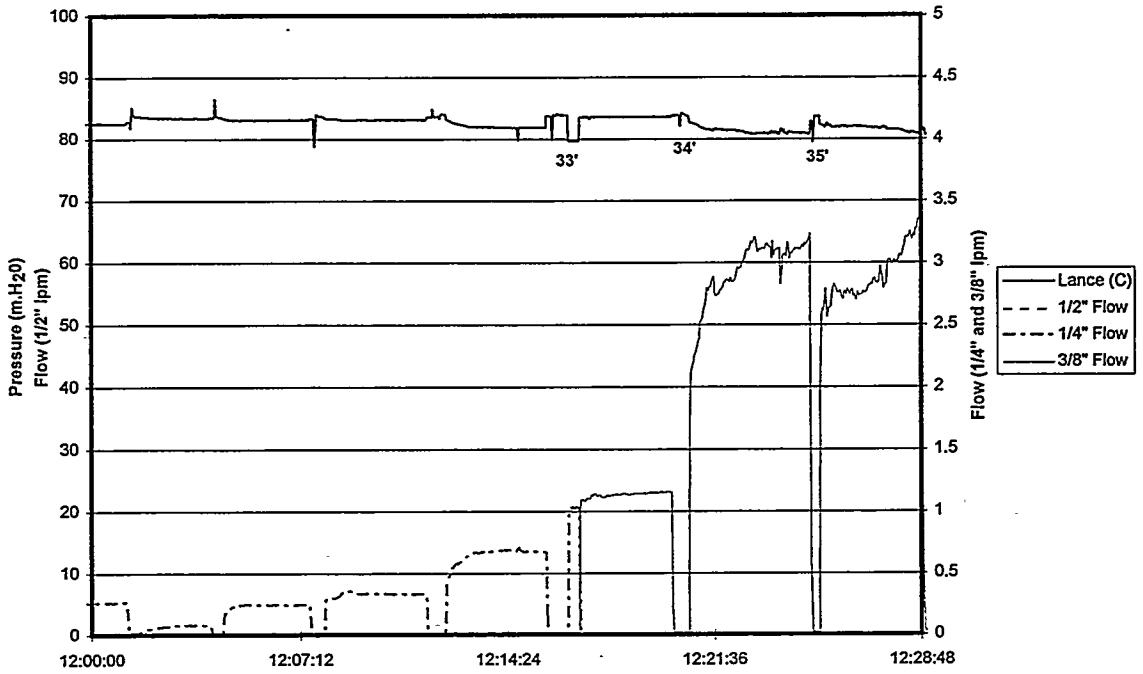
33'
34'
35'
Pressure (m.H20)
Flow (1/2" lpm)
Flow (1/4" and 3/8" lpm)
Lance (C)
1/2" Flow
1/4" Flow
3/8" Flow
12:00:00
12:07:12
12:14:24
12:21:36
12:28:48

LPT-9S

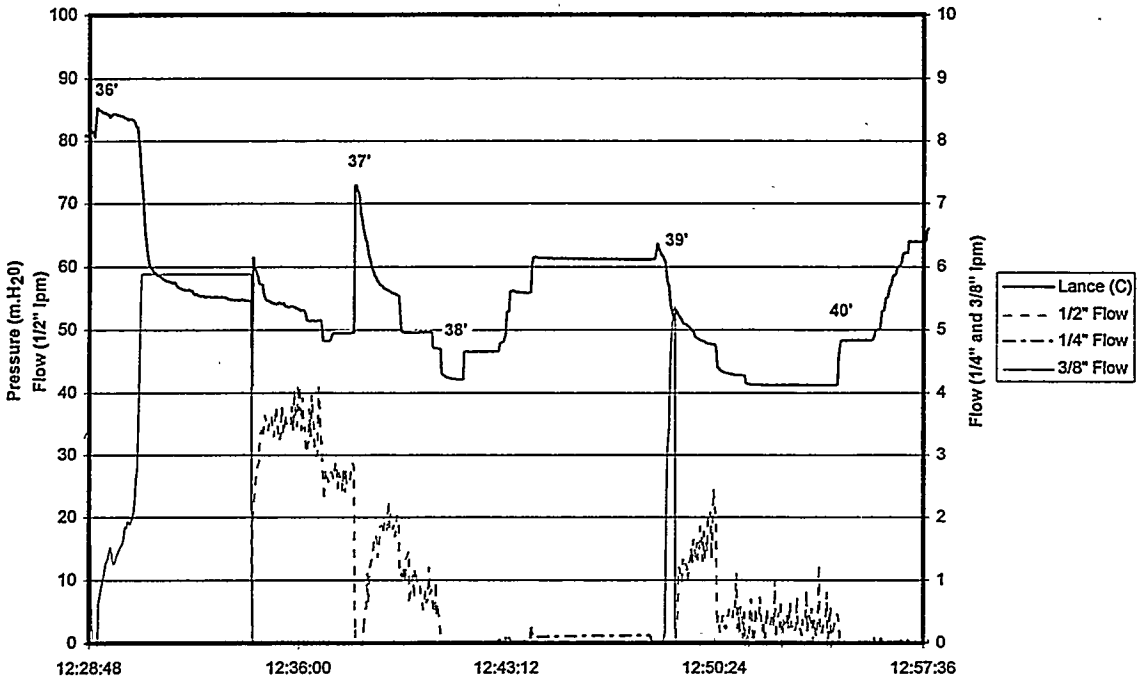
36'
37'
38'
39'
40'
Pressure (m.H20)
Flow (1/2" lpm)
Flow (1/4" and 3/8" lpm)
Lance (C)
1/2" Flow
1/4" Flow
3/8" Flow
12:28:48
12:36:00
12:43:12
12:50:24
12:57:36

LPT-9S

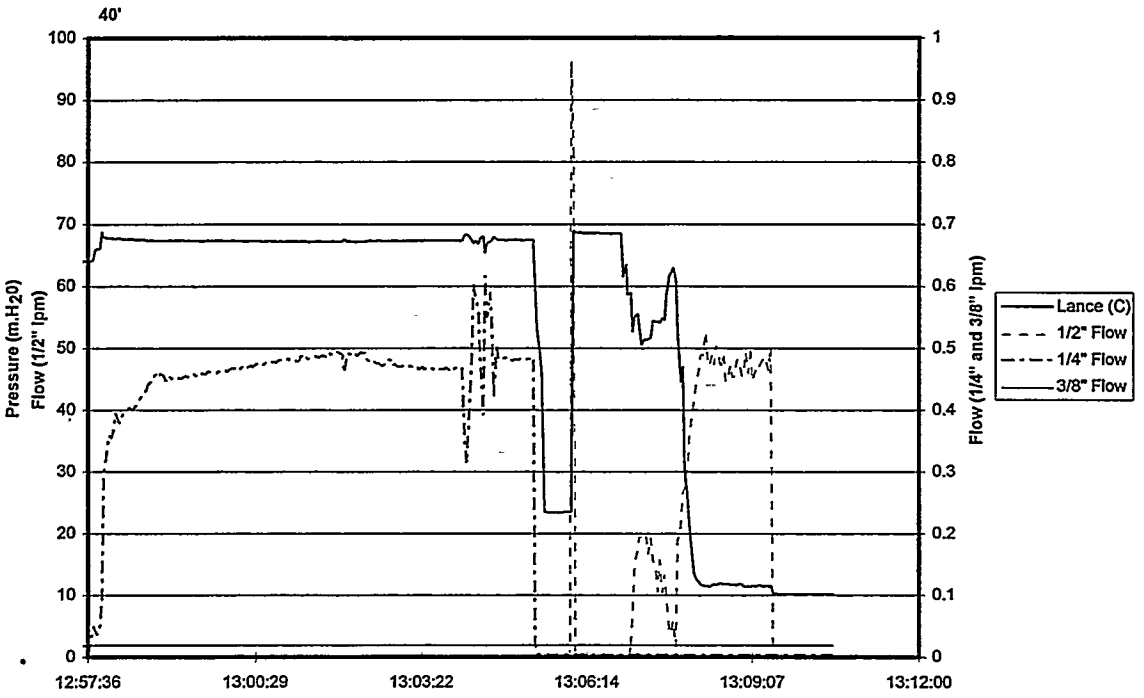
40'
Pressure (m.H20)
Flow (1/2" lpm)
Flow (1/4" and 3/8" lpm)
Lance (C)
1/2" Flow
1/4" Flow
3/8" Flow
12:57:36
13:00:29
13:03:22
13:06:14
13:09:07
13:12:00

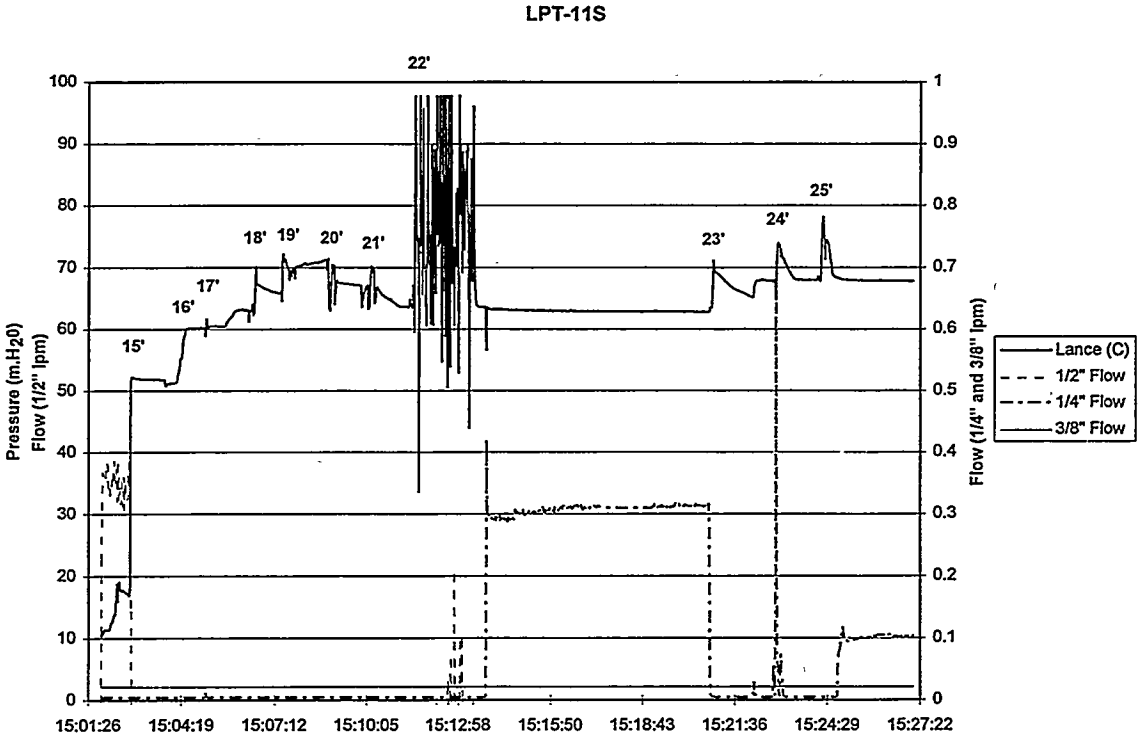
LPT-11S
Pressure (m.H2O)
Flow (1/2" lpm)
Flow (1/4" and 3/8" lpm)
Lance (C)
1/2" Flow
1/4" Flow
3/8" Flow
15'
16'
17'
18'
19'
20'
21'
22'
23'
24'
25'
15:01:26
15:04:19
15:07:12
15:10:05
15:12:58
15:15:50
15:18:43
15:21:36
15:24:29
15:27:22

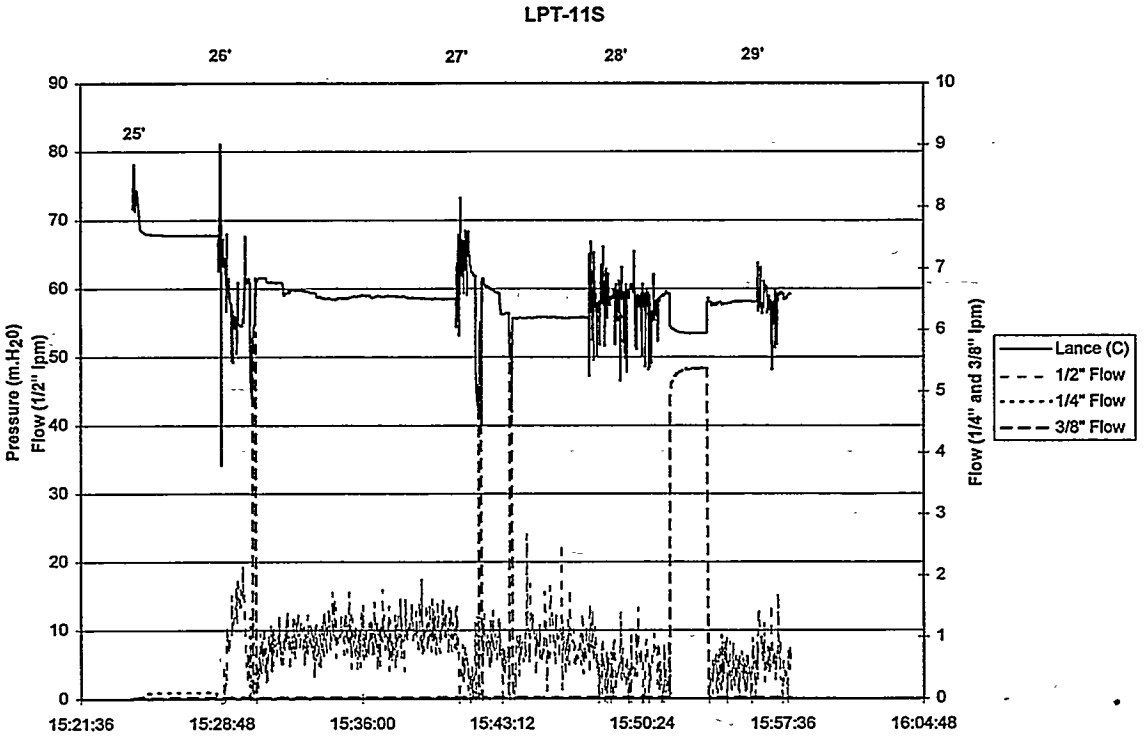
LPT-11S
Pressure (m.H2O)
Flow (1/2" lpm)
Flow (1/4" and 3/8" lpm)
Lance (C)
1/2" Flow
1/4" Flow
3/8" Flow
25'
26'
27'
28'
29'
15:21:36
15:28:48
15:36:00
15:43:12
15:50:24
15:57:36
16:04:48

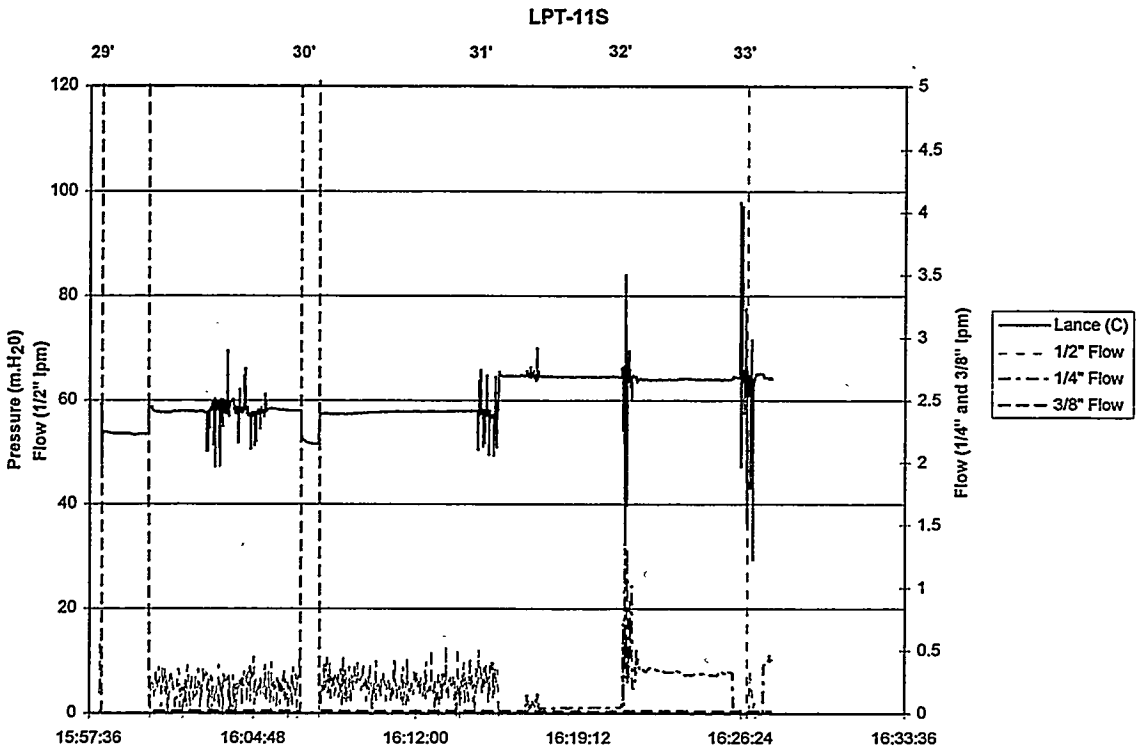
LPT-11S
29'
30'
31'
32'
33'
120
100
80
60
40
20
0
5
4.5
4
3.5
3
2.5
2
1.5
1
0.5
0
Pressure (m.H20)
Flow (1/2" lpm)
Flow (1/4" and 3/8" lpm)
15:57:36
16:04:48
16:12:00
16:19:12
16:26:24
16:33:36
Lance (C)
1/2" Flow
1/4" Flow
3/8" Flow

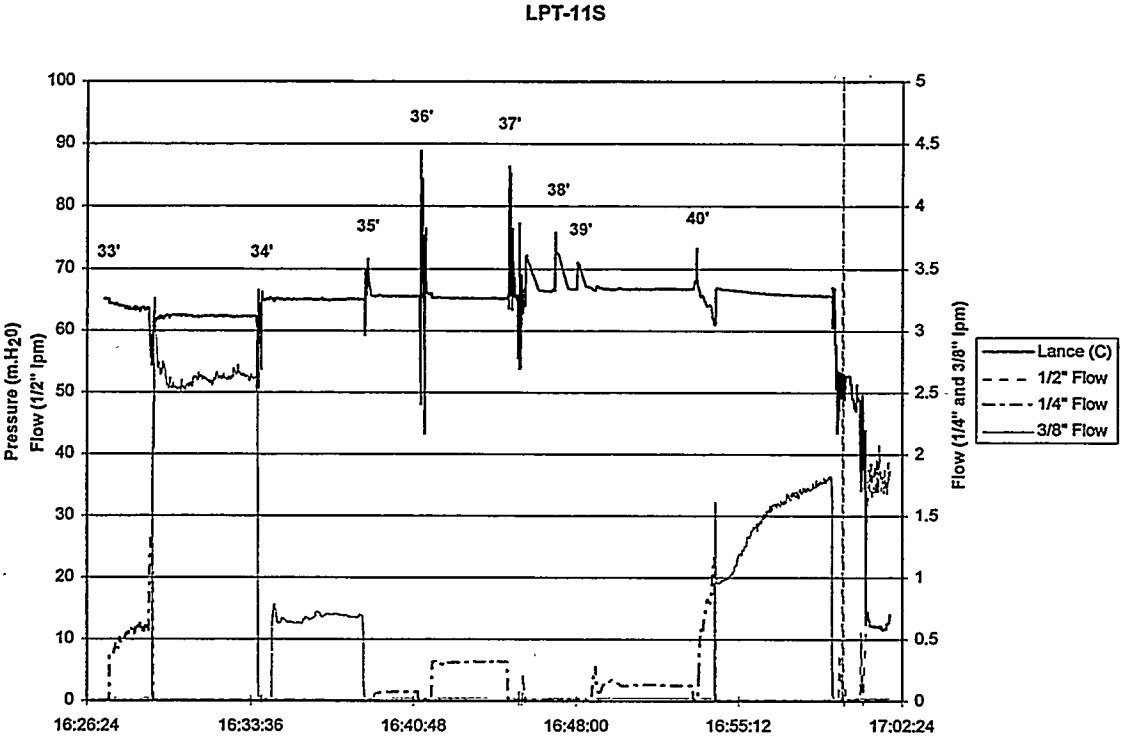
LPT-11S
100
90
80
70
60
50
40
30
20
10
0
5
4.5
4
3.5
3
2.5
2
1.5
1
0.5
0
33'
34'
35'
36'
37'
38'
39'
40'
Pressure (m.H20)
Flow (1/2" lpm)
Flow (1/4" and 3/8" lpm)
16:26:24
16:33:36
16:40:48
16:48:00
16:55:12
17:02:24
Lance (C)
1/2" Flow
1/4" Flow
3/8" Flow

LPT-16S

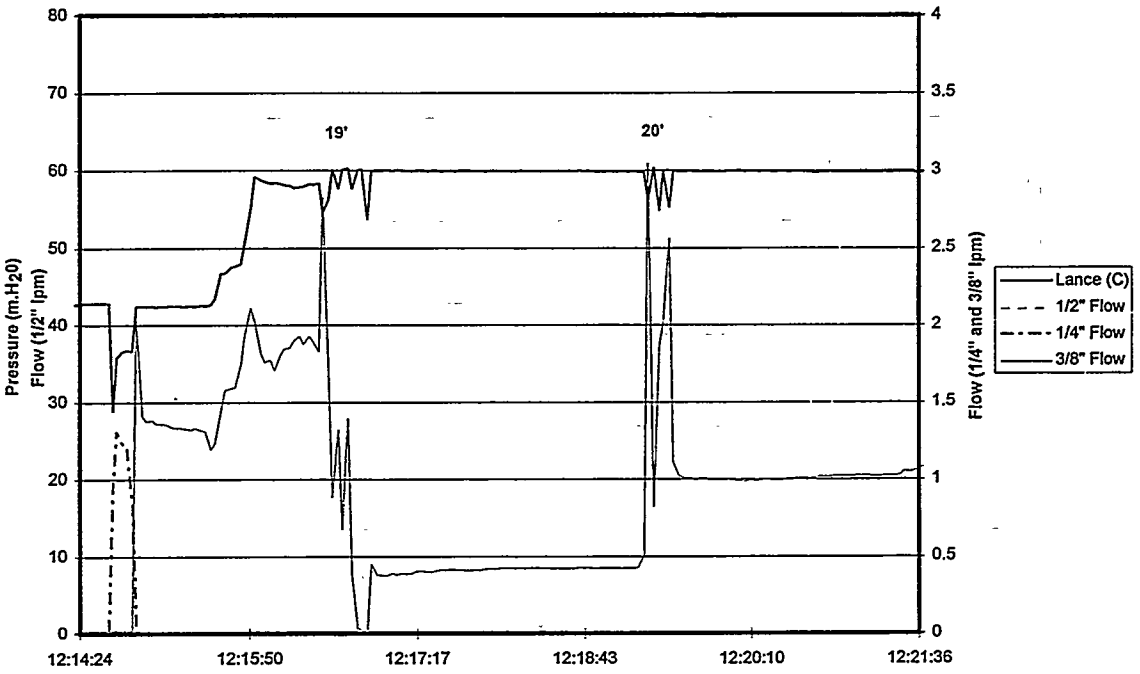

LPT-16S

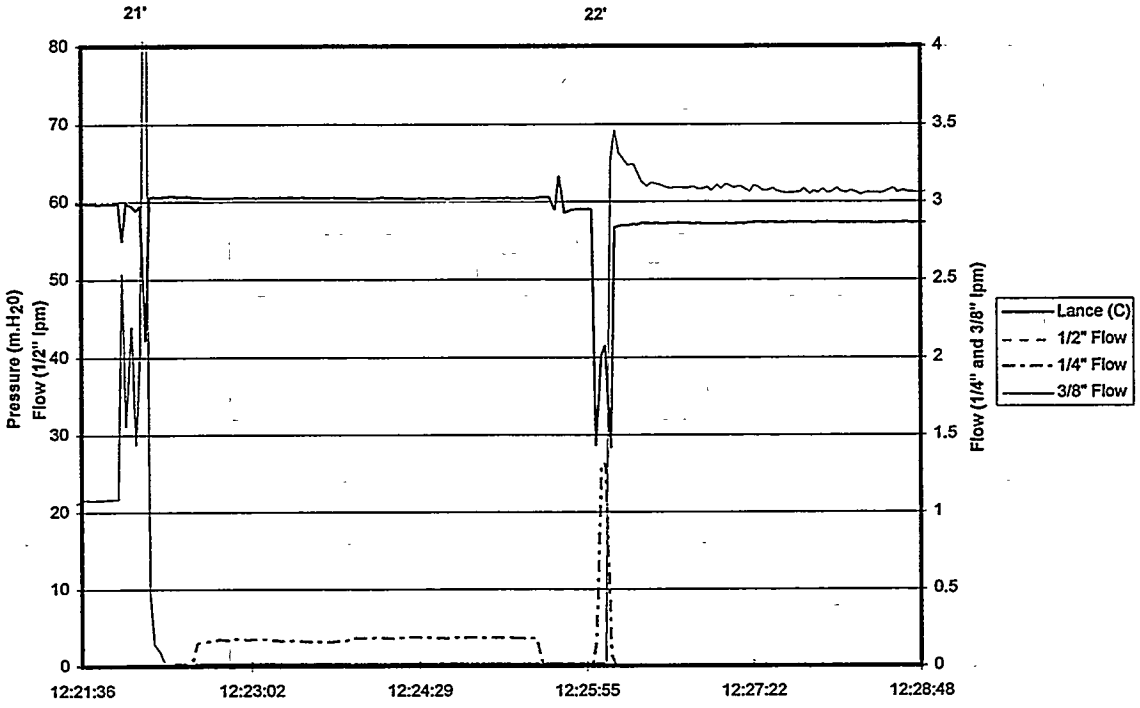

LPT-16S

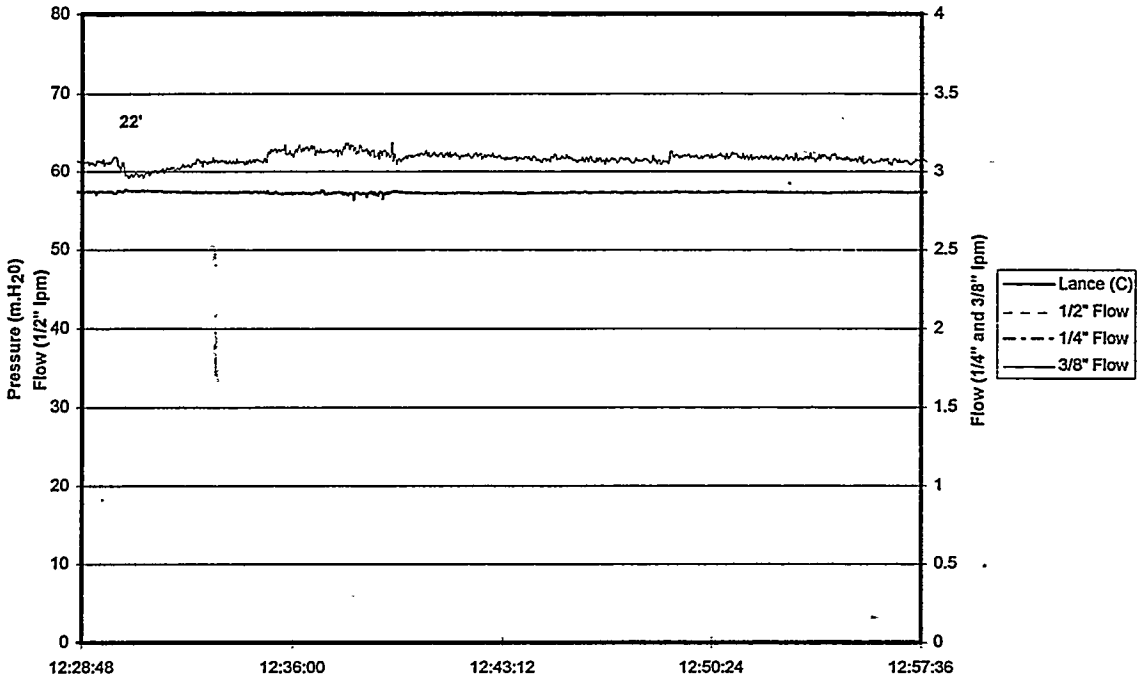

LPT-16S

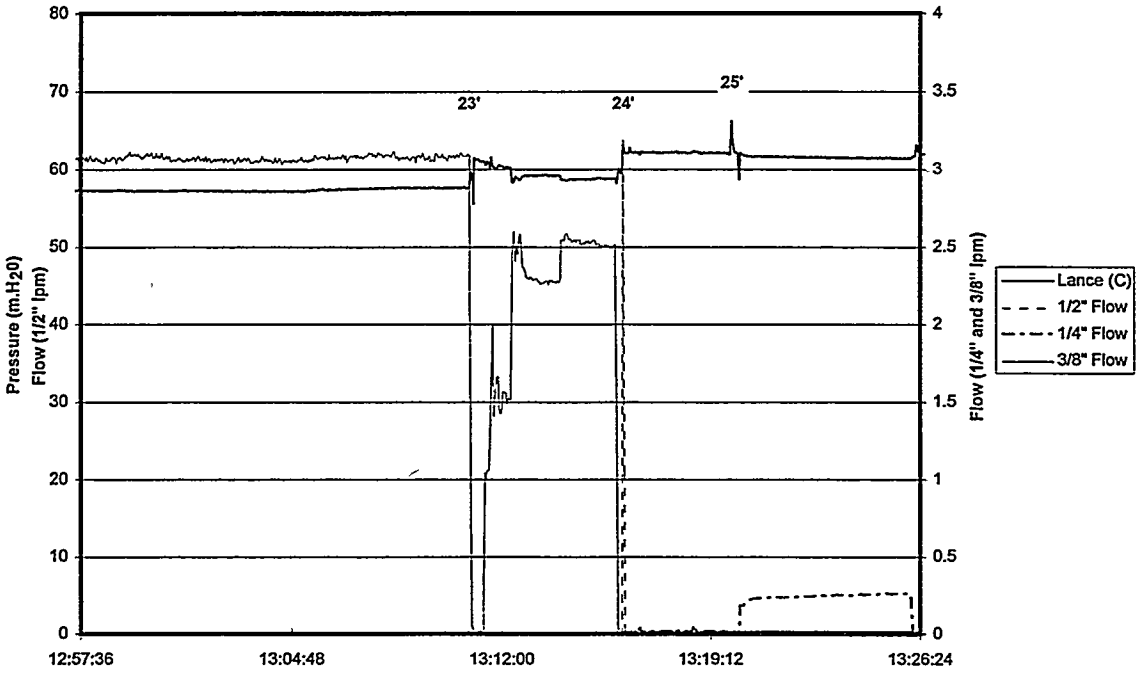

LPT-16S

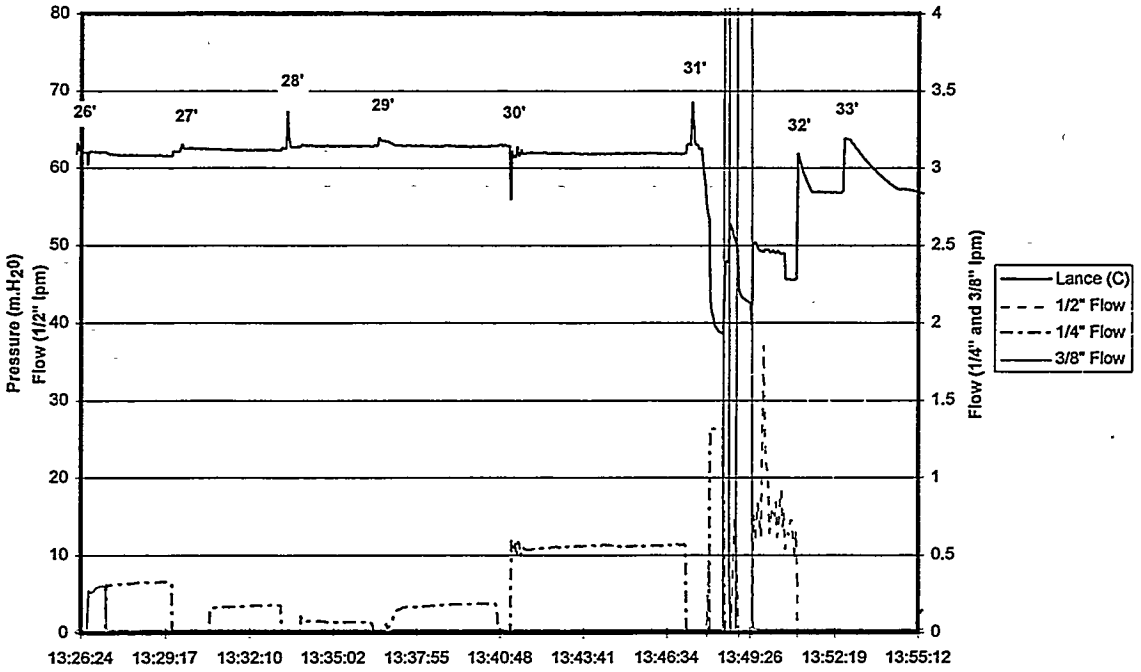

LPT-16S

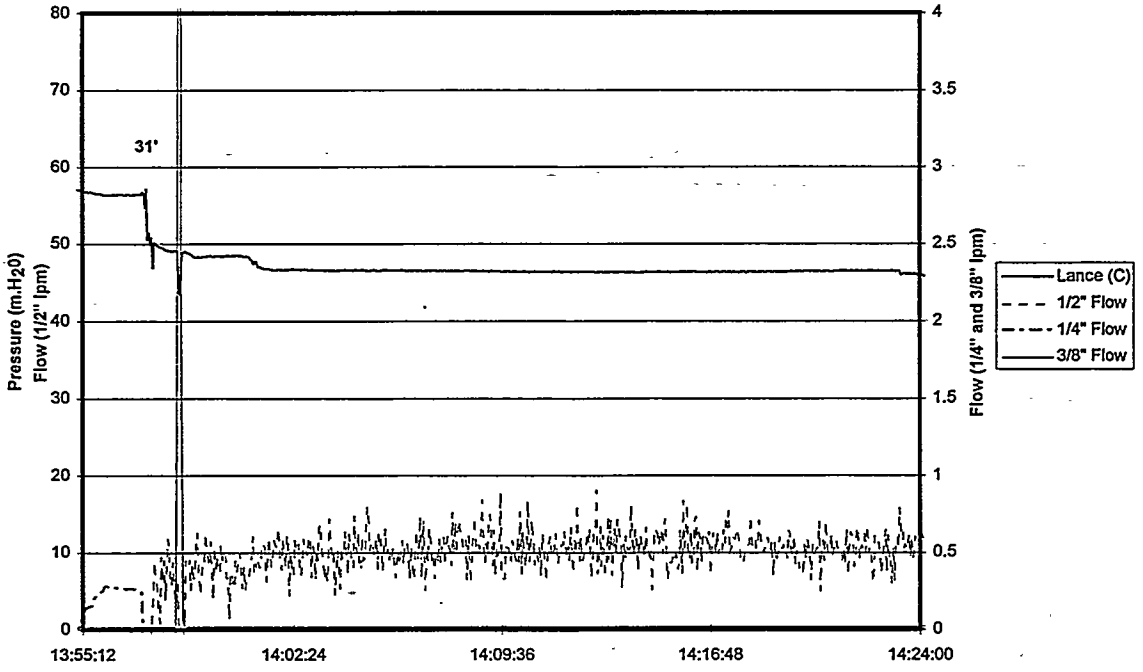

LPT-19.5S

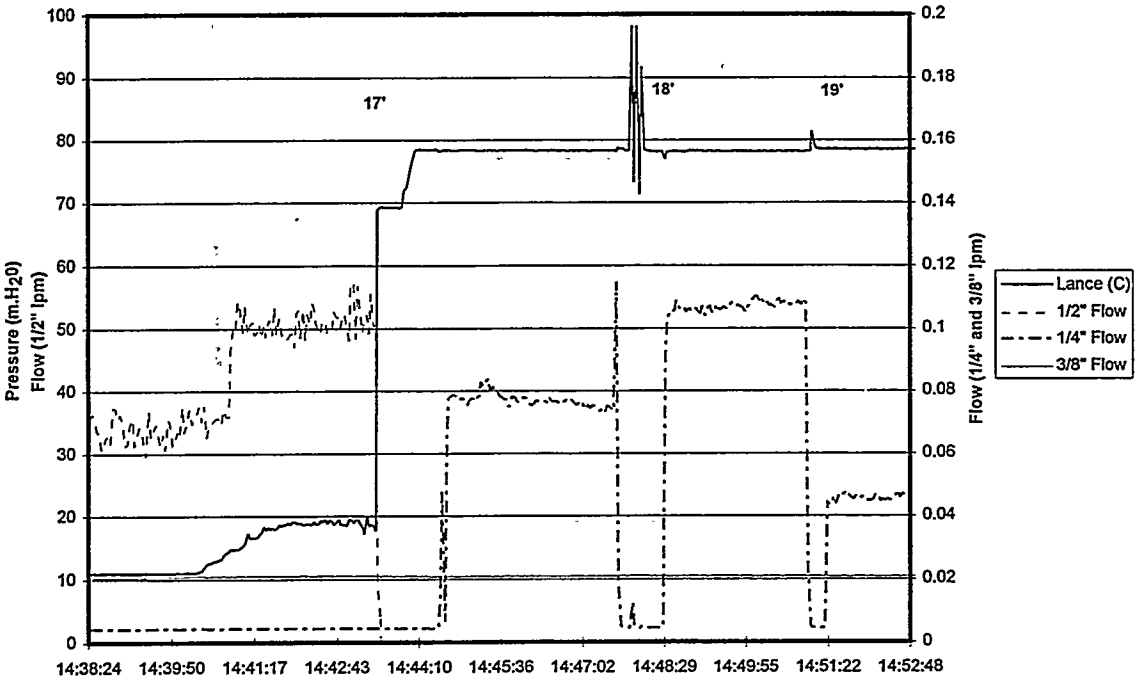

LPT-19.5S

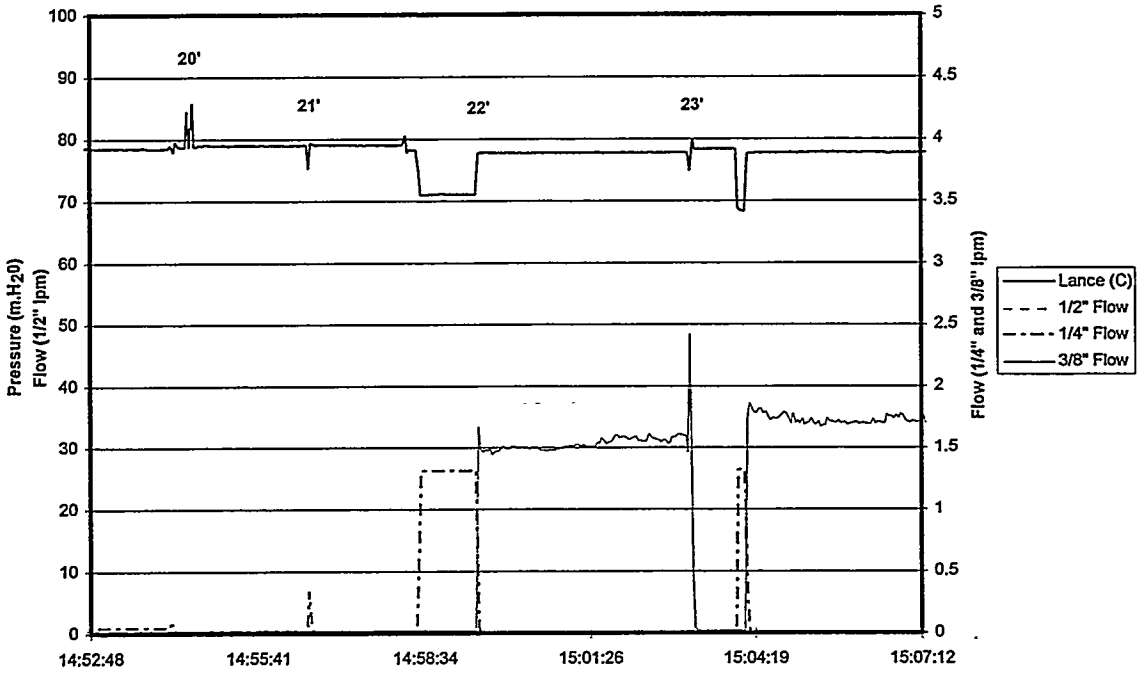

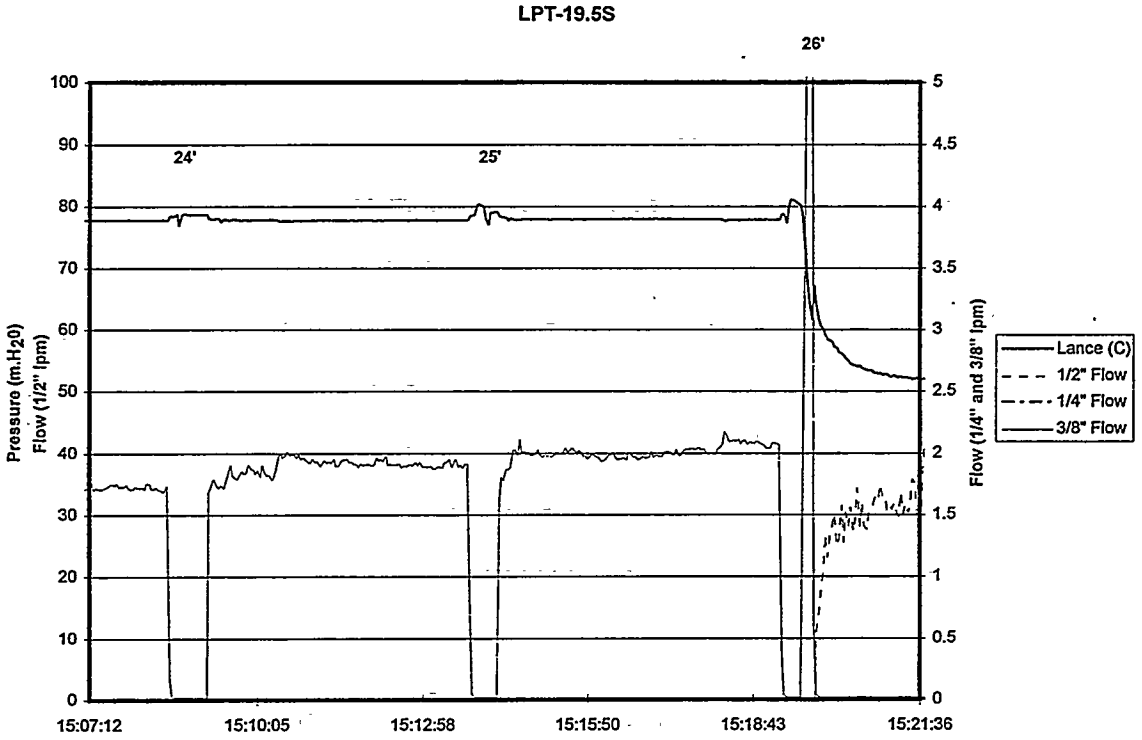
LPT-19.5S
26'
24'
25'
Pressuro (m.H20)
Flow (1/2" lpm)
Flow (1/4" and 3/8" lpm)
Lance (C)
1/2" Flow
1/4" Flow
3/8" Flow
15:07:12
15:10:05
15:12:58
15:15:50
15:18:43
15:21:36

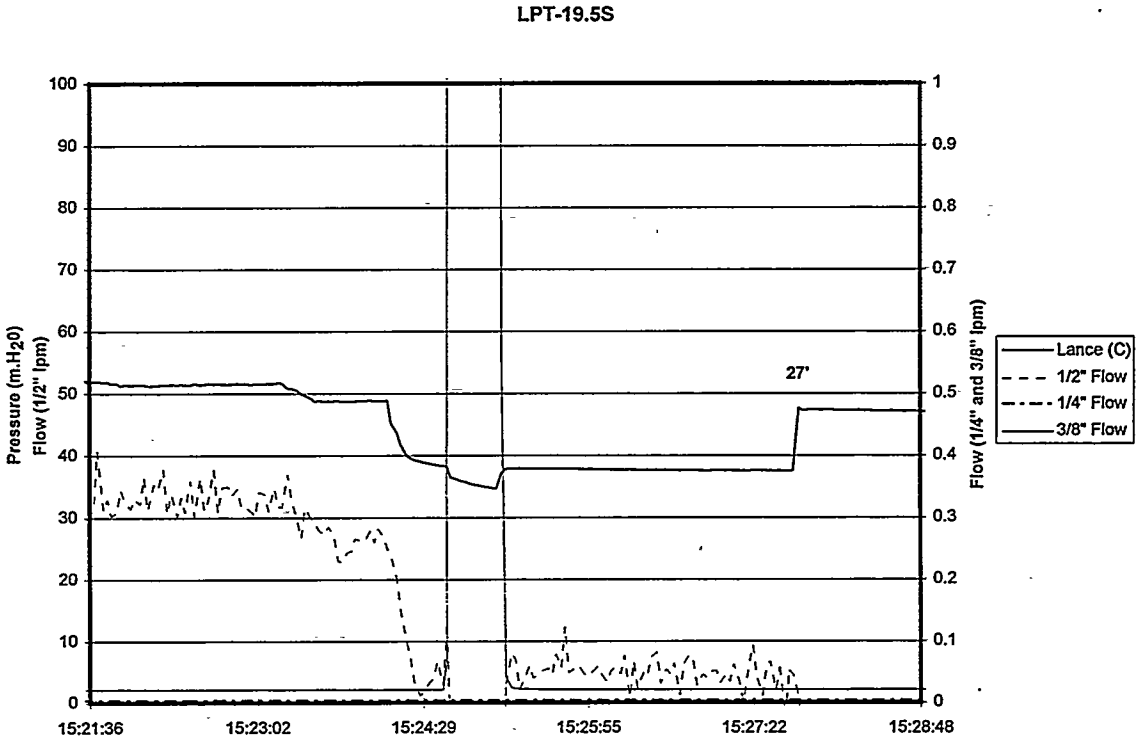
LPT-19.5S
27'
Pressuro (m.H20)
Flow (1/2" lpm)
Flow (1/4" and 3/8" lpm)
Lance (C)
1/2" Flow
1/4" Flow
3/8" Flow
15:21:36
15:23:02
15:24:29
15:25:55
15:27:22
15:28:48

LPT-19.5S

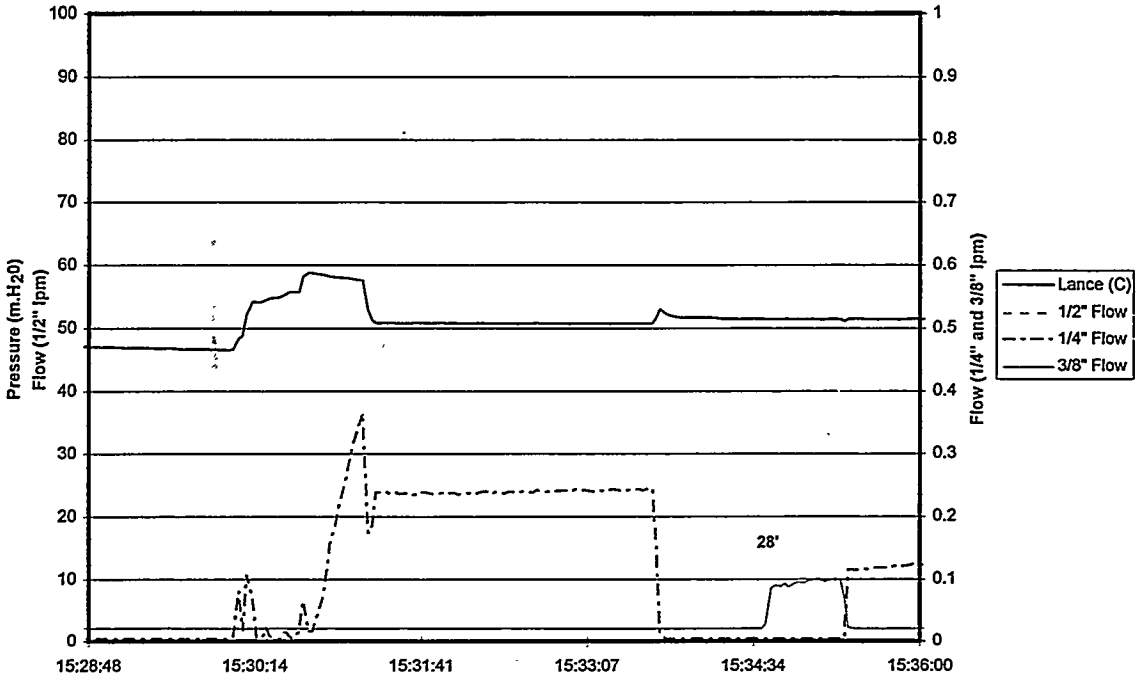

LPT-19.5S

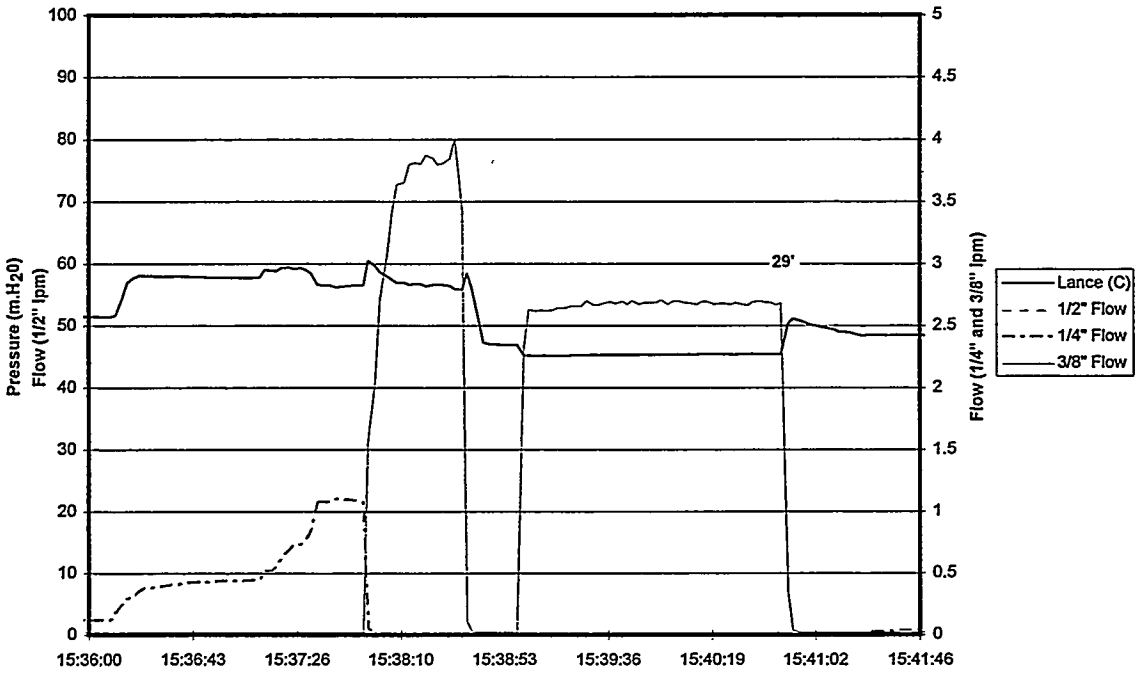

LPT-19.5S

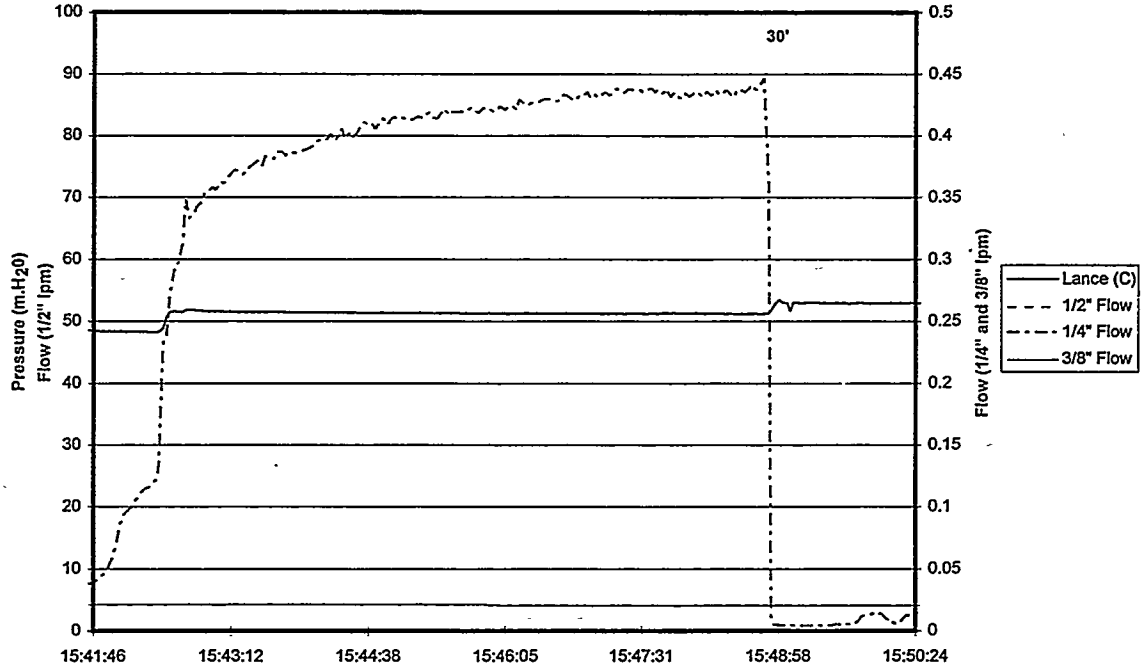

LPT-19.5S

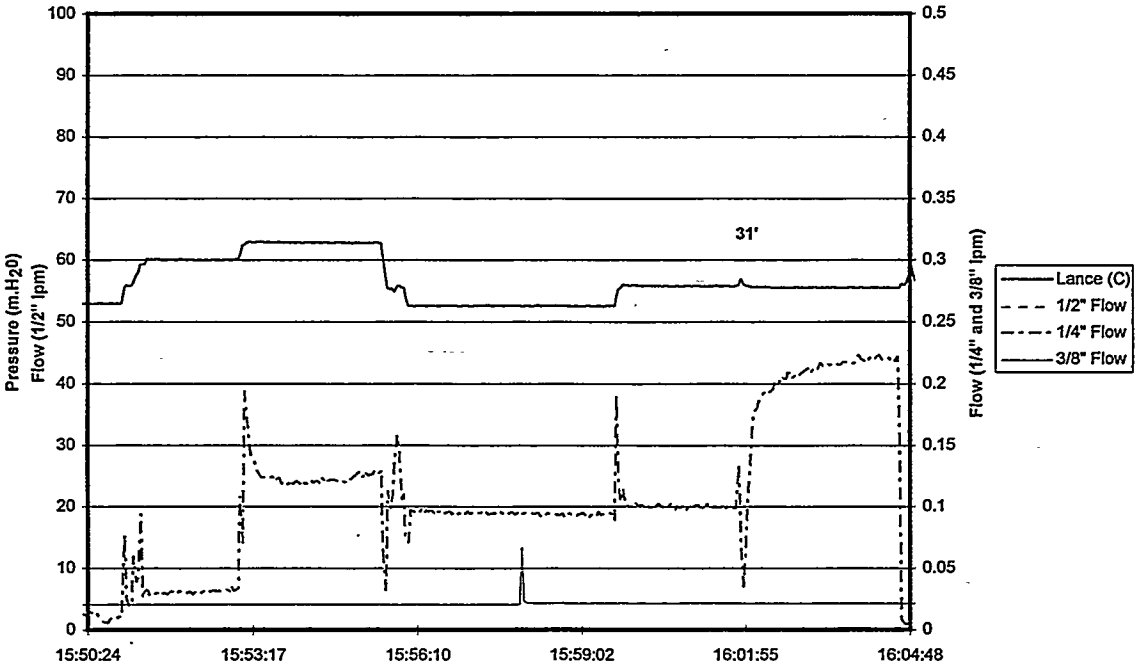

LPT-19.5S

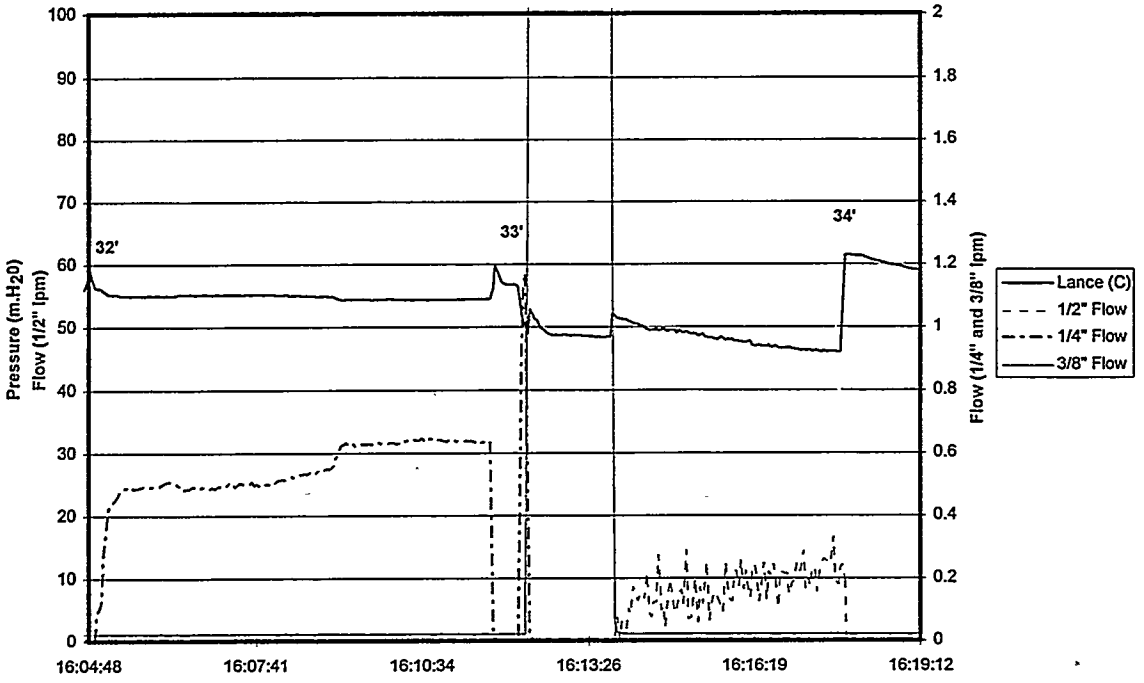

LPT-19.5S

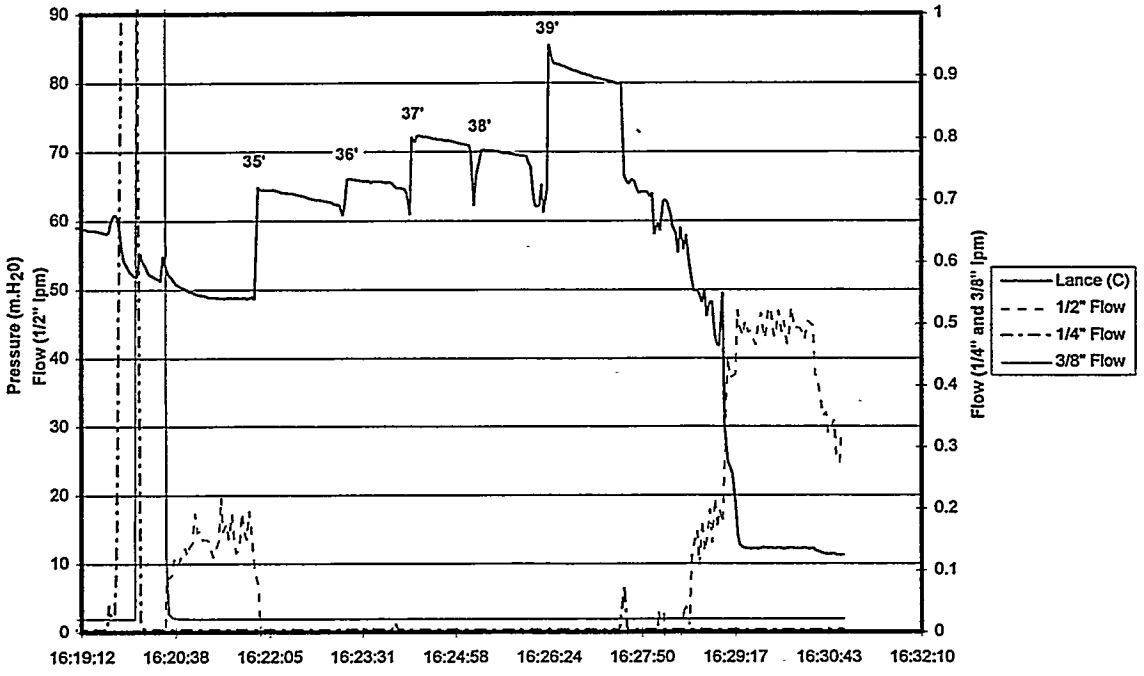

LPT-20

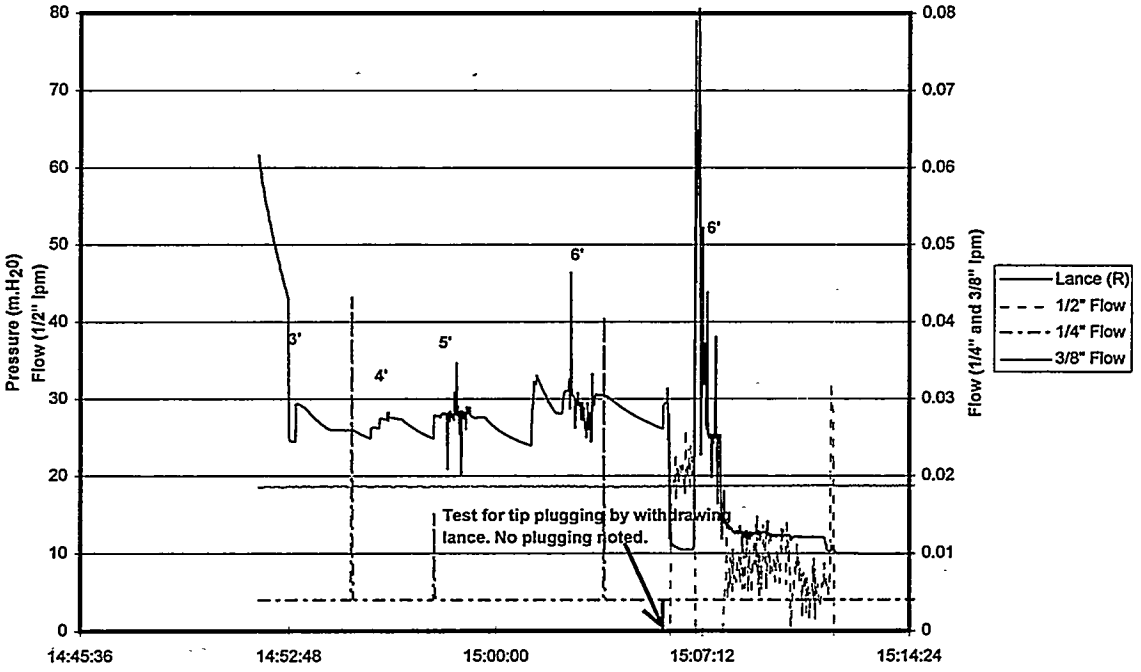
Pressure (m.H20)
Flow (1/2" lpm)
Flow (1/4" and 3/8" lpm)
Lance (R)
1/2" Flow
1/4" Flow
3/8" Flow
3'
4'
5'
6'
6'
6'
Test for tip plugging by withdrawing lance. No plugging noted.
14:45:36
14:52:48
15:00:00
15:07:12
15:14:24

LPT-20

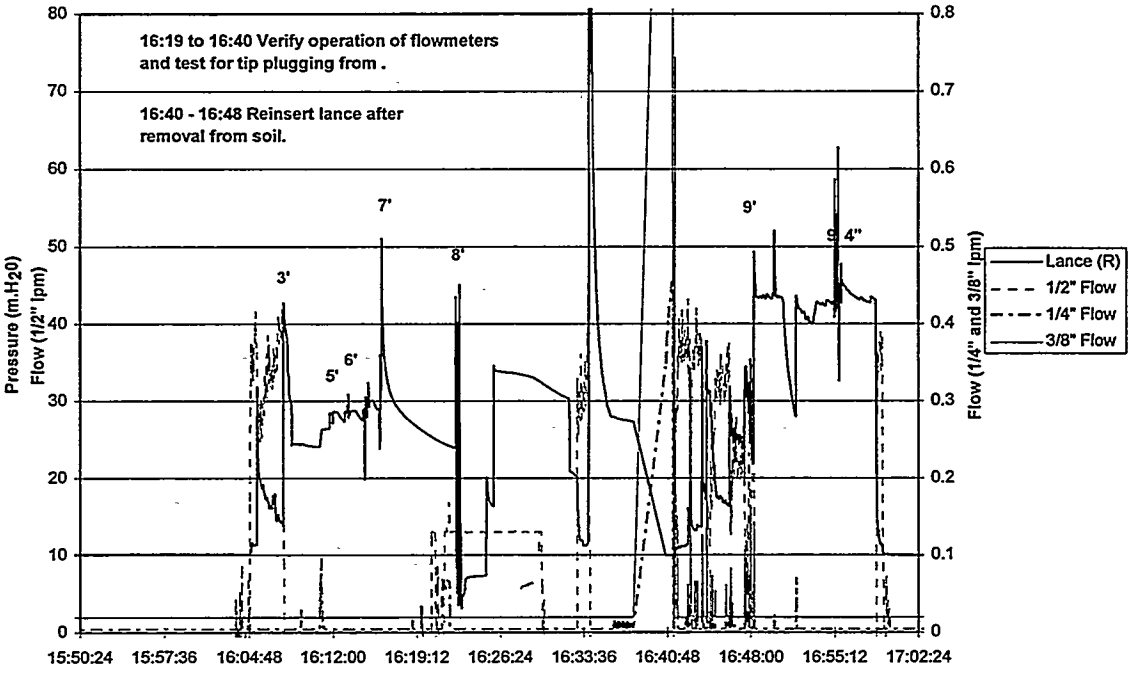
16:19 to 16:40 Verify operation of flowmeters and test for tip plugging from .
16:40 - 16:48 Reinsert lance after removal from soil.
Pressure (m.H20)
Flow (1/2" lpm)
Flow (1/4" and 3/8" lpm)
Lance (R)
1/2" Flow
1/4" Flow
3/8" Flow
3'
5'
6'
7'
8'
9'
9 4"
15:50:24
15:57:36
16:04:48
16:12:00
16:19:12
16:26:24
16:33:36
16:40:48
16:48:00
16:55:12
17:02:24

Appendix B

Analytical Model Simulation Results for Lance Injection Tests

Injection Radius:		0.0174	Boundary Radius:		1.0 meters	Assumed rad. thick:		0.1 meters		
						*Spherical	*Radial	*Radial K	Comments	
Location	Depth (ft)	Start Time	Pressure	Flow(lpm)	Flow (m3/sec)	K (m/s)	T(m2/sec)	K (m/s)		
LPT-5S	16	8:07	43	0.028	4.58E-07	5.30E-08	1.70E-09	1.70E-08		
LPT-5S	16	8:09	50.5	0.032	5.33E-07	5.02E-08	1.61E-09	1.61E-08		
LPT-5S	17	8:13	62	0.060	1.00E-06	7.31E-08	2.34E-09	2.34E-08		
LPT-5S	18	8:16	62	0.098	1.63E-06	1.19E-07	3.80E-09	3.80E-08		
LPT-5S	19	8:19	62	0.075	1.25E-06	9.14E-08	2.93E-09	2.93E-08		
LPT-5S	20	8:21	61	0.460	7.67E-06	5.72E-07	1.83E-08	1.83E-07		
LPT-5S	21	8:25	62	0.260	4.33E-06	3.17E-07	1.01E-08	1.01E-07		
LPT-5S	22	8:39	63	0.100	1.67E-06	1.20E-07	3.83E-09	3.83E-08		
LPT-5S	23	8:35	61.2	0.600	1.00E-05	7.43E-07	2.38E-08	2.38E-07		
LPT-5S	24	8:42	59.3	3.000	5.00E-05	3.86E-06	1.23E-07	1.23E-06		
LPT-5S	25	8:46	63.8	< 0.01	1.67E-07	1.18E-08	3.77E-10	3.77E-09	No Detectable Flow	
LPT-5S	26	8:49	63	0.400	6.67E-06	4.78E-07	1.53E-08	1.53E-07		
LPT-5S	27	8:55	63	0.500	8.33E-06	5.98E-07	1.91E-08	1.91E-07		
LPT-5S	28	9:00	42	22.000	3.67E-04	4.38E-05	1.40E-06	1.40E-05	Post Fracture	
LPT-5S	29	9:04	60.5	0.750	1.25E-05	9.42E-07	3.01E-08	3.01E-07		
LPT-5S	30	9:17	60.5	2.200	3.67E-05	2.76E-06	8.84E-08	8.84E-07		
LPT-5S	31	9:22	48	16.000	2.67E-04	2.68E-05	8.56E-07	8.56E-06	Post Fracture	
LPT-5S	32	9:31	61	0.125	2.08E-06	1.55E-07	4.97E-09	4.97E-08		
LPT-5S	33	9:39	50	<0.01	1.67E-07	1.59E-08	5.08E-10	5.08E-09		
LPT-11S	15	15:02	52	< 0.01	1.67E-07	1.51E-08	4.84E-10	4.84E-09	No Detectable Flow	
LPT-11S	16	15:04	60	< 0.01	1.67E-07	1.27E-08	4.06E-10	4.06E-09	No Detectable Flow	
LPT-11S	17	15:05	60.5	< 0.01	1.67E-07	1.26E-08	4.02E-10	4.02E-09	No Detectable Flow	
LPT-11S	18	15:07	64	< 0.01	1.67E-07	1.17E-08	3.75E-10	3.75E-09	No Detectable Flow	
LPT-11S	19	15:08	70	< 0.01	1.67E-07	1.06E-08	3.38E-10	3.38E-09	No Detectable Flow	
LPT-11S	20	15:09	69	< 0.01	1.67E-07	1.07E-08	3.43E-10	3.43E-09	No Detectable Flow	
LPT-11S	21	15:11	64	< 0.01	1.67E-07	1.17E-08	3.75E-10	3.75E-09	No Detectable Flow	
LPT-11S	22	15:12	62	0.315	5.25E-06	3.84E-07	1.23E-08	1.23E-07		
LPT-11S	23	15:20	68	< 0.01	1.67E-07	1.09E-08	3.49E-10	3.49E-09	No Detectable Flow	
LPT-11S	24	15:22	68	< 0.01	1.67E-07	1.09E-08	3.49E-10	3.49E-09	No Detectable Flow	
LPT-11S	25	15:25	68	0.100	1.67E-06	1.09E-07	3.49E-09	3.49E-08		
LPT-11S	26	15:28	58	9.000	1.50E-04	1.19E-05	3.80E-07	3.80E-06		
LPT-11S	27	15:41	56	7.000	1.17E-04	9.65E-06	3.09E-07	3.09E-06		
LPT-11S	28	15:52	54	5.500	9.17E-05	7.93E-06	2.54E-07	2.54E-06		
LPT-11S	29	15:57	54	5.400	9.00E-05	7.79E-06	2.49E-07	2.49E-06		
LPT-11S	30	16:06	52	6.000	1.00E-04	9.07E-06	2.90E-07	2.90E-06		
LPT-11S	31	16:16	64	< 0.01	1.67E-07	1.17E-08	3.75E-10	3.75E-09	No Detectable Flow	
LPT-11S	32	16:20	64	0.350	5.83E-06	4.11E-07	1.31E-08	1.31E-07		
LPT-11S	33	16:26	52	2.600	4.33E-05	3.93E-06	1.26E-07	1.26E-06		
LPT-11S	34	16:33	65	0.700	1.17E-05	8.06E-07	2.58E-08	2.58E-07		
LPT-11S	35	16:38	66	0.080	1.33E-06	9.05E-08	2.90E-09	2.90E-08		
LPT-11S	36	16:41	65	0.300	5.00E-06	3.46E-07	1.11E-08	1.11E-07		
LPT-11S	37	16:46	66	< 0.01	1.67E-07	1.13E-08	3.62E-10	3.62E-09	No Detectable Flow	
LPT-11S	38	16:47	67	< 0.01	1.67E-07	1.11E-08	3.56E-10	3.56E-09	No Detectable Flow	
LPT-11S	39	16:48	67	0.120	2.00E-06	1.33E-07	4.27E-09	4.27E-08		
LPT-11S	40	16:52	66	1.700	2.83E-05	1.92E-06	6.15E-08	6.15E-07		
LPT-16S	19	12:16	60	0.400	6.67E-06	5.07E-07	1.62E-08	1.62E-07		
LPT-16S	20	12:19	60	1.050	1.75E-05	1.33E-06	4.26E-08	4.26E-07		
LPT-16S	21	12:21	60	0.200	3.33E-06	2.54E-07	8.11E-09	8.11E-08		
LPT-16S	22	12:25	57.5	3.100	5.17E-05	4.14E-06	1.32E-07	1.32E-06		
LPT-16S	23	13:11	59	2.500	4.17E-05	3.24E-06	1.04E-07	1.04E-06		
LPT-16S	24	13:16	62	< 0.01	1.67E-07	1.22E-08	3.90E-10	3.90E-09	No Detectable Flow	
LPT-16S	25	13:19	62	0.250	4.17E-06	3.05E-07	9.75E-09	9.75E-08		
LPT-16S	26	13:26	62	0.300	5.00E-06	3.66E-07	1.17E-08	1.17E-07		
LPT-16S	27	13:29	62	0.175	2.92E-06	2.13E-07	6.83E-09	6.83E-08		
LPT-16S	28	13:33	63	0.075	1.25E-06	8.97E-08	2.87E-09	2.87E-08		
LPT-16S	29	13:36	63	0.200	3.33E-06	2.39E-07	7.65E-09	7.65E-08		
LPT-16S	30	13:40	62	0.550	9.17E-06	6.70E-07	2.15E-08	2.15E-07		
LPT-16S	31	13:47	49	10.000	1.67E-04	1.63E-05	5.21E-07	5.21E-06		

*Note: Permeability for tests with no measureable flow indicates an upper bound. Actual permeability may be considerably less.

LPT-16S	31	13:57	46.5	10.000	1.67E-04	1.74E-05	5.57E-07	5.57E-06	
LPT-16S	32	13:51	57	< 0.01	1.67E-07	1.35E-08	4.32E-10	4.32E-09	No Detectable Flow
LPT-16S	33	13:52	57	< 0.01	1.67E-07	1.35E-08	4.32E-10	4.32E-09	No Detectable Flow
LPT-16S	34	14:24	62	< 0.01	1.67E-07	1.22E-08	3.90E-10	3.90E-09	No Detectable Flow
LPT-16S	35	14:26	62	< 0.01	1.67E-07	1.22E-08	3.90E-10	3.90E-09	No Detectable Flow
LPT-16S	36	14:27	64	< 0.01	1.67E-07	1.17E-08	3.75E-10	3.75E-09	No Detectable Flow
LPT-16S	37	14:28	63	< 0.01	1.67E-07	1.20E-08	3.83E-10	3.83E-09	No Detectable Flow
LPT-16S	38	14:29	62	< 0.01	1.67E-07	1.22E-08	3.90E-10	3.90E-09	No Detectable Flow
LPT-16S	39	14:31	60	< 0.01	1.67E-07	1.27E-08	4.06E-10	4.06E-09	No Detectable Flow
LPT-16S	40	14:32	62	< 0.01	1.67E-07	1.22E-08	3.90E-10	3.90E-09	No Detectable Flow
LPT-16S	40	14:35	54	33.000	5.50E-04	4.76E-05	1.52E-06	1.52E-05	Post Fracture
LPT-20	3	14:51	24	< 0.01	1.67E-07	4.61E-08	1.48E-09	1.48E-08	No Detectable Flow
LPT-20	5	14:56	26	< 0.01	1.67E-07	4.02E-08	1.29E-09	1.29E-08	No Detectable Flow
LPT-20	6	15:02	28	< 0.01	1.67E-07	3.57E-08	1.14E-09	1.14E-08	No Detectable Flow
LPT-20	7	16:16	24	< 0.01	1.67E-07	4.61E-08	1.48E-09	1.48E-08	No Detectable Flow
LPT-20	8	16:22	34	< 0.01	1.67E-07	2.66E-08	8.52E-10	8.52E-09	No Detectable Flow
LPT-20	9	16:48	44	< 0.01	1.67E-07	1.87E-08	5.99E-10	5.99E-09	No Detectable Flow
LPT-2	5	8:59	82	< 0.01	1.67E-07	8.79E-09	2.81E-10	2.81E-09	No Detectable Flow
LPT-2	6	9:01	82	0.025	4.17E-07	2.20E-08	7.03E-10	7.03E-09	
LPT-2	7	9:06	82	0.030	5.00E-07	2.64E-08	8.43E-10	8.43E-09	
LPT-2	8	9:12	82	0.060	1.00E-06	5.27E-08	1.69E-09	1.69E-08	
LPT-2	9	9:18	82.25	0.030	5.00E-07	2.63E-08	8.41E-10	8.41E-09	
LPT-2	10	9:23	82.25	0.150	2.50E-06	1.31E-07	4.20E-09	4.20E-08	
LPT-2S	18	9:15	49	0.067	1.12E-06	1.09E-07	3.49E-09	3.49E-08	
LPT-2S	19	9:20	64	0.115	1.92E-06	1.35E-07	4.32E-09	4.32E-08	
LPT-2S	20	9:22	98	< 0.01	1.67E-07	7.18E-09	2.30E-10	2.30E-09	No Detectable Flow
LPT-2S	21	9:26	64	< 0.01	1.67E-07	1.17E-08	3.75E-10	3.75E-09	No Detectable Flow
LPT-2S	22	9:28	64	0.170	2.83E-06	2.00E-07	6.38E-09	6.38E-08	
LPT-2S	23	9:32	64	0.075	1.25E-06	8.80E-08	2.82E-09	2.82E-08	
LPT-2S	24	9:36	64.5	< 0.01	1.67E-07	1.16E-08	3.72E-10	3.72E-09	
LPT-2S	25	9:39	65	< 0.01	1.67E-07	1.15E-08	3.69E-10	3.69E-09	No Detectable Flow
LPT-2S	26	9:42	85	< 0.01	1.67E-07	8.43E-09	2.70E-10	2.70E-09	
LPT-2S	27	9:47	64	1.200	2.00E-05	1.41E-06	4.51E-08	4.51E-07	
LPT-2S	28	9:50	63	0.550	9.17E-06	6.58E-07	2.10E-08	2.10E-07	
LPT-2S	29	9:55	46	20.000	3.33E-04	3.53E-05	1.13E-06	1.13E-05	Post Fracture
LPT-2S	30	9:59	64	< 0.01	1.67E-07	1.17E-08	3.75E-10	3.75E-09	No Detectable Flow
LPT-2S	31	10:02	62	1.400	2.33E-05	1.71E-06	5.46E-08	5.46E-07	
LPT-2S	32	10:06	50	18.000	3.00E-04	2.86E-05	9.15E-07	9.15E-06	Post Fracture
LPT-2S	33	10:07	55	< 0.01	1.67E-07	1.41E-08	4.51E-10	4.51E-09	No Detectable Flow
LPT-2S	34	10:09	60	< 0.01	1.67E-07	1.27E-08	4.06E-10	4.06E-09	No Detectable Flow
LPT-2S	35	10:12	60	< 0.01	1.67E-07	1.27E-08	4.06E-10	4.06E-09	No Detectable Flow
LPT-2S	36	10:14	60	< 0.01	1.67E-07	1.27E-08	4.06E-10	4.06E-09	No Detectable Flow
LPT-2S	37	10:16	62	< 0.01	1.67E-07	1.22E-08	3.90E-10	3.90E-09	No Detectable Flow
LPT-2S	38	10:17	60	< 0.01	1.67E-07	1.27E-08	4.06E-10	4.06E-09	No Detectable Flow
LPT-9	4	19:31	44	< 0.01	1.67E-07	1.87E-08	5.99E-10	5.99E-09	No Detectable Flow
LPT-9	5	19:32	46	< 0.01	1.67E-07	1.77E-08	5.65E-10	5.65E-09	No Detectable Flow
LPT-9	6	19:33	44	< 0.01	1.67E-07	1.87E-08	5.99E-10	5.99E-09	No Detectable Flow
LPT-9	7	19:35	44	< 0.01	1.67E-07	1.87E-08	5.99E-10	5.99E-09	No Detectable Flow
LPT-9	7.5	19:36	44	< 0.01	1.67E-07	1.87E-08	5.99E-10	5.99E-09	No Detectable Flow
LPT-9S	16	10:45	78	0.380	6.33E-06	3.54E-07	1.13E-08	1.13E-07	
LPT-9S	17	10:50	78	0.370	6.17E-06	3.44E-07	1.10E-08	1.10E-07	
LPT-9S	18	10:55	79	0.100	1.67E-06	9.17E-08	2.93E-09	2.93E-08	
LPT-9S	19	11:00	80	0.090	1.50E-06	8.14E-08	2.60E-09	2.60E-08	
LPT-9S	20.5	11:10	76	0.800	1.33E-05	7.67E-07	2.45E-08	2.45E-07	
LPT-9S	21	11:17	80	0.200	3.33E-06	1.81E-07	5.78E-09	5.78E-08	
LPT-9S	22	11:22	80	0.220	3.67E-06	1.99E-07	6.36E-09	6.36E-08	
LPT-9S	23	11:27	80	0.280	4.67E-06	2.53E-07	8.10E-09	8.10E-08	
LPT-9S	24	11:34	79	0.460	7.67E-06	4.22E-07	1.35E-08	1.35E-07	
LPT-9S	25	11:40:00	81	0.100	1.67E-06	8.91E-08	2.85E-09	2.85E-08	
LPT-9S	26	11:47	82.5	0.110	1.83E-06	9.60E-08	3.07E-09	3.07E-08	
LPT-9S	27	11:53	82.5	0.130	2.17E-06	1.13E-07	3.63E-09	3.63E-08	

*Note: Permeability for tests with no measureable flow indicates an upper bound. Actual permeability may be considerably less.

LPT-9S	28	11:57	82.5	0.260	4.33E-06	2.27E-07	7.26E-09	7.26E-08		
LPT-9S	29	12:01	83.5	0.080	1.33E-06	6.89E-08	2.20E-09	2.20E-08		
LPT-9S	30	12:04	83	0.250	4.17E-06	2.17E-07	6.93E-09	6.93E-08		
LPT-9S	31	12:08	83	0.340	5.67E-06	2.95E-07	9.43E-09	9.43E-08		
LPT-9S	32	12:12	82	0.680	1.13E-05	5.98E-07	1.91E-08	1.91E-07		
LPT-9S	33	12:15	84	1.150	1.92E-05	9.83E-07	3.15E-08	3.15E-07		
LPT-9S	34	12:20	81	3.100	5.17E-05	2.76E-06	8.84E-08	8.84E-07		
LPT-9S	35	12:25	81	3.000	5.00E-05	2.67E-06	8.55E-08	8.55E-07		
LPT-9S	36	12:29	53	30.000	5.00E-04	4.43E-05	1.42E-06	1.42E-05	Post Fracture	
LPT-9S	37	12:38	50	10.000	1.67E-04	1.59E-05	5.08E-07	5.08E-06	Post Fracture	
LPT-9S	38	12:41	61	0.100	1.67E-06	1.24E-07	3.98E-09	3.98E-08		
LPT-9S	39	12:48	41	5.000	8.33E-05	1.03E-05	3.29E-07	3.29E-06		
LPT-9S	40	12:54	67	0.480	8.00E-06	5.33E-07	1.71E-08	1.71E-07		
LPT-19	4	18:28	48	< 0.01	1.67E-07	1.67E-08	5.35E-10	5.35E-09	No Detectable Flow	
LPT-19	5	18:30	48	< 0.01	1.67E-07	1.67E-08	5.35E-10	5.35E-09	No Detectable Flow	
LPT-19	6	18:33	49	< 0.01	1.67E-07	1.63E-08	5.21E-10	5.21E-09	No Detectable Flow	
LPT-19	7	18:35	50	< 0.01	1.67E-07	1.59E-08	5.08E-10	5.08E-09	No Detectable Flow	
LPT-19	8	18:36	48	< 0.01	1.67E-07	1.67E-08	5.35E-10	5.35E-09	No Detectable Flow	
LPT-19	9	18:38	75	< 0.01	1.67E-07	9.74E-09	3.12E-10	3.12E-09	No Detectable Flow	
LPT-19	10	18:54	65	< 0.01	1.67E-07	1.15E-08	3.69E-10	3.69E-09	No Detectable Flow	
LPT-19.5S	17	14:43	78	0.078	1.30E-06	7.26E-08	2.32E-09	2.32E-08		
LPT-19.5S	18	14:48	78	0.110	1.83E-06	1.02E-07	3.28E-09	3.28E-08		
LPT-19.5S	19	14:50	78	0.045	7.50E-07	4.19E-08	1.34E-09	1.34E-08		
LPT-19.5S	20	14:54	79	0.020	3.33E-07	1.83E-08	5.87E-10	5.87E-09		
LPT-19.5S	21	14:56	79	< 0.01	1.67E-07	9.17E-09	2.93E-10	2.93E-09	No Detectable Flow	
LPT-19.5S	22	14:59	78	1.500	2.50E-05	1.40E-06	4.47E-08	4.47E-07		
LPT-19.5S	23	15:03	78	1.700	2.83E-05	1.58E-06	5.06E-08	5.06E-07		
LPT-19.5S	24	15:08	78	1.800	3.00E-05	1.68E-06	5.36E-08	5.36E-07		
LPT-19.5S	25	15:14	78	2.000	3.33E-05	1.86E-06	5.96E-08	5.96E-07		
LPT-19.5S	26	15:19	52	33.000	5.50E-04	4.99E-05	1.60E-06	1.60E-05	Post Fracture	
LPT-19.5S	27	15:27	52	< 0.01	1.67E-07	1.51E-08	4.84E-10	4.84E-09	No Detectable Flow	
LPT-19.5S	28	15:34	55	3.500	5.83E-05	4.94E-06	1.58E-07	1.58E-06		
LPT-19.5S	29	15:40	51	0.450	7.50E-06	6.97E-07	2.23E-08	2.23E-07		
LPT-19.5S	30	15:48	56	0.100	1.67E-06	1.38E-07	4.41E-09	4.41E-08		
LPT-19.5S	31	16:02	56	0.220	3.67E-06	3.03E-07	9.71E-09	9.71E-08		
LPT-19.5S	32	16:04	56	0.620	1.03E-05	8.55E-07	2.74E-08	2.74E-07		
LPT-19.5S	33	16:12	48	10.000	1.67E-04	1.67E-05	5.35E-07	5.35E-06	Post Fracture	
LPT-19.5S	34	16:18	49	14.000	2.33E-04	2.28E-05	7.30E-07	7.30E-06	Post Fracture	
LPT-19.5S	35	16:21	62	< 0.01	1.67E-07	1.22E-08	3.90E-10	3.90E-09	No Detectable Flow	
LPT-19.5S	36	16:23	64	< 0.01	1.67E-07	1.17E-08	3.75E-10	3.75E-09	No Detectable Flow	
LPT-19.5S	37	16:24	71	< 0.01	1.67E-07	1.04E-08	3.32E-10	3.32E-09	No Detectable Flow	
LPT-19.5S	38	16:25	70	< 0.01	1.67E-07	1.06E-08	3.38E-10	3.38E-09	No Detectable Flow	
LPT-19.5S	39	16:26	78	< 0.01	1.67E-07	9.31E-09	2.98E-10	2.98E-09	No Detectable Flow	
LPT-20	3	14:52	27	< 0.01	1.67E-07	3.78E-08	1.21E-09	1.21E-08	No Detectable Flow	
LPT-20	4	14:55	27	< 0.01	1.67E-07	3.78E-08	1.21E-09	1.21E-08	No Detectable Flow	
LPT-20	5	14:58	27	< 0.01	1.67E-07	3.78E-08	1.21E-09	1.21E-08	No Detectable Flow	
LPT-20	6	15:02	28	< 0.01	1.67E-07	3.57E-08	1.14E-09	1.14E-08	No Detectable Flow	
LPT-20	7	16:15	28	< 0.01	1.67E-07	3.57E-08	1.14E-09	1.14E-08	No Detectable Flow	
LPT-20	8	16:21	32	< 0.01	1.67E-07	2.91E-08	9.30E-10	9.30E-09	No Detectable Flow	
LPT-20	9	16:48	44	< 0.01	1.67E-07	1.87E-08	5.99E-10	5.99E-09	No Detectable Flow	
							Average Permeability:	9.15E-07		
							Avg. Perm. w/o fracture flow data included:	3.05E-07		

*Note: Permeability for tests with no measureable flow indicates an upper bound. Actual permeability may be considerably less.

Appendix C

Axial Lance Load Data

Peak Force Needed to Advance Lance to Next Test Zone

Lancing	Depth(ft.)	Force(lbs)
LPT-2	3	1000
LPT-2	4	2500
LPT-2	5	3500
LPT-2	6	4000
LPT-2	7	3250
LPT-2	8	3000
LPT-2	9	4200
LPT-2	10	6500
LPT-2S	18	5400
LPT-2S	19	4800
LPT-2S	20	5100
LPT-2S	21	4200
LPT-2S	22	5000
LPT-2S	23	4000
LPT-2S	24	4000
LPT-2S	25	7000
LPT-2S	26	2300
LPT-2S	27	1900
LPT-2S	28	2000
LPT-2S	29	2400
LPT-2S	30	2200
LPT-2S	31	3000
LPT-2S	32	3300
LPT-2S	33	4600
LPT-2S	34	5600
LPT-2S	35	4500
LPT-2S	36	3800
LPT-2S	37	3000
LPT-2S	38	5200
LPT-5S	19	6200
LPT-5S	20	6000
LPT-5S	21	6600
LPT-5S	22	5000
LPT-5S	23	6300
LPT-5S	24	2000
LPT-5S	25	2600
LPT-5S	26	4500
LPT-5S	27	4300
LPT-5S	28	5300
LPT-5S	29	4800
LPT-5S	30	3700
LPT-5S	31	6100
LPT-5S	32	4500
LPT-5S	33	5700
LPT-9	2	2300
LPT-9	3	1800
LPT-9	4	4000
LPT-9	5	5200
LPT-9	6	7500
LPT-9	7	5700
LPT-9	7.5	5500
LPT-11S	15	2600
LPT-11S	16	3400
LPT-11S	17	4000
LPT-11S	18	5200
LPT-11S	19	5200
LPT-11S	20	5600
LPT-11S	21	6000
LPT-11S	22	6000
LPT-11S	23	5800
LPT-11S	24	5700
LPT-11S	25	5500
LPT-11S	26	7600
LPT-11S	27	7500
LPT-11S	28	9000
LPT-11S	29	7600
LPT-11S	30	8600
LPT-11S	31	7000
LPT-11S	32	7400
LPT-11S	33	6200
LPT-16S	19	4500
LPT-16S	20	3600
LPT-16S	21	5200
LPT-16S	22	2600
LPT-16S	23	5700
LPT-16S	24	6000
LPT-16S	25	2200
LPT-16S	26	2300
LPT-16S	27	2300
LPT-16S	28	2700
LPT-16S	29	4000
LPT-16S	30	4500
LPT-16S	31	4500
LPT-16S	32	5000
LPT-16S	33	5300
LPT-20	1	5000
LPT-20	2	6500
LPT-20	3	7000
LPT-20	4	9000
LPT-20	5	5500
LPT-20	6	5600
LPT-20	7	5000
LPT-20	8	6000
LPT-20	9	5600

LPT-2

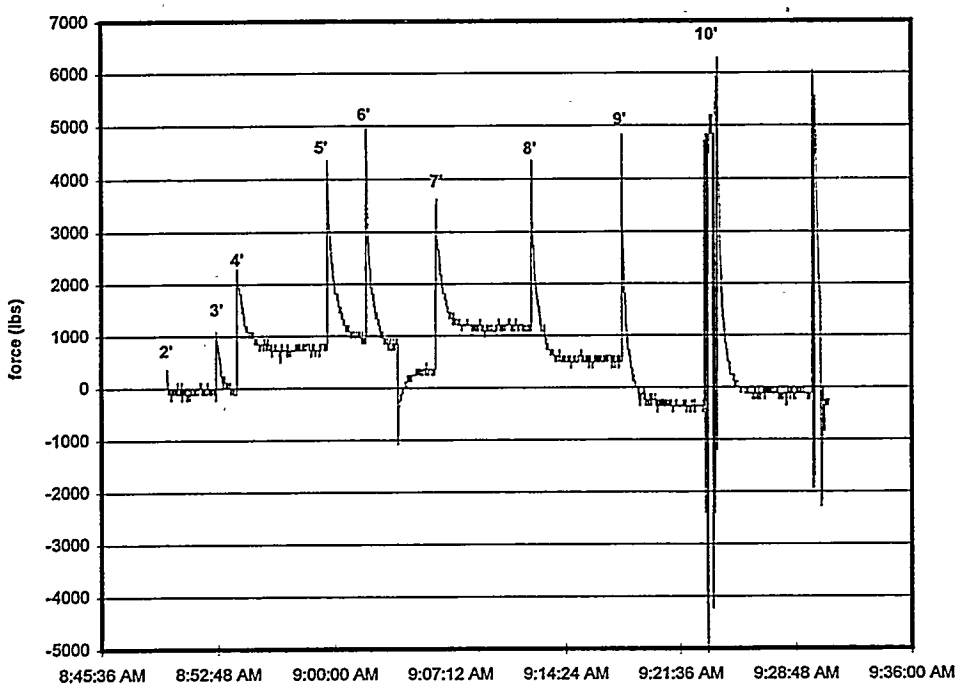
7000
6000
5000
4000
3000
2000
1000
0
-1000
-2000
-3000
-4000
-5000
force (lbs)
2'
3'
4'
5'
6'
7'
8'
9'
10'
8:45:36 AM
8:52:48 AM
9:00:00 AM
9:07:12 AM
9:14:24 AM
9:21:36 AM
9:28:48 AM
9:36:00 AM

LPT-2S

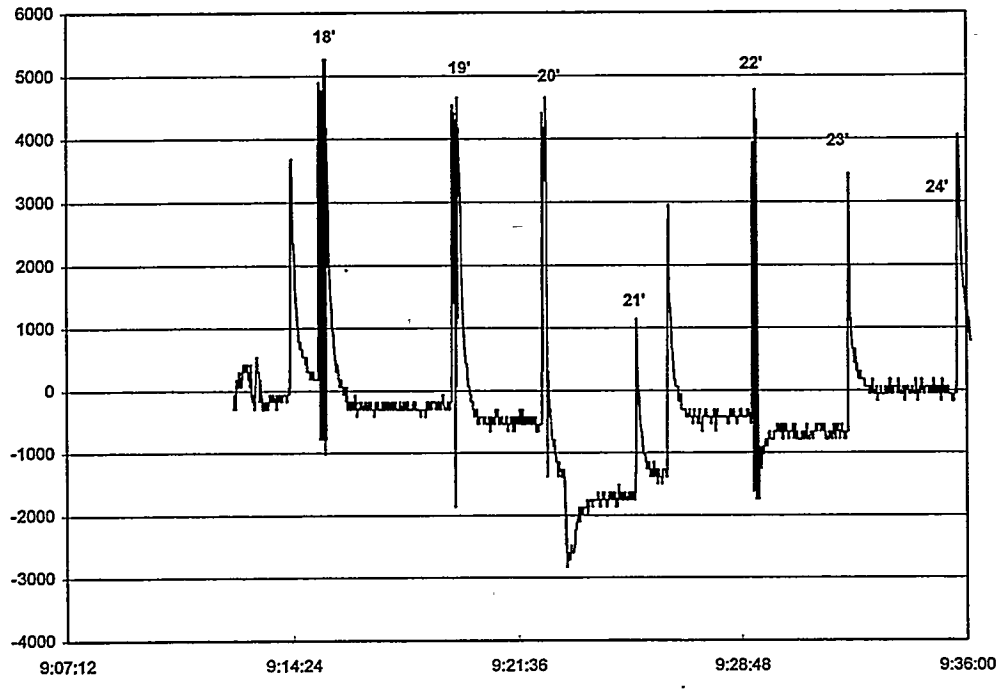
6000
5000
4000
3000
2000
1000
0
-1000
-2000
-3000
-4000
18'
19'
20'
21'
22'
23'
24'
9:07:12
9:14:24
9:21:36
9:28:48
9:36:00

LPT-2S

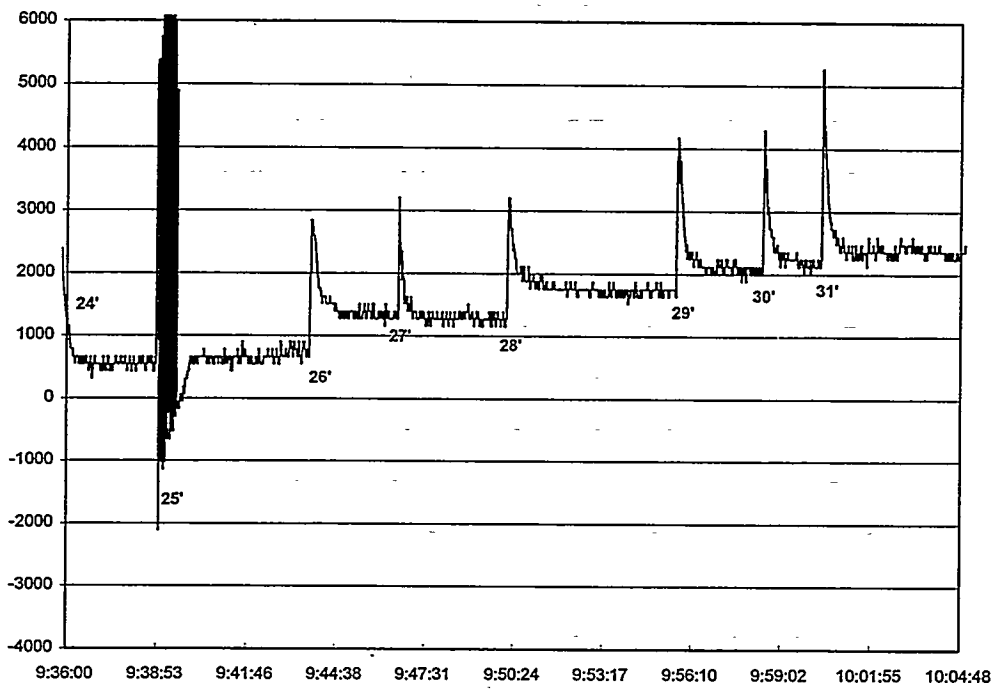
6000
5000
4000
3000
2000
1000
0
-1000
-2000
-3000
-4000
24'
25'
26'
27'
28'
29'
30'
31'
9:36:00
9:38:53
9:41:46
9:44:38
9:47:31
9:50:24
9:53:17
9:56:10
9:59:02
10:01:55
10:04:48

LPT-2S

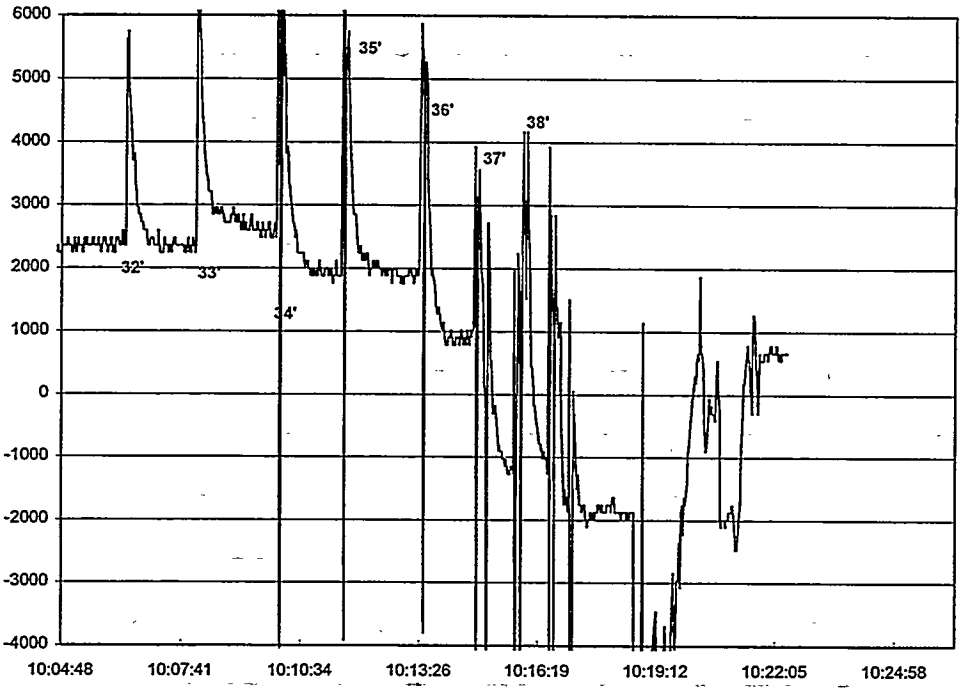
6000
5000
4000
3000
2000
1000
0
-1000
-2000
-3000
-4000
32'
33'
34'
35'
36'
37'
38'
10:04:48
10:07:41
10:10:34
10:13:26
10:16:19
10:19:12
10:22:05
10:24:58

LPT-5S

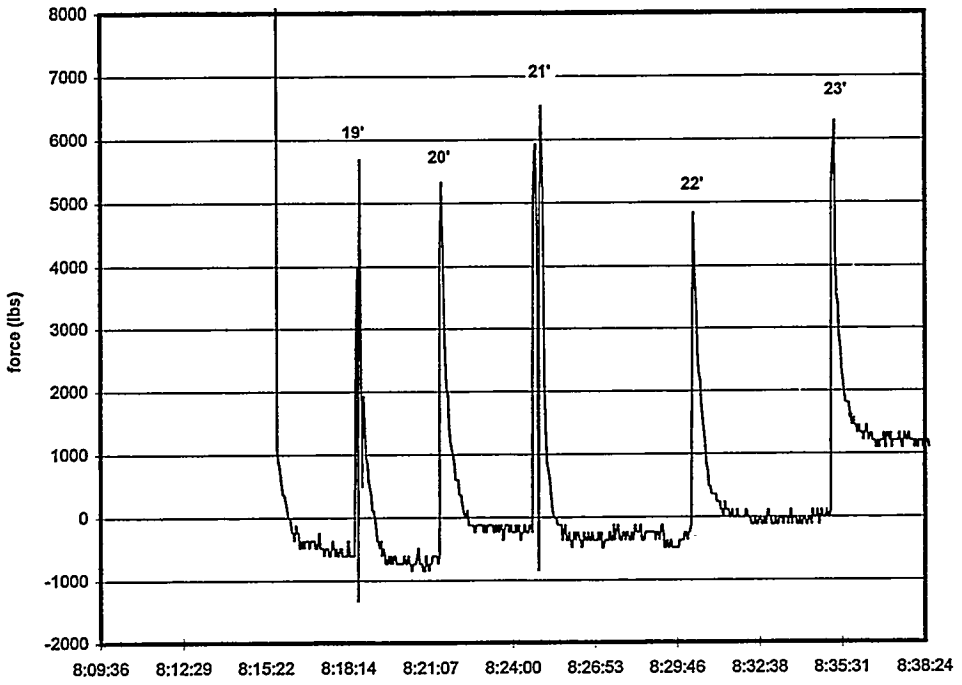
8000
7000
6000
5000
4000
3000
2000
1000
0
-1000
-2000
force (lbs)
19'
20'
21'
22'
23'
8:09:36
8:12:29
8:15:22
8:18:14
8:21:07
8:24:00
8:26:53
8:29:46
8:32:38
8:35:31
8:38:24

LPT-5S

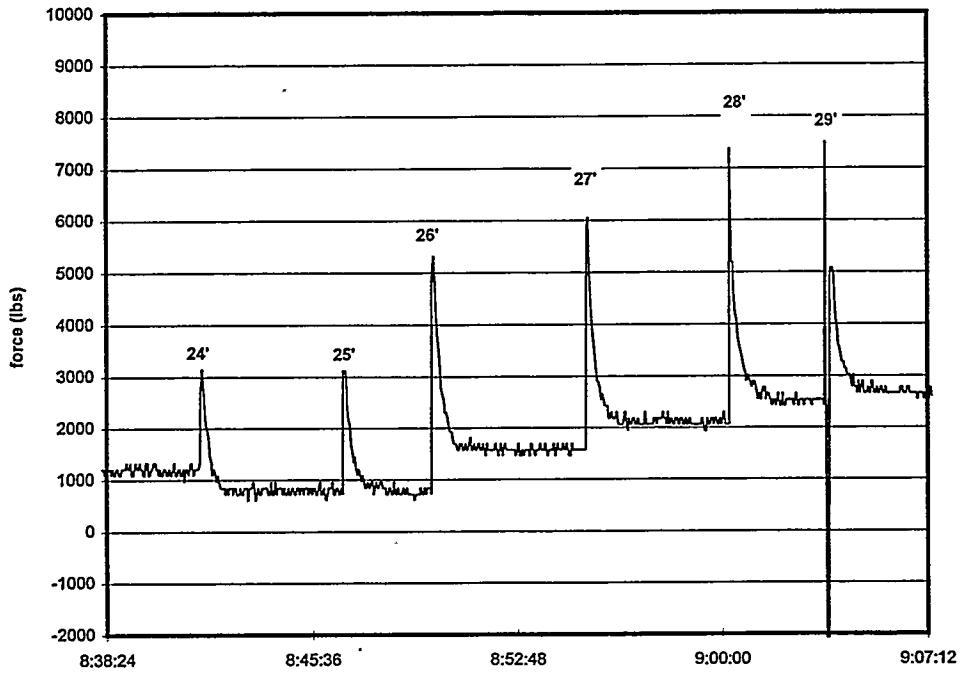
10000
9000
8000
7000
6000
5000
4000
3000
2000
1000
0
-1000
-2000
force (lbs)
24'
25'
26'
27'
28'
29'
8:38:24
8:45:36
8:52:48
9:00:00
9:07:12

LPT-5S

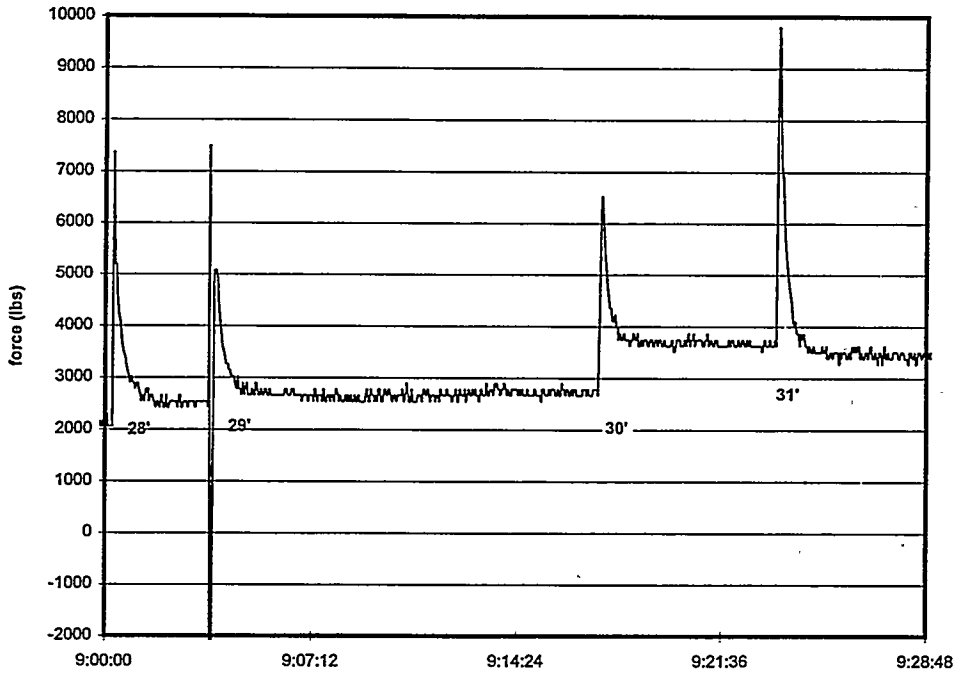
10000
9000
8000
7000
6000
5000
4000
3000
2000
1000
0
-1000
-2000
force (lbs)
28'
29'
30'
31'
9:00:00
9:07:12
9:14:24
9:21:36
9:28:48

LPT-5S

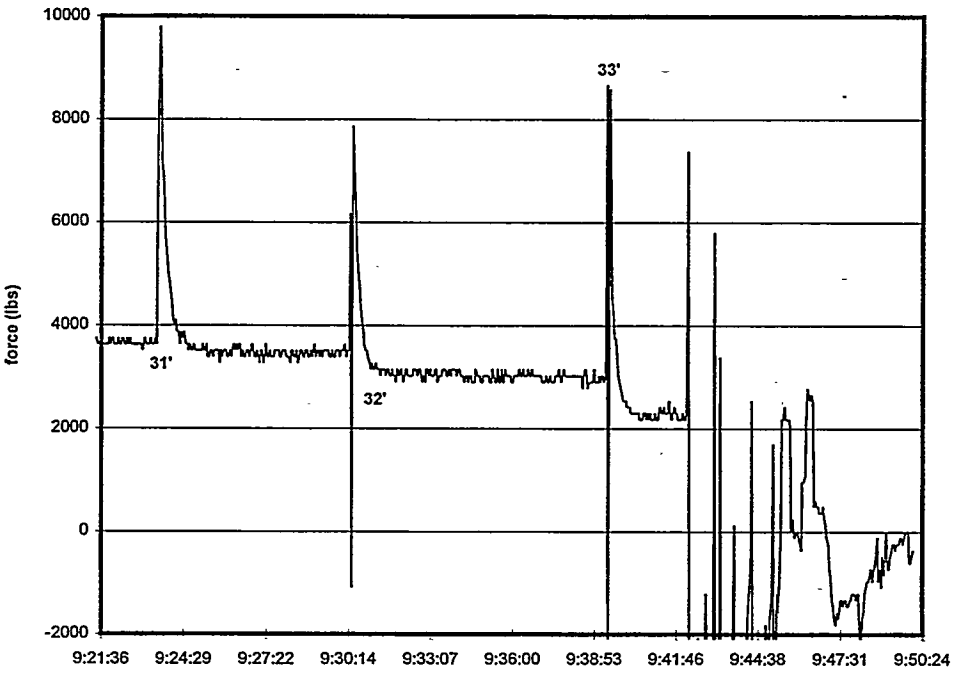
10000
8000
6000
4000
2000
0
-2000
force (lbs)
31'
32'
33'
9:21:36
9:24:29
9:27:22
9:30:14
9:33:07
9:36:00
9:38:53
9:41:46
9:44:38
9:47:31
9:50:24

LPT-9

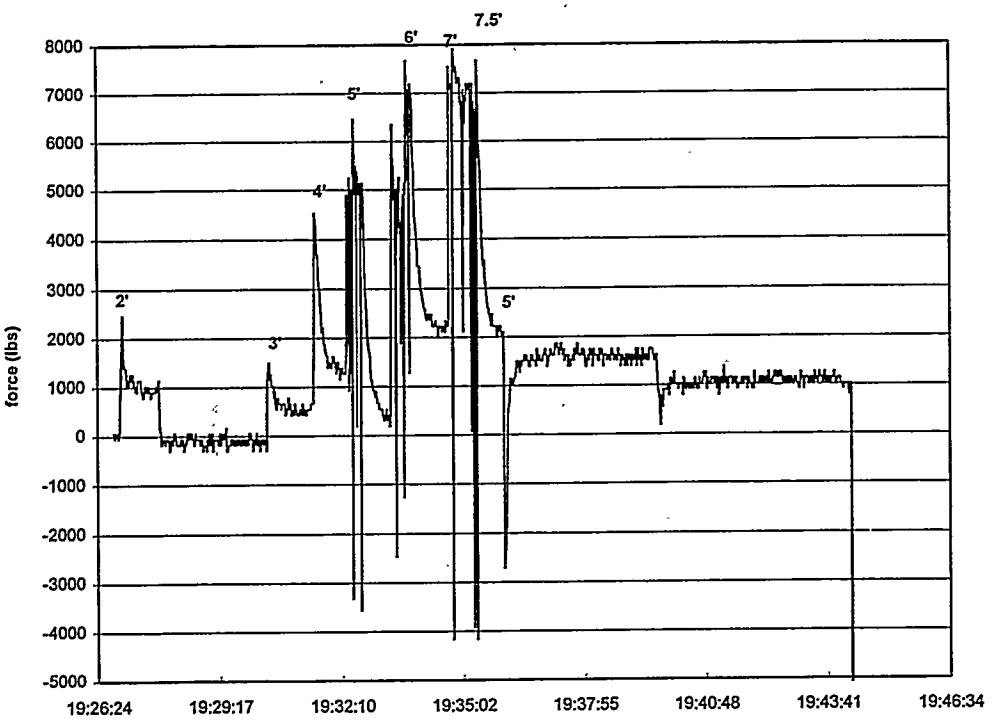
force (lbs)
8000
7000
6000
5000
4000
3000
2000
1000
0
-1000
-2000
-3000
-4000
-5000
19:26:24
19:29:17
19:32:10
19:35:02
19:37:55
19:40:48
19:43:41
19:46:34
2'
3'
4'
5'
6'
7'
7.5'
5'

LPT-11S

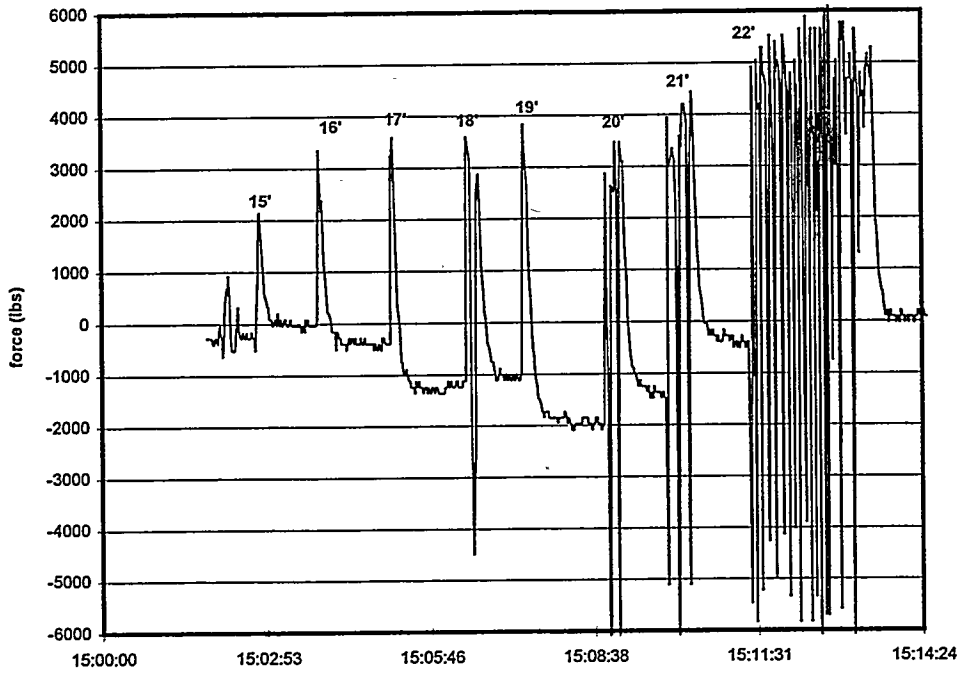
force (lbs)
6000
5000
4000
3000
2000
1000
0
-1000
-2000
-3000
-4000
-5000
-6000
15:00:00
15:02:53
15:05:46
15:08:38
15:11:31
15:14:24
15'
16'
17'
18'
19'
20'
21'
22'

LPT-11S

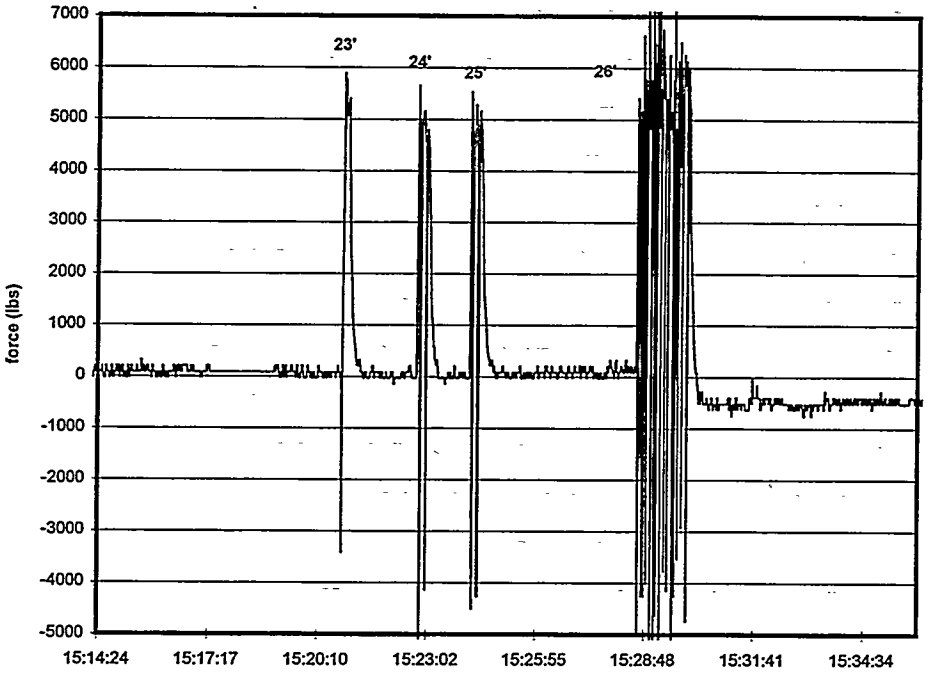

LPT-11S

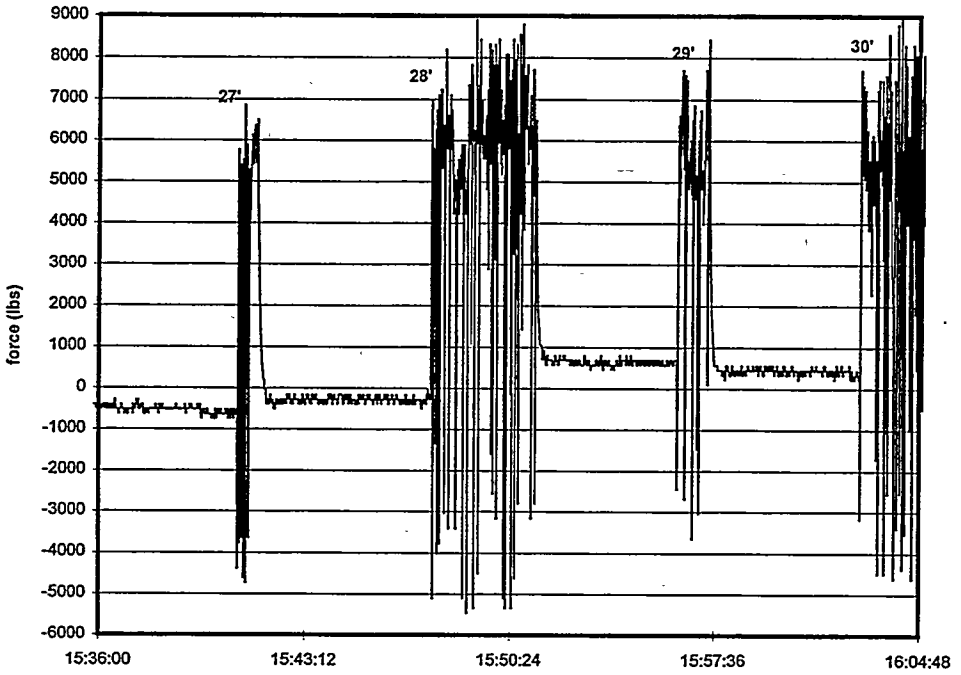

LPT-11S

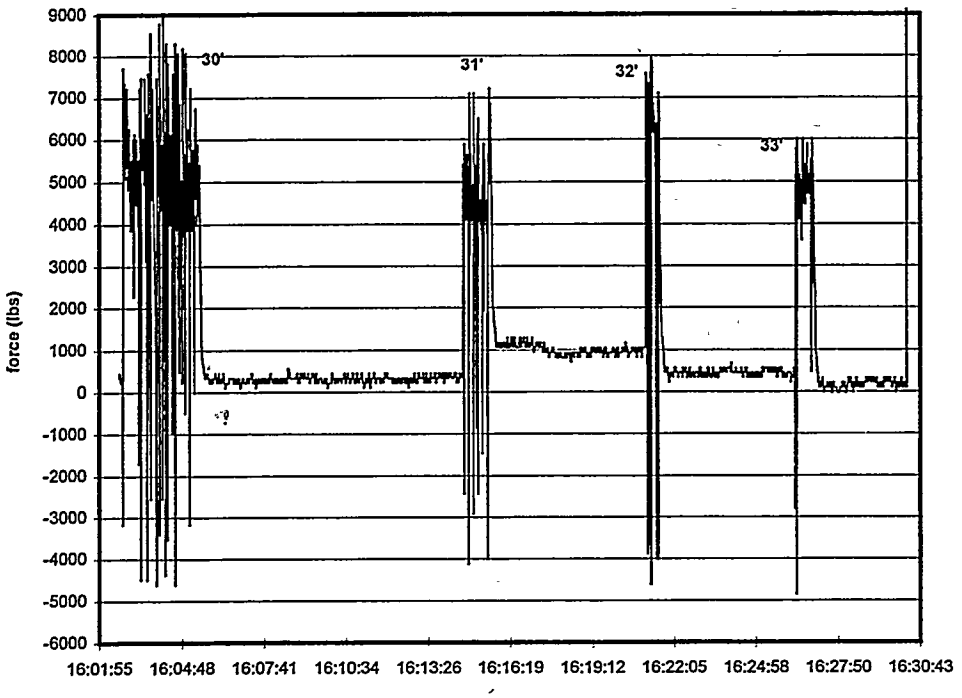

LPT-16S

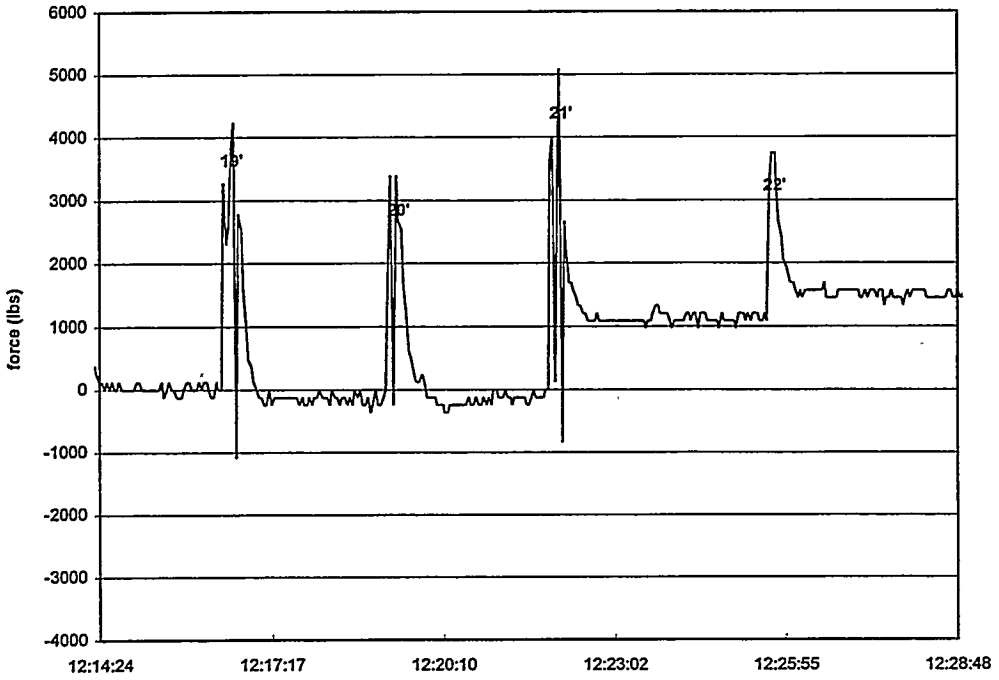

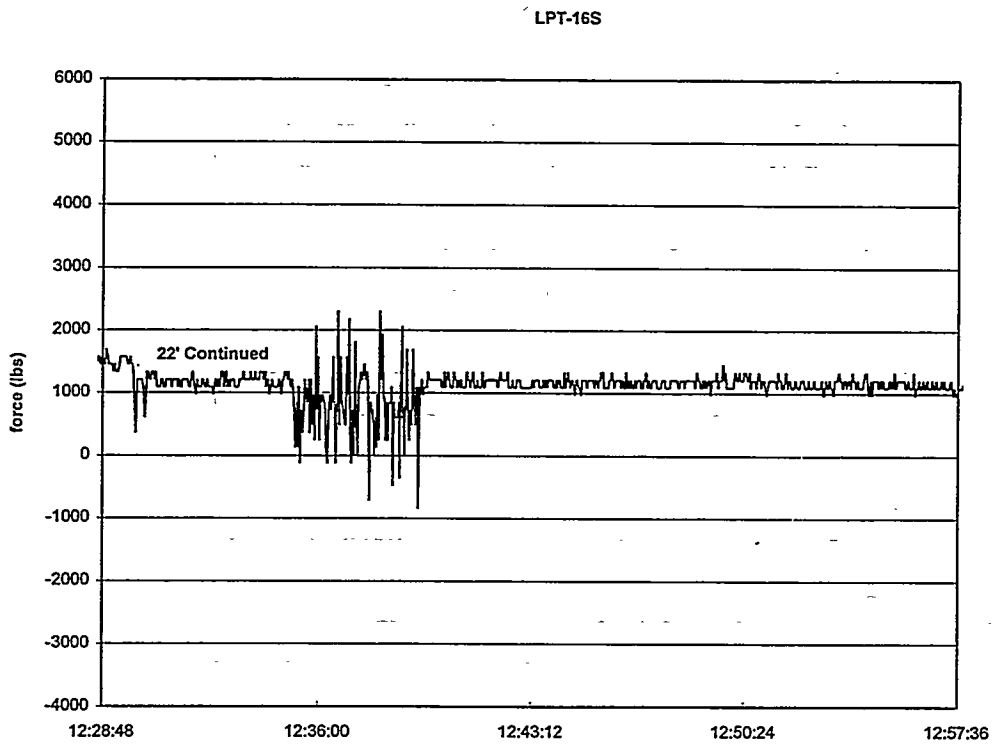
LPT-16S
6000
5000
4000
3000
2000
1000
0
-1000
-2000
-3000
-4000
force (lbs)
22' Continued
12:28:48
12:36:00
12:43:12
12:50:24
12:57:36

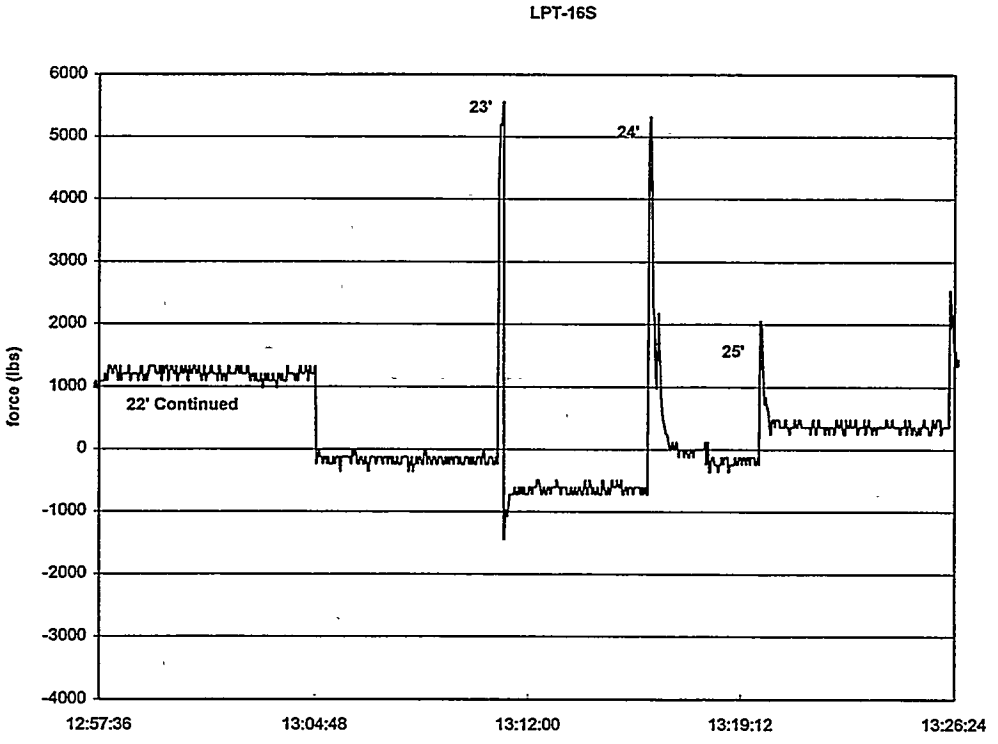
LPT-16S
6000
5000
4000
3000
2000
1000
0
-1000
-2000
-3000
-4000
force (lbs)
22' Continued
23'
24'
25'
12:57:36
13:04:48
13:12:00
13:19:12
13:26:24

LPT-16S

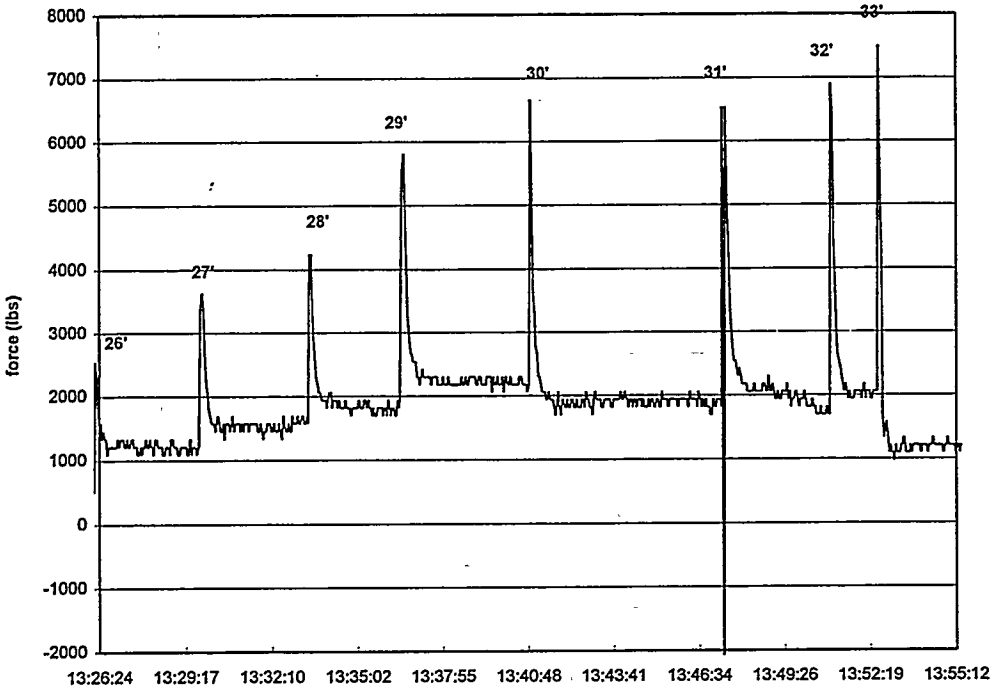

LPT-16S

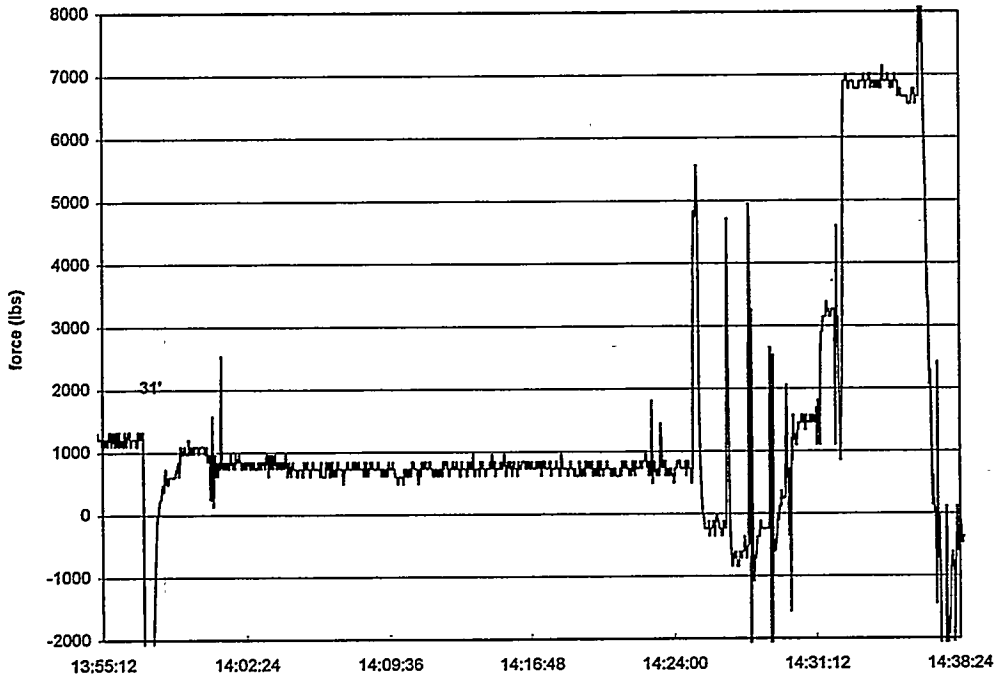

LPT-20

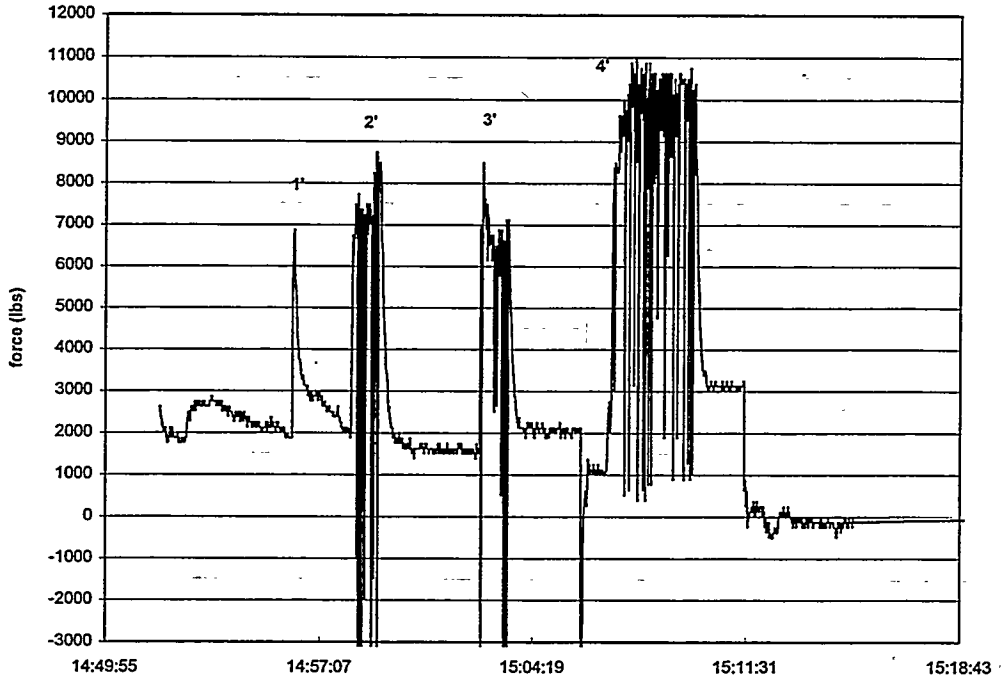
force (lbs)
12000
11000
10000
9000
8000
7000
6000
5000
4000
3000
2000
1000
0
-1000
-2000
-3000
1'
2'
3'
4'
14:49:55
14:57:07
15:04:19
15:11:31
15:18:43

LPT-20

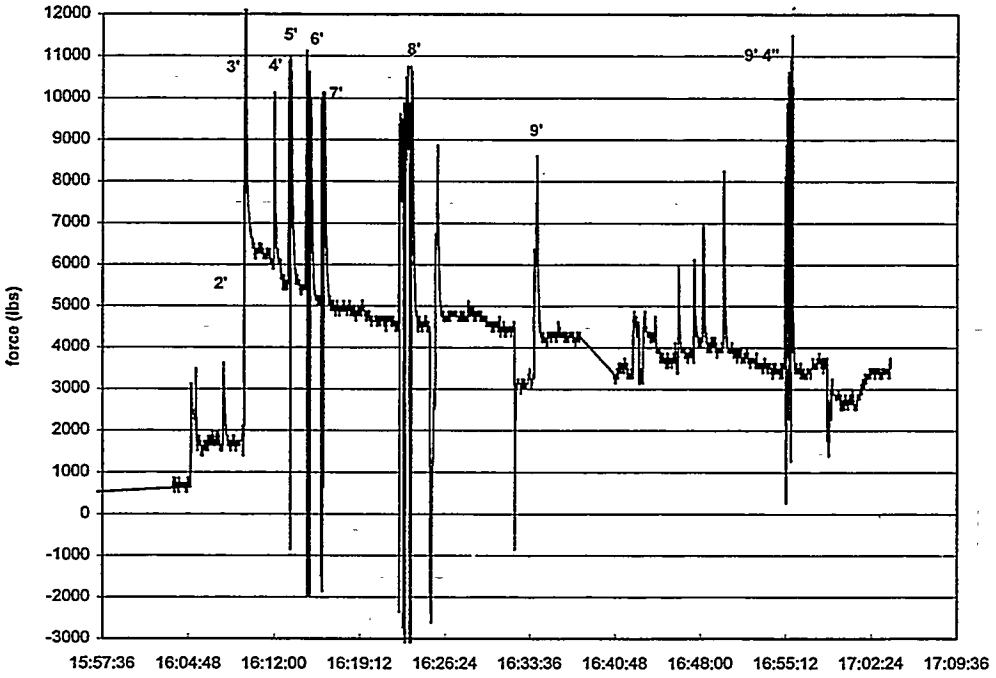
force (lbs)
12000
11000
10000
9000
8000
7000
6000
5000
4000
3000
2000
1000
0
-1000
-2000
-3000
2'
3'
4'
5'
6'
7'
8'
9'
9'-4"
15:57:36
16:04:48
16:12:00
16:19:12
16:26:24
16:33:36
16:40:48
16:48:00
16:55:12
17:02:24
17:09:36